

Numerical Modelling of Ball Bearing Stiffness to Predict Contact Stress Caused by Vibration Induced Gapping

Antonios Papakonstantinou

UNIVERSITY
— OF CENTRAL —
LANCASHIRE



JOST INSTITUTE FOR TRIBOTECHNOLOGY
UNIVERSITY OF CENTRAL LANCASHIRE

in collaboration with

THE EUROPEAN SPACE TRIBOLOGY LABORATORY

Submitted in fulfilment of
the requirements for the degree of
Master of Science

December 2004

Abstract

Award: Master of Science (by research)

**Title: NUMERICAL MODELLING OF BALL BEARING STIFFNESS TO
PREDICT CONTACT STRESS CAUSED BY VIBRATION INDUCED GAPPING**

Author: ANTONIOS PAPAKONSTANTINOU

Submission date: December 2004

The ball bearings that form part of mechanisms in space applications are subjected to vibrations. The result of these vibrations is gapping between the rings of the bearing. This gap allows collisions of the ball with the races, which produce high contact stresses. These high stresses can cause indentation damage on the ball and the raceways, and may lead to malfunction of the bearing, and therefore the mechanism the bearing forms a part.

Previous studies have develop a 2-DOF model in order to predict gapping using for the calculation, the bearing stiffness predicted by a computer software called CABARET, with satisfactory results. In the present study the model optimized, as the comparison with available measured gapping values verifies, by the introduction of the non-linear stiffness to the existing prediction model.

A method of contact stress prediction developed, based on the analysis of the collisions between the ball and the rings of the bearing, considering the laws of conservation of energy and the laws of motion, involving evaluations of the closing velocity, the collision acceleration and the impact force. Comparison of the Hertzian stress predicted by the author showed better agreement to experimental indentation damage (made by another investigator), than the CABARET predicted stress.

TABLE OF CONTENTS

Abstract.....	i
TABLE OF CONTENTS.....	ii
LIST OF FIGURES	v
Acknowledgments	viii
NOMECLATURE.....	ix
1 Introduction.....	1
1.1 The need for research	2
1.2 Aims of the current project	3
1.3 Chapters of the project	4
2 Literature Survey.....	5
2.1 Types of bearings	6
2.1.1 Ball Bearings	6
2.1.2 Radial or deep groove or Conrad bearings	7
2.1.2.1 Description.....	7
2.1.1.1 Applications.....	8
2.1.3 Angular contact bearings	8
2.1.3.1 Description.....	8
2.1.3.2 Applications	10
2.1.4 Four-Point-Contact ball bearings.....	10
2.1.4.1 Description.....	10
2.1.4.2 Applications	11
2.1.5 Wire race bearings	11
2.1.6 Thrust ball bearings	12
2.2 Roller bearings	12
2.3 Plain, Spherical and rod end bearings	12
2.4 Magnetic bearings.....	13
2.5 Linear bearings	13
2.6 Lubrication	13
2.7 Liquid and Grease Lubricants.....	14
2.7.1 Types of liquid lubricants	14
2.7.1.1 Mineral oils.....	14
2.7.1.2 Synthetic oils.....	14
2.7.2 Greases	15
2.8 Solid Lubricants	15
2.8.1 Applications.....	15
Types of solid lubricants.....	15
2.9 Performance Characteristics.....	15

2.10	Theoretical methods.....	16
2.11	Components of coulombic torque.....	16
2.11.1	Assumptions	17
2.12	Methodology	17
2.12.1	Limitations.....	18
2.13	Geometrical parameters	18
2.13.1	Ball size	19
2.13.2	Variation of Ball Complement.....	19
2.13.3	Variation of ball diameter	19
2.13.4	Variation in Conformity Number.....	19
2.13.5	Variation in Free Contact angle.....	20
2.14	Test methods.....	20
2.14.1	Test Environment.....	20
2.14.2	Test chamber.....	21
2.15	Factors that influence the frictional forces and coefficients.....	21
2.16	Lubrication Mechanisms.....	21
2.16.1	Liquid lubrication	22
2.16.1.1	Hydrodynamic lubrication	22
2.16.2	Elasto- hydrodynamic lubrication (EHL)	22
2.16.3	Boundary lubrication	23
2.16.4	Mixed lubrication.....	24
2.17	Solid lubrication	24
Chapter 3		27
3	<i>Theoretical background and previous studies</i>	27
3.1	Gapping.....	28
3.2	Mass-spring model.....	28
3.3	Vibration test.....	32
3.4	Raceway damage.....	32
3.5	Theoretical background to the current study.....	33
3.6	Evaluation of bearing stiffness.....	33
3.6.1	Angular contact bearings	34
3.6.2	ANGULAR CONTACT BEARING PAIR	42
3.6.3	ASSUMPTIONS	43
3.6.4	Other bearing types and load conditions	43
3.7	Evaluation of Hertzian stress	44
3.7.1	Equivalent radius	44
3.7.2	Equivalent elastic modulus	45
3.7.3	Impact Force	46
3.7.4	Closing acceleration	48
3.7.5	Impact force calculation	49
4	<i>Results.....</i>	50
4.1	Introduction.....	51
4.2	Bearing stiffness	51

4.3	Gapping prediction for constant load	54
4.3.1	5-ball complement	54
4.3.2	9-ball complement	56
4.3.3	14-ball complement	57
4.4	Gapping prediction for constant 500 Hz frequency	58
	CABARET predictions	59
4.4.1	Non-linear predictions	64
4.5	Ball movement between the rings	69
4.5.1	Covered distances	70
	Closing velocity	71
4.5.2	Collision Acceleration	73
4.5.3	Impact Force	75
4.5.4	Hertzian stress	77
5	<i>Discussion</i>.....	80
5.1	Gapping prediction comparison	81
5.1.1	Constant load	81
5.1.2	Constant Frequency	84
5.1.2.1	500 Hz Frequency	84
5.1.2.1.1	5-ball complement	84
5.1.2.1.2	14-ball complement	85
5.1.2.1.3	9-ball complement	86
5.1.3	1500 Hz Frequency	93
5.1.4	2000 Hertz frequency	94
5.2	Collision between ball and rings	96
6	<i>Conclusions and recommendations</i>.....	98
6.1	Summary of the work completed.....	99
6.2	Identifying sources of error.....	100
6.3	Recommendations for further work.....	101
	Theoretical work	101
6.3.1	Experimental work	101
	<i>References</i>.....	103
	APPENDIX	106

LIST OF FIGURES

Figure 2.1 Angular contact bearing.....	9
Figure 2.2 Tandem-mounted pair of angular contact bearings	9
Figure 2.3 Face-to-face mounted pair of angular contact bearings.....	10
Figure 2.4 Cross section of a four point contact bearing	11
Figure 2.5 Coefficient of friction as function of viscosity-velocity-load parameter (Stribeck Hersey curve)	22
Figure 3.1 Mass- spring model	29
Figure 3.2 Applied load - Bearing stiffness graph	36
Figure 3.3 Ball complement – Bearing stiffness graph.....	36
Figure 3.4 Ball diameter – Bearing stiffness graph	37
Figure 3.5 Contact angle – Bearing stiffness graph	37
Figure 3.6 Rate of change of bearing stiffness with applied load.....	38
Figure 3.7 Rate of change of bearing stiffness with ball complement.....	39
Figure 3.8 Rate of change of bearing stiffness with ball diameter.....	40
Figure 3.9 Rate of change of bearing stiffness with contact angle	40
Figure 3.10 Relative movement of the rings.....	46
Figure 4.1 Bearing stiffness against Input acceleration	52
Figure 4.2 Bearing Stiffness against Applied Force	52
Figure 4.3 Gapping prediction for 5-ball complement at 20g.....	54
Figure 4.4 Gapping prediction for 5-ball complement at 25g.....	55
Figure 4.5 Gapping prediction for 5-ball complement at 30g.....	55
Figure 4.6 Gapping prediction for 9-ball complement at 20g.....	56
Figure 4.7 Gapping prediction for 9-ball complement at 25g.....	56
Figure 4.8 Gapping prediction for 9-ball complement at 30g.....	57
Figure 4.9 Gapping prediction for 14-ball complement at 20g.....	57
Figure 4.10 Gapping prediction for 14-ball complement at 25g.....	58
Figure 4.11 Gapping prediction for 14-ball complement at 30g.....	58
Figure 4.12 Input acceleration – Gapping prediction (using CABARET stiffness) at 500 Hz	59
Figure 4.13 Applied Force – Gapping prediction (using CABARET stiffness) at 500 Hz.....	60
Figure 4.14 Input acceleration – Gapping prediction (using CABARET stiffness) at 1500 Hz	60
Figure 4.15 Applied Force – Gapping prediction (using CABARET stiffness) at 1500 Hz.....	61
Figure 4.16 Input acceleration – Gapping prediction (using CABARET stiffness) at 2000 Hz	61
Figure 4.17 Applied Force – Gapping prediction (using CABARET stiffness) at 2000 Hz.....	62
Figure 4.18 Input acceleration – Gapping prediction (using non-linear stiffness) at 500 Hz	64
Figure 4.19 Applied Force – Gapping prediction (using non-linear stiffness) at 500 Hz.....	65
Figure 4.20 Input acceleration – Gapping prediction (using non-linear stiffness) at 1500 Hz	65

Figure 4.21 Applied Force – Gapping prediction (using non-linear stiffness) at 1500 Hz 66
 Figure 4.22 Input acceleration – Gapping prediction (using non-linear stiffness) at 2000 Hz
 67
 Figure 4.23 Applied Force – Gapping prediction (using non-linear stiffness) at 2000 Hz 67
 Figure 4.24 Inner and outer ring covered distances for 5-ball complement 70
 Figure 4.25 Inner and outer ring covered distances for 9-ball complement 71
 Figure 4.26 Inner and outer ring covered distances for 14-ball complement 71
 Figure 4.27 Closing velocities for 5-ball complement..... 72
 Figure 4.28 Closing velocities for 14-ball complement..... 72
 Figure 4.29 Closing velocities for 14-ball complement..... 73
 Figure 4.30 Collision Accelerations for 5-ball complement..... 74
 Figure 4.31 Collision Accelerations for 9-ball complement..... 74
 Figure 4.32 Collision Accelerations for 14-ball complement..... 75
 Figure 4.33 Equivalent Closing velocity – Equivalent Collision Acceleration for 9-ball
 complement..... 75
 Figure 4.34 Input acceleration – Impact force graph for 5, 9 and 14-ball complement.... 76
 Figure 4.35 Applied Force – Impact force graph for 5, 9 and 14-ball complement 76
 Figure 4.36 Equivalent Collision Acceleration – Impact force for 9-ball complement..... 77
 Figure 4.37 Equivalent Closing Velocity – Impact force for 9-ball complement..... 77
 Figure 4.38 Input Acceleration – Maximum Hertzian Stress 78
 Figure 4.39 Applied Force – Maximum Hertzian Stress 78
 Figure 4.40 Impact Force- Maximum Hertzian Stress for 9-ball Complement 79
 Figure 4.41 Equivalent Closing Velocity – Maximum Hertzian Stress for 9-ball complement
 79
 Figure 5.1 Gapping comparison for 5-ball complement at 20g 81
 Figure 5.2 Gapping comparison for 5-ball complement at 25g 82
 Figure 5.3 Gapping comparison for 9-ball complement at 25g 82
 Figure 5.4 Gapping comparison for 9-ball complement at 30g 83
 Figure 5.5 Gapping comparison for 14-ball complement at 20g 83
 Figure 5.6 Gapping comparison for 14-ball complement at 30g 84
 Figure 5.7 Input Acceleration – Gapping Prediction Graph for 5-ball complement at 500 Hz
 85
 Figure 5.8 Input Acceleration – Gapping Prediction Graph for 14-ball complement at 500
 Hz 86
 Figure 5.9 Gapping comparison for 9-ball complement at 500 Hz 87
 Figure 5.10 Gapping comparison for 9-ball complement at 500 Hz (mean measured gap
 values) 88
 Figure 5.11 Absolute error between predicted values and test results of measurement 1 89
 Figure 5.12 Absolute error between predicted values and test results of measurement 2 89
 Figure 5.13 Absolute error between predicted values and mean value of the two
 measurements..... 90
 Figure 5.14 %Error between predicted values and test results of measurement 1 91
 Figure 5.15 %Error between predicted values and test results of measurement 2..... 91
 Figure 5.16 %Error between predicted values and mean value of the two measurements 92
 Figure 5.17 Input Acceleration – Gapping prediction graph for 5-ball complement at 1500
 Hz 93

Figure 5.18 Input Acceleration – Gapping prediction graph for 9-ball complement at 1500 Hz	93
Figure 5.19 Input Acceleration – Gapping prediction graph for 14-ball complement at 1500 Hz	94
Figure 5.20 Input Acceleration – Gapping prediction graph for 5-ball complement at 2000 Hz	94
Figure 5.21 Input Acceleration – Gapping prediction graph for 9-ball complement at 2000 Hz	95
Figure 5.22 Input Acceleration – Gapping prediction graph for 14-ball complement at 2000 Hz	95
Figure 5.23 Calculated and CABARET maximum Hertzian stress for 9-ball complement at 500 Hz	97

Acknowledgments

I would like to thank Professor I. Sherrington, Director of Studies for his support, not only on academic, but also on personal fields. I would also like to thank to Professor E. W. Roberts, second supervisor, and S. D. Lewis third supervisor for their guidance. Finally I would like to thank my parents and my sister for their support through the years.

NOMECLATURE

a	Accelerration
m	Mass
k	CABARET stiffness
ψ	Non- linear stiffness
K	Coefficient of stiffness
f	Frequency
x	Ring displacement
u	Velocity
ω	Angular velocity
A	Amplitude
R_1, R_2	Radii
R	Equivalent radius
χ	Acceleration due to vibration
Q	Rolling element load
Z	Number of balls
α	Contact angle
δ	Deflection
δ_n	Nominal approach
D	Ball diameter
E	Young's modulus
E^*	Equivalent Young's modulus
ν	Poisson's ratio
P_0	Maximum Hertzian stress
S	Distance
h	Gapping

Chapter 1

1 Introduction

This Chapter is the introduction to the thesis. Provides the aims of the current project along with a brief explanation of the chapters of the thesis.

1.1 The need for research

Mechanical components used in space applications are subjected to conditions such as extreme velocities, vibrations and the environmental conditions of the space vacuum.

Especially during launch the vibrational forces can reach extreme values, that can cause immediate failure or reduced component life. The design methods that work successfully in earth applications, cannot guarantee the same success in space applications.

(Sarafin, 1995) (Fusaro,1991).

Moreover space missions last for long periods of time and costs considerable amounts of money. A failed space mission results in significant financial loss, embarrassment and possible delay the future space missions. Therefore it is necessary to ensure that all the possible actions are made to reduce the risk of failure.

From the engineering point of view, must be ensured that all the systems will work properly as long as the mission lasts. There is no margin for error, since a failure during the mission is in progress is usually impossible to be remedied.

There are many anomalies presented in the past due to tribological problems. Well known is the failure of Galileo's high-gain antenna deployment due to loss of the MoS₂ lubricant film at the antenna rib and the supporting bracket (Miyoshi,1999)(Takano,1999). This was caused by extra ground transportation, since the original launch date was cancelled because of the Challenger tragedy. Another tribological failure, presented at the Japanese Geostationary Meteorological Satellite 3 (of the series GMS-1 to GMS-5), was the presence of wear debris of MoS₂ solid lubricant in the ball bearings, supporting the mirror rotational axis (Takano,1999).

Experiences like those presented above as well as failures of mechanisms during testing before their launch (GOES-NEXT, CERES, SPACE STATION BETA JOINT CYMBALS) (Miyoshi,1999)(Shapiro et al, 1995) show the need for research and testing of components and mechanisms in space applications (Haltner et al, 1994).

1.2 Aims of the current project

This project is a continuation of a series of studies performed for the ESTL. On a previous study a 2-degrees of freedom model created in order to evaluate the occurrence of gapping on an angular contact ball bearing in space applications. This model had to use the bearing stiffness. The bearing stiffness was calculated by sophisticated computer software called CABARET. The model worked successfully, but it was believed that the introduction of the non-linear bearing stiffness instead of that calculated by CABARET produces even more accurate gapping predictions. Therefore, the first aim of this project was the introduction of the non-linear stiffness into the existing model.

The analysis of the ball movement within the inner and outer rings of the ball bearing is another subject of importance from the tribological point of view, because the impact forces developed, can generate high contact stresses, a resulting from indentation of the balls and the rings, which can result in malfunction of the bearing. In order to calculate the Hertzian contact stresses using existing methods, the evaluation of the load, which in this case is the impact force between the ball and the ring is necessary. Therefore the second aim of this project was to apply a method that will evaluate the impact force, with the aid of which the Hertzian stresses can be calculated, relating the method with the results obtained for gapping

In summary the aims of the current project are:

- The introduction of non-linear stiffness into the existing 2-DOF model in order to predict gapping
- A method that evaluates the Impact Force generated between the ball and the rings in an angular contact bearing, in order to calculate the Hertzian contact stress.

1.3 Chapters of the project

This section provides a brief explanation of the chapters of the thesis

- The present chapter is an introduction to the problem
- The second chapter is the literature survey. It provides information on the bearing types, bearing performance characteristics and bearing test methods that find application on space missions, using the existing literature
- The third chapter provides the theoretical background of the methods used. Also the previous ESTL studies used in this project are presented.
- The fourth chapter presents the results obtained using the methods described in chapter 3
- The fifth chapter provides a discussion on the results along with comparisons with experimental results obtained on the previous ESTL studies.
- The sixth and last chapter contains the conclusions and recommendations for further work.

Chapter 2

2 Literature Survey

This chapter presents the literature survey. The information related to the bearing types that find use in space applications, their performance characteristics, their test methods, as well as the information about lubrication in space is given in this chapter, based on the existing literature.

2.1 Types of bearings

The common types of bearings used in space applications are:

- 1) Ball bearings (including wire race and thrust types)
 - Radial or Deep Groove or Conrad Bearings
 - Angular contact bearings
 - Four-Point-Contact ball bearings
 - Wire race bearings
 - Thrust ball bearings

- 2) Roller bearings

- 3) Plain, Spherical and rod end bearings

- 4) Magnetic bearings

- 5) Linear bearings

2.1.1 Ball Bearings

Ball bearing as the name states refer to those bearings that consist of an inner raceway and an outer raceway separated by a complement of balls. There are several different types of ball bearings with respect to the application intended for (i.e. the type of load they intend to support). The different types of ball bearings will be discussed in more detail in the following sections.

Advantages:

Due to the advantages that ball bearings have in respect of those suitable for use in space they are the most commonly used bearings in space applications. These advantages include :

- High load carrying capacity
- Relative ease of lubrication
- High stiffness when preloaded
- Low friction
- Wide availability of sizes

Typical applications:

Ball bearings are used typically in spacecraft systems such as high speed control momentum gyroscopes (liquid lubricated bearings) (sanders et al, 2000), space drive mechanisms like solar array drive assemblies or antenna drive mechanisms (solid lubricated bearings) (Nishimura et al, 1995)

2.1.2 Radial or deep groove or Conrad bearings

2.1.2.1 Description

Deep-groove ball bearings are currently the most commonly used bearings but they find less use than angular contact bearings in space applications (Sarafin et al, 1995). Radial bearings, as their name makes clear, are designed to carry radial loads. Even though they perform well under combined radial and relatively small thrust load alone (Palmgren, 1946). They offer a high load-carrying capacity due to the high osculation (i.e. percentage conformity) and relatively large ball diameter. For even greater radial load capacity double rows of balls can be used.

2.1.1.1 Applications

According to “space tribology handbook” (ESTL, 1997) the radial bearings are used for:

- Applications which call for little or no axial load capacity
- Applications in which a high radial stiffness is required
- Wave-generator bearings on harmonic drives (bearing has a reduced section)

2.1.3 Angular contact bearings

2.1.3.1 Description

Angular contact ball bearings are similar to the radial bearings, but with a contact angle that allows the bearing to accommodate combined loads in both the axial and radial directions. The contact angle is designed according to the ratio of the radial to the thrust load needed to be accommodated. A small ratio denotes high axial load, therefore, a large contact angle is needed. On the contrary for large radial to axial load ratio a small contact angle is needed.

The thrust contact angle generally does not exceed 40° (Palmgren, 1946) . The bearings generally have groove curvature radii in the range of 52 to 53 % of the ball diameter (Harris, 1966).

Angular contact bearings usually mounted in duplex pairs, in back- to- back and face- to- face arrangements in order to accommodate axial loads in both directions, and increase bearing stiffness due to preload.



Figure 2.1 Angular contact bearing

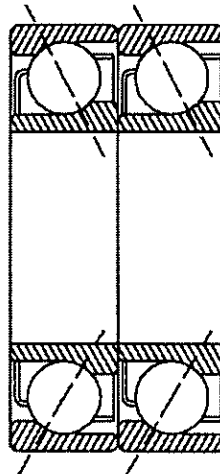


Figure 2.2 Tandem-mounted pair of angular contact bearings

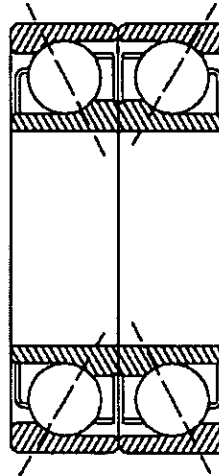


Figure 2.3 Face-to-face mounted pair of angular contact bearings

2.1.3.2 Applications

According to “space tribology handbook” (ESTL, 1997), angular contact bearings used for high stiffness high precision applications (e.g. where accurate positioning with high stiffness is required).

2.1.4 Four-Point-Contact ball bearings

2.1.4.1 Description

Four-point contact ball bearings are single row angular contact ball bearings having raceways that are so designed that the bearings can support axial loads acting in both directions (SKF). A four-point-contact ball bearing is called so, because there are four contact points between a ball and races. This is achieved due to the design of the races, where each one has 2 radii, whose centres are offset from the plane of the ball centres. (ESTL, 1997).

2.1.4.2 Applications

According to “space tribology handbook” (ESTL, 1997) four-point-contact ball bearings are used for:

- Applications which call for high radial, axial and moment stiffness
- High stiffness coupled with low weight and size (for thin section bearings)
- Large diameter, hollow shafted mechanisms that need to accommodate mechanical and electrical devices within the shaft (bearings in thin-section form)

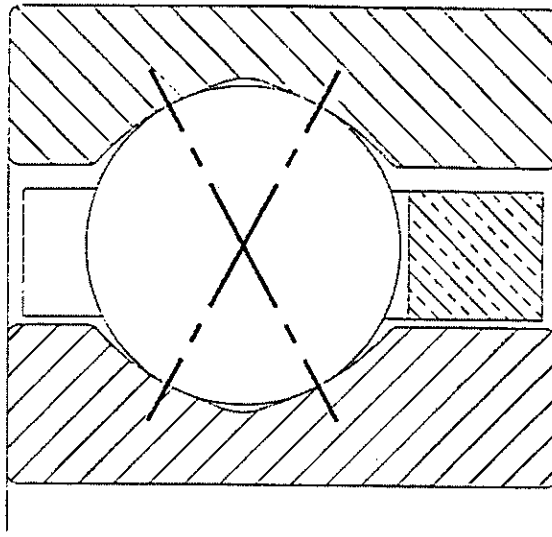


Figure 2.4 Cross section of a four point contact bearing

2.1.5 Wire race bearings

In a wire race bearing four hardened spring or stainless steel wires are replace the conventional raceways of a four-point contact. The wires are supplied machined to be conformal with respect to the ball and are located in the corners of the bearing housing

(ESTL, 1997). The application area of the wire race bearings is limited to low precision assemblies.

2.1.6 Thrust ball bearings

All the ball bearings with contact angles greater than 45° are classified as thrust bearings. When the contact angle is 90° no radial load can be supported. Their use in space applications is limited, where axial loads are applied and there is no concern as to the radial stiffness (ESTL, 1997)..

2.2 Roller bearings

Roller bearings are used for applications requiring exceptionally large load-supporting capability. As their name states they have rollers instead of balls. Roller bearings are stiffer than ball bearings and provide greater fatigue endurance, but they require greater care in mounting and accuracy of alignment (Harris, 1966). **Cylindrical roller bearings** have high radial-load-capacity and used in such applications. **Needle roller bearings** are cylindrical roller bearings with large roller length to diameter ratio. They are used in applications in which radial space is at a premium. **Tapered roller bearings** can support combinations of large radial and axial loads or axial loads alone. They are alternatives to angular contact ball bearings for high loads.

2.3 Plain, Spherical and rod end bearings

Spherical bearings are internally self-aligning and they have high load carrying capacity. They are designed to carry radial loads, but they can also accommodate small axial loads. Rod end bearings can carry strictly radial loads (ESTL, 1997).

2.4 Magnetic bearings

Magnetic bearings have been developed in recent years and although they are not used excessively they are considered as the bearing of the future in space applications. There are no balls or rollers on them, but they use instead opposing magnetic fields.(NASA)

2.5 Linear bearings

There are three types of linear bearings: **linear slider bearing**, in which there are no rolling elements, **linear ball bearing**, single row or multi-row, and **linear roller bearing**, in which the rolling elements are rollers. Their use in space applications is rare. (ESTL, 1997)

2.6 Lubrication

An important aspect for the proper operation of the bearings is the lubrication. Failure to lubricate can lead to failure of bearings. “Lubricants for use in space must meet one or more requirements: (1) low coefficient of friction, (2) constant coefficient of friction, (3) mitigation of wear, especially if the mission is one of long duration” (Haltner et al, 1983).

There are two types of lubricants:

1. Liquid and grease lubricants
2. Solid lubricants

2.7 Liquid and Grease Lubricants

2.7.1 Types of liquid lubricants

There are two types of liquid lubricants:

- a) Mineral oils
- b) Synthetic oils

2.7.1.1 Mineral oils

Mineral oils have a wide range of terrestrial applications, but their use in space is limited to sealed lubricant systems due to their high vapour pressure.

2.7.1.2 Synthetic oils

Synthesized hydrocarbon fluids or polyalphaolephines (PAO): They are chemically similar to mineral oils, but have lower vapour pressures. Can be blended with conventional additives to provide wear, oxidation and corrosion protection.

Perfluorinated oils (perfluoroalkylpolyethers – PFPEs): they comprise long-chain linear polymers build up from carbon, oxygen and fluorine atoms. Their use in space applications is extensive due to their very low vapour pressures.

Multiply alkylated cyclopentanes (MAC): They prepared from dicyclopentadiene by reaction with aliphatic alcohols. Their use in space has little heritage.

Synthetic esters: a group of compounds of which polyol or neopentyl esters have generated the most interest. They have little heritage in space.

Silicones: They had extensive use in early space mechanisms, because of their low vapour pressure, low pour point and high viscosity index. There are no longer serious candidates for space lubrication because of poor creep properties and tendency to degrade in contact zones.

(Fusaro, 1994)

2.7.2 Greases

Greases are in the same category as the liquid lubricants, because the lubrication is achieved by the liquid that forms the grease. The difference is that the liquid is mixed with a thickener in order to give a semi-solid product. Greases are used for a variety of space applications: low-to high-speed, angular contact ball bearings; journal bearings; and gears (Fusaro, 1994).

2.8 Solid Lubricants

2.8.1 Applications

The typical applications of solid lubricants in space include the lubrication of the following mechanical components: rolling element bearings, journal bearings, gears, bushings, electrical sliding contacts, clamps and latches, bolts, seals, rotating nuts, robotic and telescopic joints, backup bearings, fluid transfer joints, various release mechanisms, valves, and harmonic drives (Fusaro, 1994).

Types of solid lubricants

The types of solid lubricants used in space applications are:

Soft metal films: gold, silver, lead, indium, and barium.

Lamellar solids: molybdenum disulfide, tungsten disulfide, cadmium iodide, lead iodide, molybdenum diselenide, intercalated graphite, fluorinated graphite, and phthalocyanines.

Polymers: PTFE, polyimides, fluorinated ethylene-propylene, ultra-high-molecular weight polyethylene, polyether ether ketone, polyacetal, and phenolic and epoxy resins.

Other low-shear-strength materials: fluorides of calcium, lithium, barium, and rare earths; sulfides of bismuth and cadmium, and oxides of lead, cadmium, cobalt, and zinc.

(Fusaro, 1994)

2.9 Performance Characteristics

For the bearings used in space applications the most important performance characteristics are the mean torque (Coulombic torque), the stiffness, and the contact stress (Lewis). A number of factors such as the geometrical characteristics, the choice of the preloading system, and the thermal environment, influence the operational performance of bearings. The methods used to predict bearing performance and fatigue life of the component are both theoretical and experimental. The theoretical methods which can predict the bearing behaviour are good design tool, in an early stage, but since there are phenomena that cannot be taken into account in modelling, realistic testing is appropriate in order to verify the predicted values. Since the ball bearings are the dominant type of bearings used in space applications they are considered here in order to present the main theoretical as well as test methods for predicting bearing performance characteristics.

2.10 Theoretical methods

There are two numerical methods used for calculation of coulombic torque. These are the Non- interactive model (NIM) and the Simplified interactive model (SIM). Both methods are required in order to cover the wide range of bearing types. Usually one of the models is significantly closer to experiment than the other, depending on the bearing type (Todd, 1990).

2.11 Components of coulombic torque

The components of coulombic torque are:

- Heathcote or conformity microslip due to the differential velocities of the raceway across the contact ellipse
- Spinning of the ball about a normal to the Hertzian contact area (microslip can arise from partial spin)
- Sub-surface hysteretic losses due to stress cycling of material flowing beneath the contact (Todd, 1990).

2.11.1 Assumptions

Non- interactive model (NIM)

- Saturation spin occurs at only one contact (that with the lesser spin moment)
- At the other contact there is only pure rolling and no spin (i.e. conformity microslip with allowance for stick and slip regions).

Simplified interactive model (SIM)

- Microslip from spin and conformity (Heathcote) occur together at both contacts.
- Except at the bands of no slip, there is complete slip over the whole contact area (i.e. regions of stick due to elastic compliance are neglected)
- Microslip due to spin, in a direction perpendicular to the rolling direction is negligible compared to that in the roll direction.

(Todd, 1990).

2.12 Methodology

The basic methodology is the following (Todd, 1990).

- All the forces and moments acting on the balls are in equilibrium. The calculation of forces is based on a numerical method , which varies the ring deflections until convergence occurs. Convergence is defined, when internal and external forces (and moments) are equal.
- Bearing mean torque predictions are made by the summation of the forces and moments generated by frictional effects within each ball- raceway contact ellipse. All three frictional energy dissipation mechanisms, conformity microslip, ball spin and sub-surface hysteresis, are taken into account. The resulting frictional effects can be balanced and an equilibrium achieved.

The resulting torque prediction is called **Coulombic torque**. The Coulombic torque is applicable to solid lubricated bearings, and to liquid lubricated bearings with low operational speeds, it cannot be used for liquid lubricated bearings operating on mixed or hydrodynamic regimes.

2.12.1 Limitations

In the theoretical predictions there are some limitations (Todd, 1990).:

- The torque prediction relies on an assumed sliding friction coefficient, which has some non-quantifiable natural variability.
- Some non-quantifiable uncertainty to the predicted torque can be added by a non-uniform ball loading due to form errors, misalignment or ring flexure.
- The presence of the cage will inevitably produce a torque increase within the bearing.
- Ball-race contact stresses generated due to preload, have to taken into account since torque is a function of contact stresses.

2.13 Geometrical parameters

The geometrical parameters that are taken into account in a ball bearing design are

1. Ball size (PCD)
2. Ball complement
3. Ball diameter
4. Conformity number
5. Free contact angle.

2.13.1 Ball size

The variation of the PCD has negligible effect on torque, stiffness and contact stress, when dealing with purely axial loads. This assumption is correct with the exception that a larger PCD implies larger inner and outer race diameters, having as result the corresponding changes in maximum ball-race contact stresses (increasing outer race contact stress, decreasing inner race contact stress due to the changing effective radius of curvature) (ESTL, 1996)

2.13.2 Variation of Ball Complement

An increase in the ball complement produces a corresponding decrease in ball race normal contact force for each ball, and hence a reduction in peak contact stress. The bearing axial stiffness is directly proportional to the ball complement and the operating contact angle is inversely proportional. The bearing torque also is proportional to the ball complement. (ESTL, 1996)

2.13.3 Variation of ball diameter

The bearing torque the axial stiffness and the contact stresses are proportional to the ball diameter. (ESTL, 1996)

2.13.4 Variation in Conformity Number

The conformity number (i.e the ratio of the radius of the track to the radius of the ball, which always exceeds 1 and usually ranges from 1.03 to 1.15) is inversely proportional to the the bearing torque and the axial stiffness whilst is proportional to the peak contact stress (since increased conformity reduces the size of Hertzian contact). (ESTL, 1996)

2.13.5 Variation in Free Contact angle

The bearing contact angle is proportional to the axial stiffness. By increasing bearing contact results to reduced normal loads on the balls, so reduced Hertzian contact stresses. The net effect is that increased contact angle reduces mean bearing torque. (ESTL, 1996) Graphs for the effect of the variation of contact angle, as well as of variation of ball diameter, and of ball complement, presented in chapter 3.

2.14 Test methods

Although the theoretical predictions are a useful design tool at an early stage it is necessary that the results should be verified by realistic testing of the component. In the particular case of ball bearings, it is possible to perform complex oscillation profiles. This can be done by a tribometer test, which generates the oscillation profile and also simulates the space environment (i.e. pin-on-disk placed on a vacuum chamber), but it is unlikely that a full representation of the component in operation could be achieved by a simple tribometer. (ESTL, 1996)

A mechanism test on the mechanism which the bearing forms a part of is possible, but in many cases this approach is not very practical, as the mechanism may mask or even alter the performance of the individual components (ESTL, 1996) For this reason testing on component level has to be performed.

2.14.1 Test Environment

There are two basic parameters on space simulation tests. These are temperature and vacuum pressure (ESTL, 1996). At geostationary orbital height the vacuum level is in the order of 10^{-13} torr. However as a result of the out-gassing of materials that emit gases such as water vapour and carbon monoxide, a geostationary spacecraft will experience higher pressures of the level of 10^{-10} torr close to the spacecraft exterior surfaces and between 10^{-6} to 10^{-8} within partially sealed mechanisms located inside the spacecraft. (Roberts, 1990)

2.14.2 Test chamber

The tests performed inside a test chamber where the environmental parameters can be simulated. The desired test environment defines the test chamber will be used. For inert gas environment, the test environment may be as simple as a perspex box purged with dry gas. For a vacuum environment, a more complex chamber is required, usually a steel chamber with an associated pumping system. (ESTL, 1996).

2.15 Factors that influence the frictional forces and coefficients

The frictional forces of bearings in space application are dependent on the lubricants used. Therefore the factors that influence the lubricants affect the frictional forces on the bearings. It is important to know that two materials in contact do not have a unique coefficient of friction. Friction has not a specific value for a given material, its value depends on factors such as the roughness of mating surfaces. These factors can be taken into account only if we understand the lubrication mechanisms

2.16 Lubrication Mechanisms

2.16.1 Liquid lubrication

In liquid lubrication there are four defined regimes: hydrodynamic, elastohydrodynamic, boundary and mixed. Figure 2.5, known as the Stribeck- Hersey curve, shows the coefficient of friction in respect of viscosity, velocity and load. The friction coefficient is proportional to the oil viscosity Z the relative velocity V and inversely proportional to the load L .

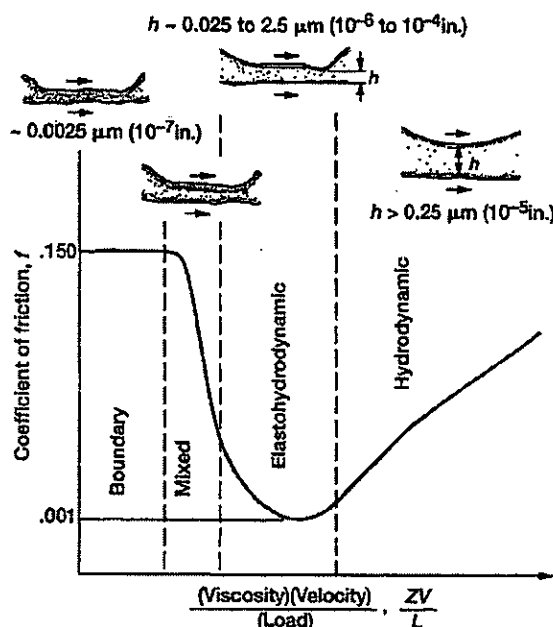


Figure 2.5 Coefficient of friction as function of viscosity-velocity-load parameter (Stribeck Hersey curve) (Fusaro, 1994)

2.16.1.1 Hydrodynamic lubrication

The first regime is known as hydrodynamic lubrication. In hydrodynamic lubrication the surfaces are completely separated by the fluid film which fully supports the load. Hydrodynamic lubrication depends upon three factors: the viscosity of the lubricant, the convergence of the surfaces and the speed of the lubricated surfaces (ESTL, 1997).

2.16.2 Elasto- hydrodynamic lubrication (EHL)

The phenomenon of elastic deformation of the mating surfaces can occur when a load of significant size imposed on a contact. This regime has a great interest because rolling element bearings are non conforming machine elements.

The nominal point contact (as occurs between two crossed cylinders) or line contact changes into a footprint. In order to consider that EHD prevails the area of the footprint must be significant in comparison with the hydrodynamic film thickness (Arnell et al,

1991). This produces a “flat” on balls, with the load carried by a pressure spread over this flattened area. Then the two surfaces, when they are in motion, drag lubricant into the convergent inlet zone which passes through the flattened zone, to emerge in the diverged zone where cavitation takes place (Arnell et al, 1991). The presence of the film does not significantly affect, in many cases, the size or the shape of the flattened area and the Hertzian pressure distribution cannot essentially change. The lubricant is subjected to an increasing pressure, as it passes through the gap. Under the high pressures generated the lubricant properties are different from those of the bulk liquid (Bhushan et al, 1991). An enormous increase in viscosity may occur in most fluids (water is a notable exception). As result of this increase of viscosity the lubricant behaves more as an amorphous solid than a liquid. The result of both these phenomena is drastically to increase the load-carrying abilities of the lubricated contact relative to that for rigid body, isoviscous theory (Arnell et al, 1991).

2.16.3 Boundary lubrication

In boundary lubrication asperity contact between the sliding surfaces takes place, and the lubrication process becomes the shear of chemical compounds on the surface. This regime is dependent on lubricant additives within the oil that produce compounds on the surface which have the ability to shear and provide lubrication. Boundary lubrication is highly complex, involving surface topography, physical and chemical adsorption, corrosion, catalysis, and reaction kinetics (Fusaro, 1994).

One way of presenting boundary lubricants to surfaces is via grease. Greases are liquid lubricants mixed with a thickening agent. The thickener improves the rheological properties and may provide boundary lubrication properties of its own (ESTL, 1997)

2.16.4 Mixed lubrication

This regime is the transition state between the fluid film lubrication and the boundary lubrication. It is called mixed, because it consists of some elastohydrodynamic and some boundary lubrication. (ESTL, 1997)

2.17 Solid lubrication

Solid lubrication is essentially the same as liquid boundary lubrication. The difference is that there is no liquid carrier to resupply a solid material to the surfaces to produce a lubricating solid film (Fusaro, 1994). There are two ways of achieving solid lubrication. The first is a part of the bearing can be made by a solid lubricant, as for example the with self lubricating cages in ball bearings. The second method is that a solid film can be applied to one counterface, as with techniques such as sputter deposition (Roberts, 1990)

The first method produces a discontinuous, uneven in its thickness and poorly adherent film. It provides a lubrication that is characterized by appreciable variations in friction coefficient (thus for example ball bearings so lubricated exhibit a noisy torque).

The second method, in contrast, produces a thin, continuous lubricant film of nominally uniform thickness which, if correctly applied, is well adhered to the substrate. The reasons that such films are used in spacecraft mechanisms are:

- a) Low shear strength materials confer their lowest friction when present as films of thickness in the order 1 μm . Such low-friction films (and those of low frictional noise) are necessitated in applications which call for low power dissipation and low torque noise, such as the cryogenic devices and precision pointing mechanisms respectively.
- b) Because of their thinness they can be applied to the most finely machined tribo-components without detracting from the components precision (Roberts, 1990)

According to Roberts (1990) friction arising between solid lubricating bodies is described by the equation

$$\text{Friction coefficient} = sA / W$$

Where s is the shear strength of the lubricant film

A is the true contact area

W is the normal contact load

Small contact areas can be achieved by ensuring that the solid lubricant is applied in the form of thin (in the order of $1 \mu\text{m}$) films onto substrates of high elastic modulus and hardness. Under these conditions the contact load will largely be supported by the hard contact materials and the true contact area will, in consequence, be small. For a smooth sphere sliding under elastically loaded (Hertzian) conditions against a smooth, flat substrate coated with a thin film: (Roberts, 1990)

$$\text{Friction coefficient} = [s / W^{1/3}] [3R / E^*]^{2/3}$$

Where R is the radius of the sphere

E^* is the effective elastic modulus of the contact materials

The effective elastic modulus is given by:

$$\frac{1}{E^*} = \frac{1 - \nu_1^2}{E_1} + \frac{1 - \nu_2^2}{E_2}$$

where E_1, E_2 are the modulus of elasticity of the two bodies

ν_1, ν_2 are the Poisson's ratios

For a given contact geometry equation shows that:

- a) Friction varies linearly with film shear strength
- b) Friction decreases with increasing contact load
- c) Friction is determined by the substrate material to which the film is applied such that the higher the elastic modulus of the substrate materials the lower the friction

- d) The methodology is applicable to semi-infinite solids or coated surfaces with thick layers. (Roberts, 1990).

Chapter 3

3 Theoretical background and previous studies

This chapter provides the theoretical background to the project. The theories used are stated here along with explanation of the formulae and their derivation.

In this chapter, there are also the references to the previous ESTL studies, the results of which are used in the current thesis.

3.1 Gapping

Gapping in ball bearing is called the phenomenon of the creation of a “gap” between the ball and the raceway, due to bearing vibration. More specifically, in space applications, the bearings are preloaded in order to achieve the desired mechanism stiffness. There are two types of preloading system, soft and hard preloading.

Hard preloading: This type of preload is used, when very high stiffness during satellite launch is desired. It is achieved by the use of matched bearings. In this type of preloading the off-loading which results in gapping occurs, when the axial load exceeds the preload by a factor of 2.83, when dealing with angular contact ball bearings.

Soft preloading : In this type of preloading a spring or diaphragm is used in a way that the preloading is achieved by the spring compression. The off-loading in this case occurs when the spring is in the load path. The off-loading occurs in the second bearing of the pair, when the spring preload is overcome.

3.2 Mass-spring model

A mass-spring model with two degrees of freedom was constructed by Sven Sochting and Simon Lewis of ESTL, in order to determine the relationship between bearings gapping and acceleration level. This model helps to define the correct acceleration levels for the vibration test. Figure 3.4 shows the 2-degree-of-freedom mass-spring model of bearing test housing with harmonic force input.

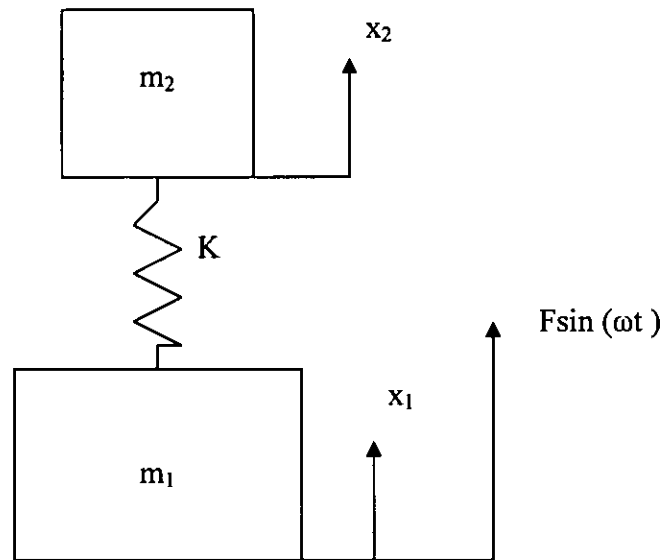


Figure 3.1 Mass- spring model

In this model, the housing assembly is assumed to be an un-damped structure subjected to a harmonic force input. m_1 is the mass of the shaft including the outer races, clamp rings and fasteners. m_2 is the mass of the outer housing assembly, including the outer races, the balls and clamp rings and all the fasteners. The shaft assembly mass total (m_1) is 1.9 Kg, and the outer housing assembly mass (m_2) is 0.783 Kg.

An appropriate software called CABARET analysis used in order to derive the values of bearing stiffness. Experimental data used to verify the CABARET analysis values. Experimental verification was performed by identifying the natural frequency f_n , with a sine sweep test on the assembled bearing housing.

Then by using the equation (Lewis et al, 2002)

$$k = (2\pi f_n)^2 m_2 \quad [3.1]$$

the bearing stiffness k can be calculated. This method gives a constant stiffness value dependent on the natural frequency and the mass of the outer ring.

Table 1 shows the stiffness obtained by CABARET and experimental values for 5, 9 and 14-ball complements,

Ball Complement	CABARET Stiffness (N/m)	Experimental Stiffness (N/m)
5-ball	$9.85 \cdot 10^6$	N/A
9-ball	$1.64 \cdot 10^7$	$1.73 \cdot 10^7$
14-ball	$2.6 \cdot 10^7$	$2.4 \cdot 10^7$

Table 3-1 Stiffness predictions

The input force according to Newton's second law of motion is given by

$$F = (m_1 + m_2) \alpha \quad [3.2]$$

Where α is the input acceleration

For two-degrees of freedom system the equations of motion can be written:

$$m_1 \chi_1 + k (x_1 - x_2) = F \sin(\omega t) \quad [3.3]$$

$$m_2 \chi_2 - k (x_1 - x_2) = 0 \quad [3.4]$$

The solution of normal mode vibrations is described by the equation

$$x = A \sin (\omega t) \quad [3.5]$$

Where A is the amplitude

Since in normal mode the whole system vibrates at one of the natural frequencies the twice-differentiated equations of the responses have the form:

$$\chi_1 = -\omega^2 A_1 \sin (\omega t) = -\omega^2 x_1 \quad [3.6]$$

$$\chi_2 = -\omega^2 A_2 \sin (\omega t) = -\omega^2 x_2 \quad [3.7]$$

where χ_1 and χ_2 are the accelerations associated with x_1 and x_2

By substituting the expression of displacement and accelerations into the equations of motion:

$$-\omega^2 m_1 A_1 + k (A_1 - A_2) = A_1 (k - \omega^2 m_1) - k A_2 = F \quad [3.8]$$

$$-\omega^2 m_2 A_2 - k (A_1 - A_2) = A_2 (k - \omega^2 m_2) - k A_1 = 0 \quad [3.9]$$

Solving for A_1, A_2

$$A_1 = F(k - \omega^2 m_2) / (k - \omega^2 m_1) (k - \omega^2 m_2) - k^2 \quad [3.10]$$

$$A_2 = Fk / (k - \omega^2 m_1) (k - \omega^2 m_2) - k^2 \quad [3.11]$$

The relative displacement is given by ΔA

$$d = \Delta A = A_2 - A_1 \quad [3.12]$$

Therefore:

$$d = - F\omega^2 m_2 / (k - \omega^2 m_1) (k - \omega^2 m_2) - k^2 \quad [3.13]$$

From the last equation it can be seen that the model is not applied when the denominator is zero (relative displacement of the rings tends to infinity, something impossible).

The denominator is

$$(k - \omega^2 m_1) (k - \omega^2 m_2) - k^2$$

And:

$$\omega^2 (\omega^2 m_1 m_2 - k m_1 - k m_2)$$

The sign of the denominator depends on

$$\omega^2 m_1 m_2 - k(m_1 + m_2)$$

The ratio $m_1 m_2 / (m_1 + m_2)$ is 1.8

Therefore, when: $1.8\omega^2 = k \quad [3.14]$

the denominator is zero. This means that gapping tends to infinity. This will result to a bearing failure. This graph behaviour is not probably due to physical phenomena, since that behaviour occurs at values well above the natural frequency, and therefore the tuning cannot be considered responsible. Probably is a disadvantage of the method that the equation [3.13] cannot cover the values where [3.14] applies.

3.3 Vibration test

In the previous program of studies vibration tests were performed by Sochting and Lewis for a SNFA SEA 65 angular contact bearing pair. The test performed for constant frequency of 500 Hz and input acceleration range from 1 to 100 g. Another test series was performed, considering constant input acceleration of 20, 25 and 30g and frequency range from 100 to 600 Hz. Therefore, all the gapping measurements used on the thesis are from the above tests. The table below summarizes the main characteristics of the bearing pair used.

SNFA SEA 65 7 CE 1 FFL	
Bore (mm)	65
Outer diameter (mm)	85
Bearing Width (mm)	10
Standard Ball Complement	29
Test Ball Complement	9
Contact Angle (degrees)	15
Preload (with full ball diameter, N)	71
Conformity No (inner and outer)	1.04
Ball Diameter (mm)	5.555
Bearing material	52100 steel

Table 3-2 SEA 65 Specification

3.4 Raceway damage

The impact forces due to the collisions between the ball and the races have as a result indentations on the bearing raceways. Indentation damage as accepted by ESTL (Lewis et al, 2002) occurs at stresses of 4.2 GPa (ISO 76 stress limit). Previous ESTL study contacted

by Lewis suggests that indentations are not visible on cleaned grease lubricated bearings (SEA 65) until a Hertzian stress of 5.5 – 6 GPa is reached (Sochting et al, 2004). Indentation measured in the previous study will be discussed in chapter 5.

3.5 Theoretical background to the current study

The objective of the current study is the introduction of non-linear stiffness into the existing mass-spring model. The term non-linear stiffness means that the bearing stiffness is changing with respect to the applied force. It is believed that the introduction of the non-linear stiffness term into the gapping prediction equation will result in more accurate prediction than with the CABARET stiffness term. This will be examined by the comparison of the two predictions with measured gapping values. The measured values are obtained by experiments performed by Sven Sochting in the previous programme of studies.

The second objective is the study of collision forces between the ball and the races of the bearing and the Hertzian stresses developed, in relation with the gapping prediction values obtained.

3.6 Evaluation of bearing stiffness

The evaluation of the non-linear bearing stiffness is based on the equations described by Palmgren in 1946 and since used in all the related literature.

The non-linear bearing stiffness ψ is given by

$$\psi = \frac{dF}{d\delta} \quad [3.15]$$

Where F is the applied load and δ is the bearing deflection

since the force can be expressed as

$$F = K\delta^{3/2} \quad [3.16] \text{ (Parssinen, 1998)}$$

Where K is the stiffness coefficient

Then, by substituting [3.16] into [3.17] and differentiating:

$$\psi = \frac{3}{2} K \sqrt{\delta} \quad [3.17]$$

3.6.1 Angular contact bearings

For angular contact bearings under thrust load (equally distributed)

$$Q = \frac{F_a}{Z \sin \alpha} \quad [3.18]$$

where Q is the rolling element load

F is the applied load

Z is the number of rolling elements per row

α is the contact angle

The axial deflection of the bearing under purely axial load is

$$\delta_a = 4.4 \times 10^{-7} \frac{Q^{2/3}}{D^{1/3} \sin \alpha} \quad [3.19]$$

where D is the ball diameter

From equations [3.18] and [3.19]:

$$\delta_a = \frac{4.4 \times 10^{-7} F_a^{2/3}}{Z^{2/3} D^{1/2} \sin^{5/3} \alpha} \quad [3.20]$$

Substituting [3.20] into [3.15] the bearing stiffness equation becomes

$$\psi = 2.27 \times 10^6 F_a^{1/3} Z^{2/3} D^{1/3} \sin^{5/3} \alpha \quad [3.21]$$

Therefore by applying equation [3.21] the bearing stiffness of a single angular contact bearing under central axial load can be calculated.

The proportionalities observed by the above equation are:

- a) ψ is proportional to the applied force
- b) ψ is proportional to the number of balls
- c) ψ is proportional to the ball diameter
- d) ψ is proportional to the sin of the contact angle

Those proportionalities are shown clearly in the following graphs. The study applies to the SAE 65 bearing of the SNFA catalogue, in respect of the masses, but for the observation of the stiffness characteristics, alternative ball complements, ball diameters and contact angles have been examined.

Graph 3.2 shows the effect of changing the applied load.

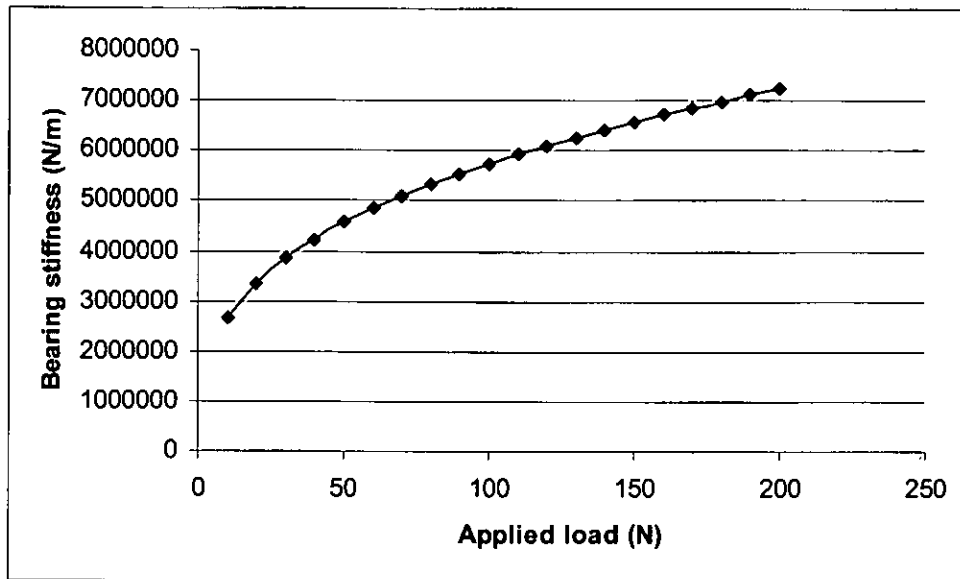


Figure 3.2 Applied load - Bearing stiffness graph

Figure 3.3 shows the effect of changing the ball complement.

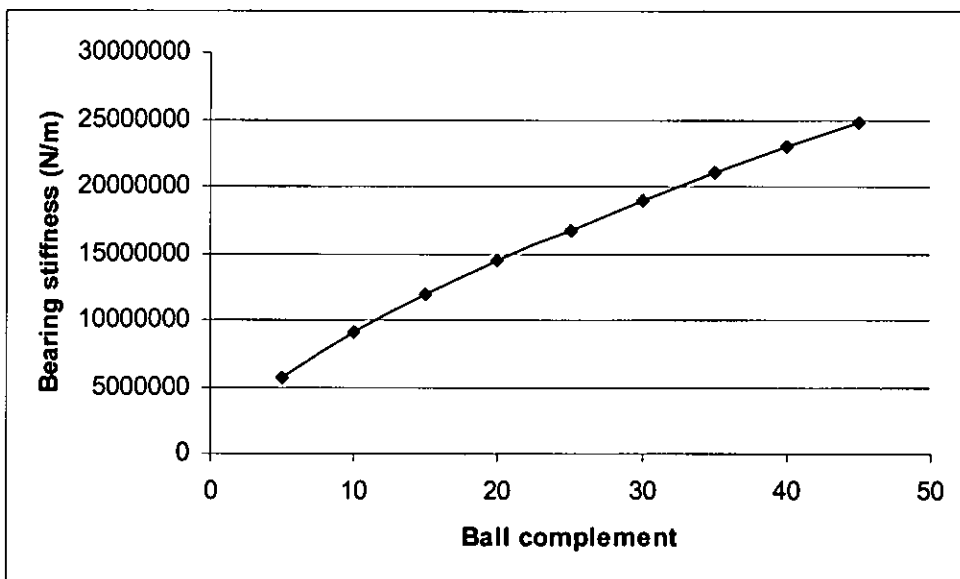


Figure 3.3 Ball complement - Bearing stiffness graph

Figure 3.4 shows the effect of changing the ball diameter.

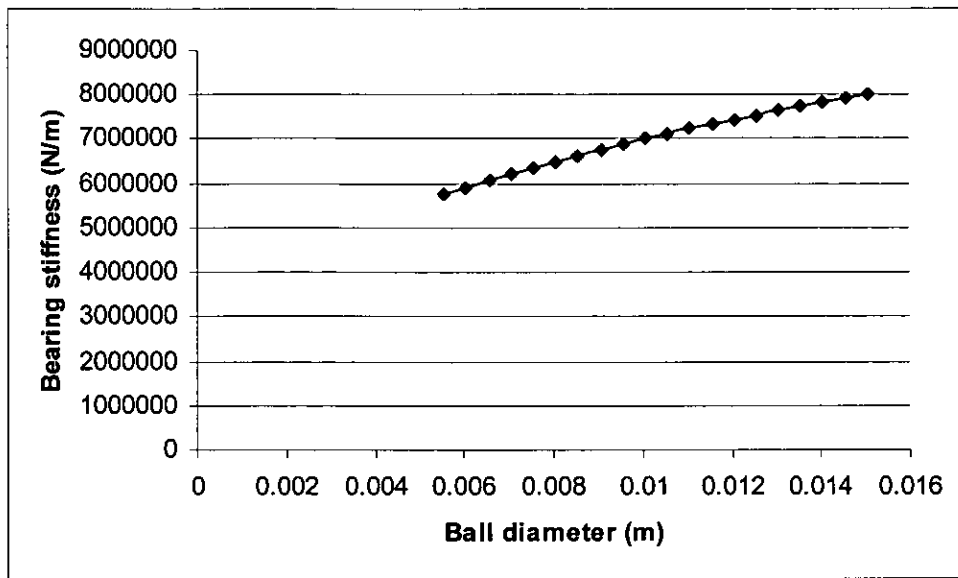


Figure 3.4 Ball diameter – Bearing stiffness graph

Figure 3.7 shows the effect of changing the contact angle.

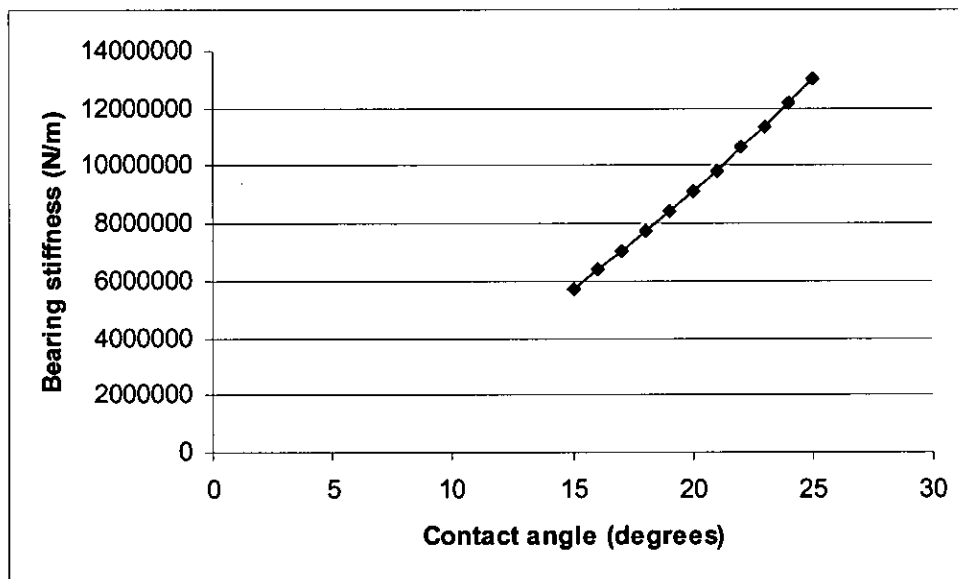


Figure 3.5 Contact angle – Bearing stiffness graph

Analysing the above graphs, it can be seen that the stiffness graph concaves down by increasing the applied force, the ball complement and the ball diameter (maintaining all the other parameters constant each time), while the graph concaves up by increasing the contact

angle. That concludes, the rate of change (increase) of the bearing stiffness is directly proportional to the contact angle and inversely proportional to the applied force, the ball complement and the ball diameter. That can be also seen by the first derivative of the stiffness equation, with respect to the variable in question each time.

The derivative of the stiffness with respect to the applied force is

$$\psi' = 2.27 \times 10^7 \times Z^{2/3} \times D^{1/3} \times \sin^{5/3} \alpha \times \frac{1}{3} \times F_a^{-2/3} \quad [3.22]$$

The graph obtained (Figure 3.6) by this equation shows the rate of change of the bearing stiffness with applied load.

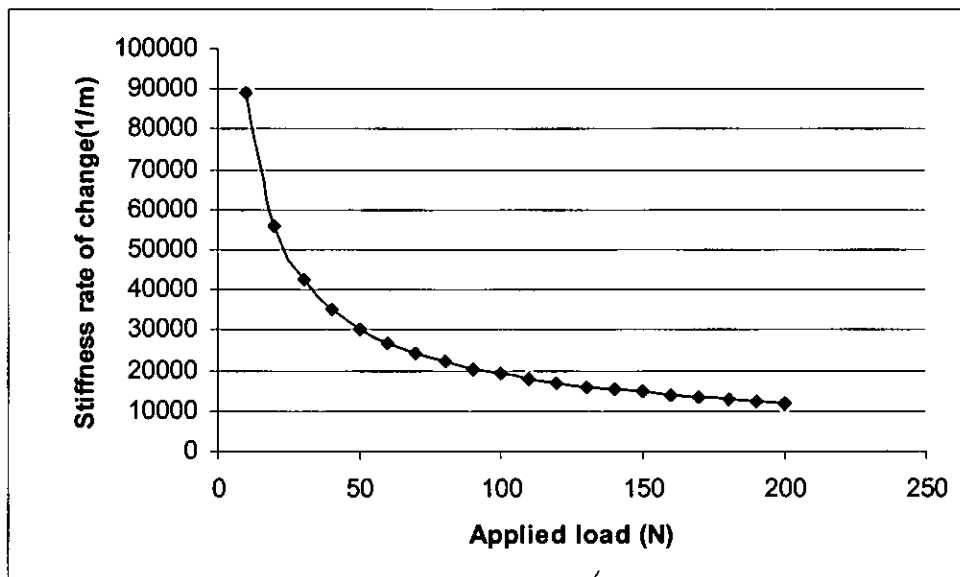


Figure 3.6 Rate of change of bearing stiffness with applied load

Similarly the rate of change of stiffness with ball complement is given by

$$\psi' = 2.27 \times 10^7 \times F_a^{1/3} \times D^{1/3} \times \sin^{5/3} \alpha \times \frac{2}{3} \times Z^{-1/3} \quad \text{Equation 3.23}$$

which provides the graph

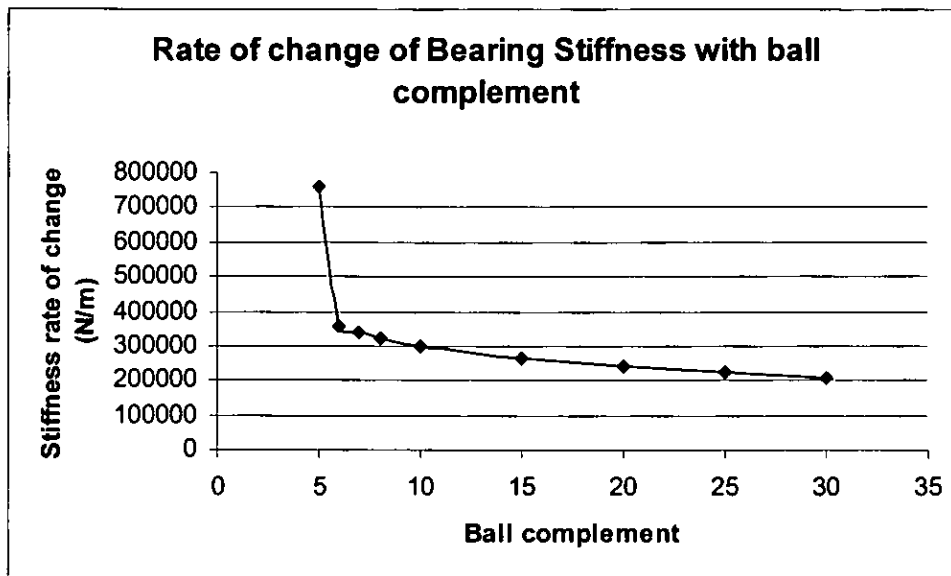


Figure 3.7 Rate of change of bearing stiffness with ball complement

The rate of change at lower values is practically impossible. That strange behaviour of the graph is due to the 5-ball complement used which is only for calculation purposes and never used in bearing design.

The rate of change of stiffness with ball diameter is given by

$$\psi' = 2.27 \times 10^7 \times Z^{2/3} \times F_a^{1/3} \times \sin^{5/3} \alpha \times \frac{1}{3} \times D^{-(2/3)} \quad [3.24]$$

and the graph produced is

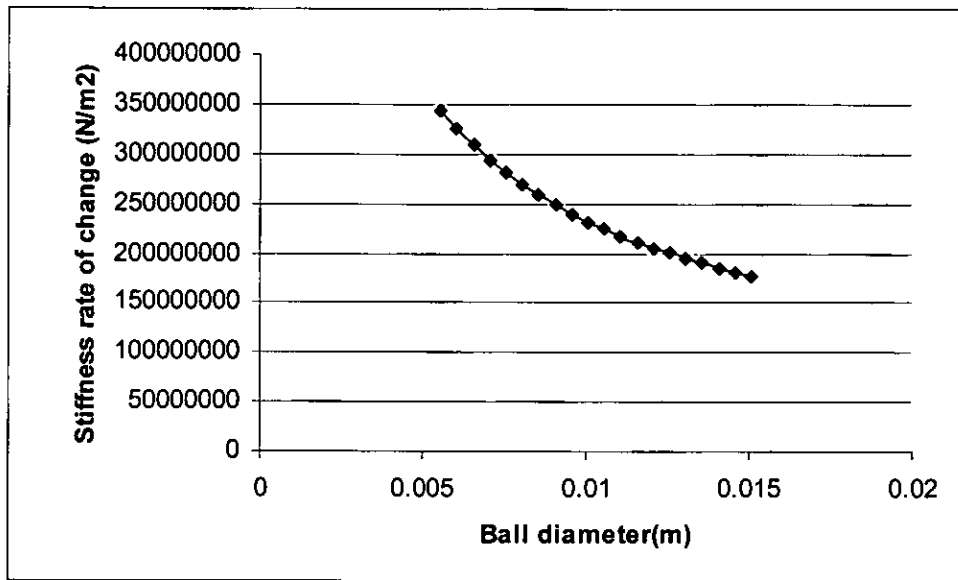


Figure 3.8 Rate of change of bearing stiffness with ball diameter

The rate of change of stiffness with contact angle is

$$\psi' = 2.27 \times 10^7 \times Z^{2/3} \times D^{1/3} \times F_a \sin^{5/3} a \times \frac{5}{3} \times \cos a \quad [3.25]$$

and the produced graph

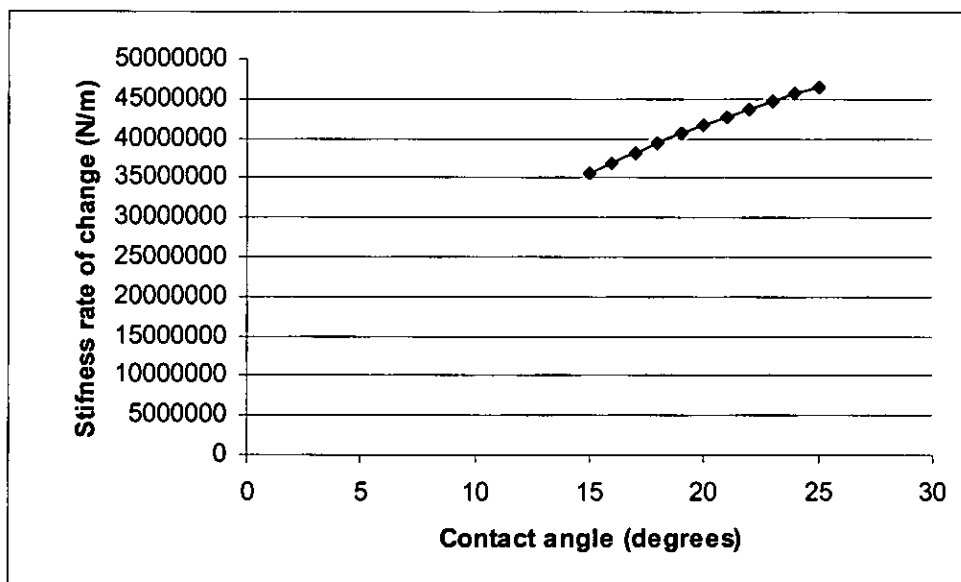


Figure 3.9 Rate of change of bearing stiffness with contact angle

The use of the above graphs is that possible sources of error can be identified. High rates of change denote high error risk, whilst for lower rate of change values that risk is reduced. More specifically analysing the information, given by the above graphs, follows that: Figure 3.5 shows the rate of change of bearing stiffness with the applied load change. For small loads the rate of change is high, decreasing for higher load values. This means that a possible error on the applied load measurement will result to a significant error on the bearing stiffness prediction for low applied load values, while a similar measurement error on the applied load for higher load values will result to less significant error on bearing stiffness prediction.

Similarly fig 3.6 shows the rate of change of the bearing stiffness with the ball complement. For low number of balls (5-ball complement) the rate of change is high while for ball complements of 10 balls and higher the rate of change of stiffness is significantly lower. Therefore a possible error in ball complement (which is very unlikely to happen in real life conditions) will result to more significant error on stiffness prediction for low ball complements than for higher.

The rate of change of the bearing stiffness with the ball diameter (fig 3.7) behaves in the same manner as for the applied load and ball complement change, with the difference that in this case the rate of change declines almost constantly. That means a possible error on the ball diameter value will produce more significant error in stiffness prediction for smaller ball diameters, but the difference since the decrease is almost constant is not as dramatic in relation to a similar change on applied force.

The rate of change of bearing stiffness with the contact angle (fig 3.8) is increasing almost constantly. So a possible error on the contact angle characteristic provides less significant error on the stiffness prediction for smaller contact angles. That means assumption that the contact angle remains constant at 15° while the actual contact angle has increased has lower error risk than a similar assumption for a 25° angle.

The following table summarises the error risks on the bearing stiffness prediction caused by errors on the four characteristics

CHARACTERISTIC	BEARING STIFFNESS PREDICTION	
	ERROR RISK	
	Low characteristic value	High characteristic value
<i>Applied force (N)</i>	HIGH to VERY HIGH	LOW
<i>Ball Complement</i>	HIGH to VERY HIGH	LOW
<i>Ball Diameter (m)</i>	HIGH	LOW
<i>Contact Angle</i>	LOW	HIGH

Table 3-3 Stiffness prediction error risk

3.6.2 ANGULAR CONTACT BEARING PAIR

The specific case under investigation is that of an angular contact bearing pair face-to-face mounted.

According to the literature (Harris, 1966) the bearing stiffness is affected by the preload of the pair. This means the preload amount has to be added to the external axial force in the calculations.

$$F = F_a + F_p \quad [3.26]$$

where F is the total axial load

F_a is the axial load

F_p is the axial preload

After the external force reaches the amount of preload the preload is “removed” and only the external force is taken into account in the formulae.

By reaching the value that the preload is removed the pair is acting as a single bearing.

Therefore the bearing stiffness for the angular contact bearing pair is

$$\psi = 2.27 \times 10^6 F^{1/3} Z^{2/3} D^{1/3} \sin^{5/3} \alpha \quad [3.27]$$

where $F = F_a + F_p$ for $2.83 F_p > F_a$
and $F = F_a$ for $2.83 F_p \leq F_a$

3.6.3 ASSUMPTIONS

In the above analysis a number of assumptions have been made:

- The bearing is subjected to purely axial load.
- The load is distributed equally to the balls (not practical, but used for simplicity of the calculations)
- The contact angle remains constant as in the unloaded condition (also not practical, but used for simplicity)

3.6.4 Other bearing types and load conditions

The above analysis described can be applied to different bearing types and load conditions. The general stiffness equation [3.15] is the same, but the equations of load distribution and bearing deflection differs for different bearing types and load condition (e.g. non-eccentric load, radial load, combined load). Dealing with radial bearings under purely radial load, the analysis is similar to the one presented for the angular-contact bearings under purely axial load.

For bearings, where the load is not acting in the centre of the bearing (hence the load is not equally distributed among the rolling elements) or under combined load the analysis is more complicated, because factors such as the eccentricity factor and the load integrals taken into account. (Changsen, 1991)

3.7 Evaluation of Hertzian stress

In angular contact bearings the ball carries load through elliptical contact areas [Sarafin et al, 1995]. With approximation the maximum Hertzian stress can be calculated from the equation for circular contact (Arnel et al, 1991) (Greenwood, 1997)

$$P_0 = \frac{1}{\pi} \left(\frac{6F_1 E^{*2}}{R^2} \right)^{1/3} \quad [3.28] \quad (\text{Johnson, 1989})$$

where P_0 is the maximum Hertzian stress
 F_1 is the impact force
 E^* is the equivalent elastic modulus
 R is the equivalent radius

3.7.1 Equivalent radius

Every Hertzian contact (i.e. contact between curved surfaces) can be represented by the equivalent contact between a spherical body against a flat surface taken into account the Hertzian assumptions which are: (Johnson, 1989)

1. the surfaces are continuous and non-conforming
2. the strains are small
3. each solid can be considered as an elastic half space
4. the surfaces are frictionless

The radius of this spherical body is the equivalent radius for circular contact given by:

$$\frac{1}{R} = \frac{1}{R_1} + \frac{1}{R_2} \Leftrightarrow [3.29]$$
$$R = \frac{R_1 R_2}{R_1 + R_2}$$

where R_1 is the radius of the first body
 R_2 is the radius of the second body

In the case the type of contact is known to be elliptical. Therefore the above equation is not considered accurate. In that case the equivalent radius evaluation suggested from Greenwood (1983) will be followed.

That is

$$A = \frac{1}{R_1} \quad [3.30] \quad \text{and} \quad B = \frac{1}{R_1} + \frac{1}{R_2} \quad [3.31]$$

where R_1 is the radius of the ball = 2.775 mm

R_2 is the radius of the ring = 42.5 mm

Then the equivalent radius is given by

$$\frac{1}{R} = \left[AB \frac{A+B}{2} \right]^{1/3} \quad [3.32]$$

Substituting the relevant values

$$R = 2.86 \text{ mm}$$

3.7.2 Equivalent elastic modulus

The equivalent elastic modulus is given by

$$\frac{1}{E^*} = \frac{1-\nu_1^2}{E_1} + \frac{1-\nu_2^2}{E_2} \quad [3.33]$$

where E_1, E_2 are the modulus of elasticity of the two bodies

ν_1, ν_2 are the Poisson's ratios

In the case examined both ball and race is from the same material so

$$E_1 = E_2 = 210 \text{ GPa}$$

$$\text{and } \nu_1 = \nu_2 = 0.3$$

Substituting to the equation the equivalent elastic modulus found to be:

$$E^* = 115GPa$$

3.7.3 Impact Force

The calculation of the impact force is the most complicated part of the analysis.

The first step to evaluate the impact force is to find the closing velocity. The term closing velocity is the velocity that the ball has at the point that reaches the outer ring. Similarly, it can be considered that the ball is moving towards the inner ring. The worst case scenario is that initially the ball is in contact with the inner ring and they are moving together towards the outer ring, while the outer ring is moving towards the inner ring and the ball. Figure 3.10 shows the relative movement of the rings

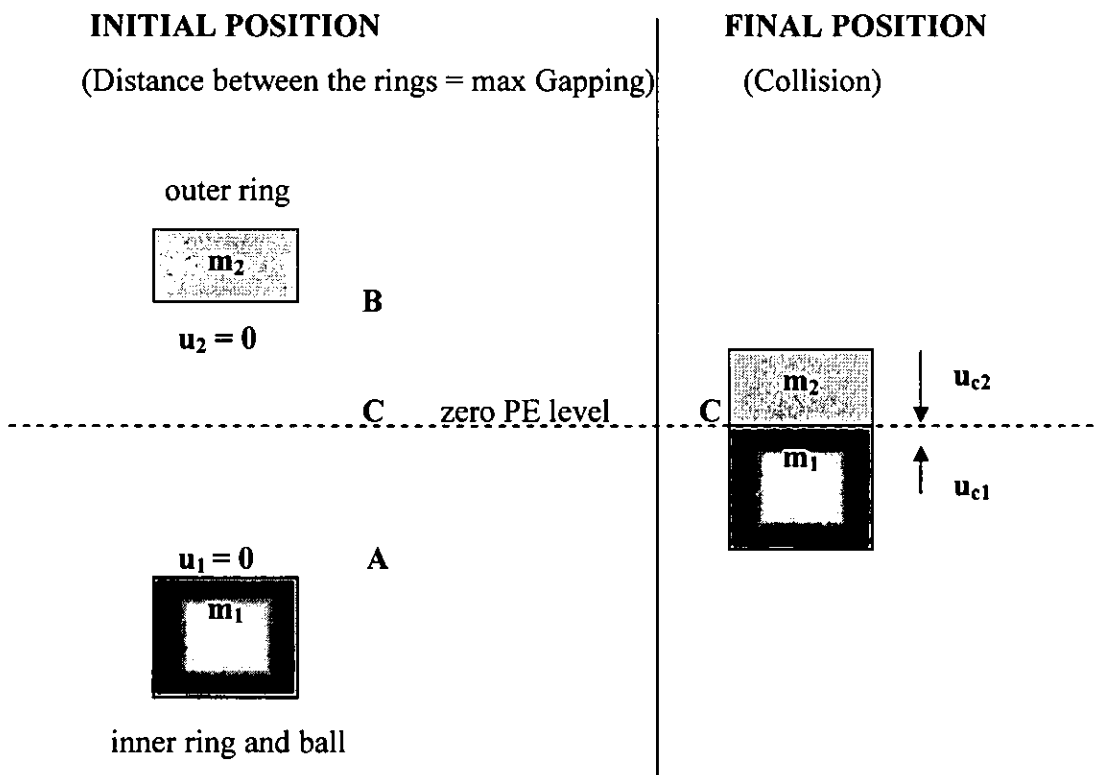


Figure 3.10 Relative movement of the rings

Position C is the position that the two rings meet is the zero potential energy (PE) position. The initial velocities are zero, while at the contact position C the inner ring with the ball (m_1) has velocity u_{C1} , while the outer ring with the ball (m_2) has velocity u_{C2} . The distance of the inner ring from the contact position is S_1 and the distance of the outer ring from the contact position is S_2 . The total distance $h = S_1 + S_2$ is the gapping. The acceleration that the rings are moving is the input acceleration.

Applying conservation of mechanical energy for the inner ring from position A to position C.

$$m_1 \alpha S_1 = \frac{1}{2} m_1 u_{C1}^2 \Rightarrow [3.34]$$

$$u_{C1} = \sqrt{2\alpha S_1}$$

working similarly for the outer ring from position B to C:

$$u_{C2} = \sqrt{2\alpha S_2} \quad [3.35]$$

Now since

$$S_1 + S_2 = h \quad [3.36]$$

then

$$u_{C1}^2 + u_{C2}^2 = 2\alpha h \quad [3.37]$$

Considering now an equivalent condition where an equivalent body of mass m travels distance h . Applying conservation of mechanical energy for distance h the equivalent velocity u is:

$$u^2 = 2\alpha h \quad [3.38]$$

therefore

$$u^2 = u_{C1}^2 + u_{C2}^2 \quad [3.39]$$

At initial positions

$$PE_1 = PE_2 \Rightarrow$$

$$m_1 a S_1 = m_2 a S_2 \quad [3.40]$$

So

$$S_1 = \frac{m_2}{m_1} S_2 \quad [3.41] \quad \text{and} \quad S_2 = \frac{m_1}{m_2} S_1 \quad [3.42]$$

Substituting for $m_1 = 1.9$ Kg and $m_2 = 0.783$ Kg and $h = S_1 + S_2$

then

$$S_1 = 0.292h \quad [3.43] \quad \text{and} \quad S_2 = 2.426h \quad [3.44]$$

The maximum kinetic energy of the equivalent body at its zero potential energy position will be equal to the total kinetic energy of the two rings at position C.

So

$$\frac{1}{2} m u^2 = \frac{1}{2} m_1 u_{C1}^2 + \frac{1}{2} m_2 u_{C2}^2 \quad [3.45]$$

but since

$$u^2 = u_{C1}^2 + u_{C2}^2$$

then

$$m = \frac{m_1 u_{C1}^2 + m_2 u_{C2}^2}{u_{C1}^2 + u_{C2}^2} \quad [3.46]$$

which by substitution gives

$$m = 1.109 \text{Kg}$$

3.7.4 Closing acceleration

Once the two rings collide with velocities u_{C1} and u_{C2} the two bodies (ball and outer ring) deformed by an amount δ_n . The nominal approach at 4.2 GPa assumed as $2.8 \cdot 10^{-6} \text{m}$

(Lewis et al, 2002). The masses stopped due to the deceleration occurred by the impact force. Applying conservation of energy for the equivalent body from the time of contact until it stops

$$\begin{aligned} u &= \sqrt{2a_c \delta_n} \Rightarrow \\ a_c &= \frac{u^2}{2\delta_n} \end{aligned} \quad [3.47]$$

where A is the closing acceleration (deceleration).

3.7.5 Impact force calculation

Since the closing acceleration and the equivalent mass are known then from Newton's second law:

$$F_I = ma_c \quad [3.48]$$

Knowing all the parameters of the appropriate equation, the Hertzian stress can be calculated by:

$$P_0 = \frac{1}{\pi} \left(\frac{6F_I E^{*2}}{R^2} \right)^{1/3} \quad [3.24]$$

Chapter 4

4 Results

Chapter 4 presents the results of calculations of bearing stiffness, gapping predictions for constant load (variable frequency) and constant frequency (variable load) using stiffness values predicted by the author and values of stiffness from CABARET. These data are compared in the next chapter, and results for the closing velocity of the rings, the collision acceleration, the impact force and the Hertzian stress are also presented. All the results are obtained using the methods described in the previous chapter.

4.1 Introduction

This chapter contains the results obtained by applying the methods described in the previous chapter. The results on the bearing stiffness for 5, 9 and 15 ball complements provided in the beginning, followed by the gapping prediction, based on the obtained stiffness values. Along with them the gapping prediction, using CABARET stiffness, used in previous study is provided in order to present a comparison between the two methods in the next chapter. The gapping prediction results can be separated into two categories. The first category is examined very briefly, since the current study is focused on the second one.

- a) The prediction for constant applied load of 20, 25 and 30N in respect of frequency for a range from 100 to 600 Hz, which is the frequency range where measured results are available.
- b) The prediction for constant 500 Hz frequency with respect to the applied load up to 100 N, which is the load up to which measured results also exist and, therefore, the validity of the method can be examined.

The gapping prediction results are followed by the results for closing velocity between the ball and the race, the closing acceleration, the impact force and the Hertzian stress.

4.2 Bearing stiffness

Figure 4.1 shows the bearing stiffness against the input acceleration while Figure 4.2 shows the bearing stiffness against the applied load for the different ball complements.

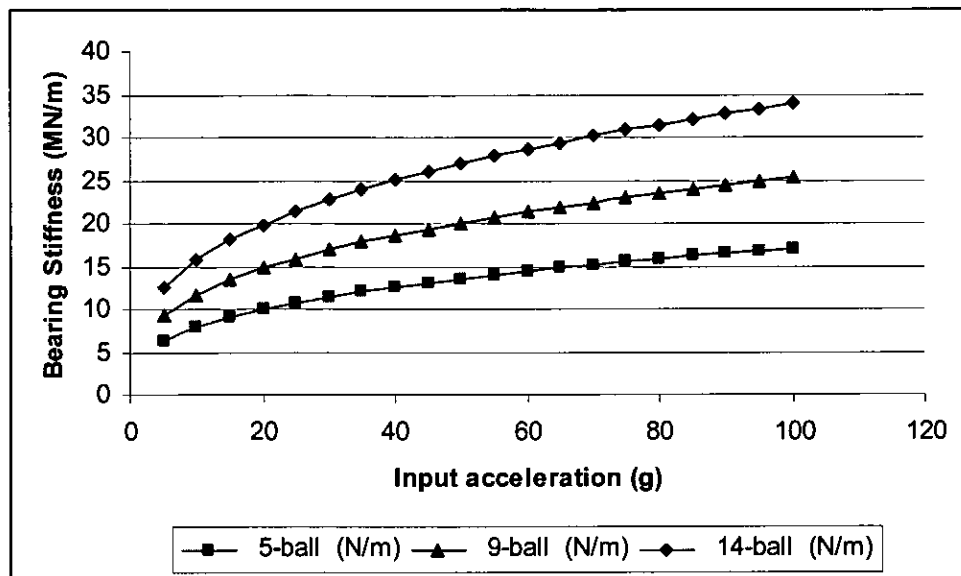


Figure 4.1 Bearing stiffness against Input acceleration

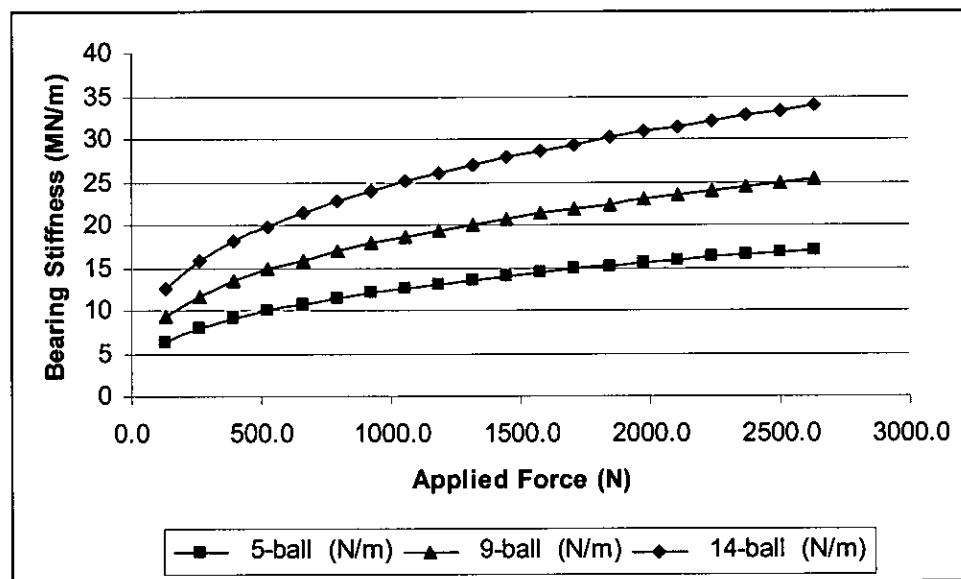


Figure 4.2 Bearing Stiffness against Applied Force

Title: BEARING STIFFNESS at 500Hz
Author: PAPAKONSTANTINOUS ANTONIOS

Input data

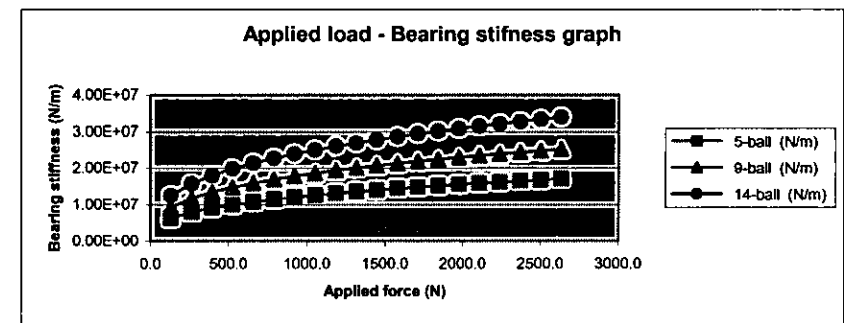
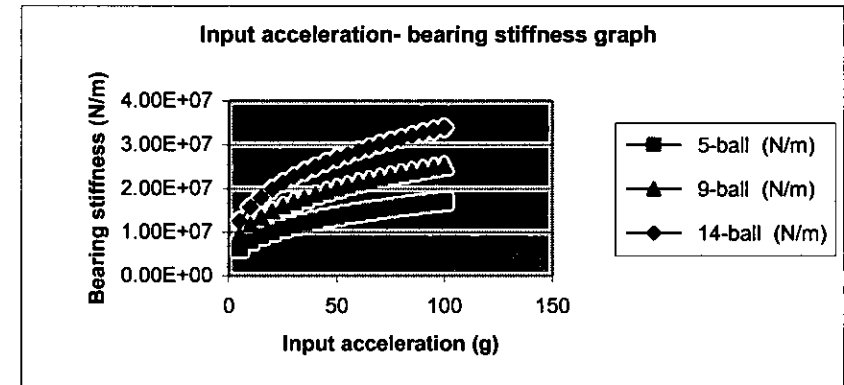
Shaft assembly mass total (m_1)	1.9	kg		
Outer housing assembly mass	0.783	kg		
Ball complement Z	5	9	14	
Ball diameter (D)	0.005555	m		
Frequency	500	Hz		
Angular acceleration ω	3140	rad/s		
CABARET stiffness	9.85E+06	1.64E+07	2.60E+07	

FORMULAE

$$F = (m_1 + m_2)a$$

$$Stiffness = 2.27 * 10^7 * Z^{2/3} * F^{1/3} * D^{1/3} * \sin^{2/3} \alpha$$

Acceleration a (g)	Applied load F (N)	Contact angle (degrees)	Calculated Bearing Stiffness		
			5-ball (N/m)	9-ball (N/m)	14-ball (N/m)
5	131.6	15	6.29E+06	9.31E+06	1.25E+07
10	263.2	15	7.93E+06	1.17E+07	1.57E+07
15	394.8	15	9.08E+06	1.34E+07	1.80E+07
20	526.4	15	9.99E+06	1.48E+07	1.98E+07
25	658.0	15	1.08E+07	1.59E+07	2.14E+07
30	789.6	15	1.14E+07	1.69E+07	2.27E+07
35	921.2	15	1.20E+07	1.78E+07	2.39E+07
40	1052.8	15	1.26E+07	1.86E+07	2.50E+07
45	1184.4	15	1.31E+07	1.94E+07	2.60E+07
50	1316.0	15	1.36E+07	2.01E+07	2.69E+07
55	1447.6	15	1.40E+07	2.07E+07	2.78E+07
60	1579.2	15	1.44E+07	2.13E+07	2.86E+07
65	1710.8	15	1.48E+07	2.19E+07	2.94E+07
70	1842.4	15	1.52E+07	2.24E+07	3.01E+07
75	1974.0	15	1.55E+07	2.30E+07	3.08E+07
80	2105.6	15	1.59E+07	2.35E+07	3.15E+07
85	2237.2	15	1.62E+07	2.39E+07	3.21E+07
90	2368.8	15	1.65E+07	2.44E+07	3.28E+07
95	2500.4	15	1.68E+07	2.48E+07	3.34E+07
100	2632.0	15	1.71E+07	2.53E+07	3.39E+07



4.3 Gapping prediction for constant load

The following graphs shows the results for the different ball complements in respect with frequency, for applied loads of 196.2, 245.25 and 249.3 N i.e. input acceleration of 20g, 25g and 30g respectively. In every graph two lines are present. The rhombi denote the gapping prediction using CABARET stiffness, referred as “CABARET gap” on the graphs. The squares denote the gapping prediction using the non-linear stiffness values, referred as “non-linear gap” on the graph.

4.3.1 5-ball complement

The following figures show the gapping prediction results obtained for 5-ball complement angular contact bearing pair.

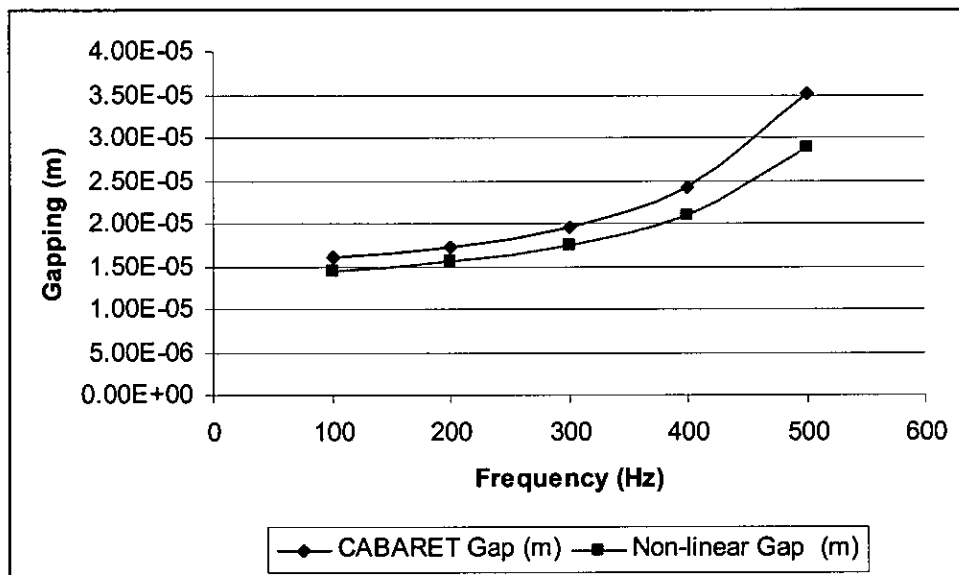


Figure 4.3 Gapping prediction for 5-ball complement at 20g

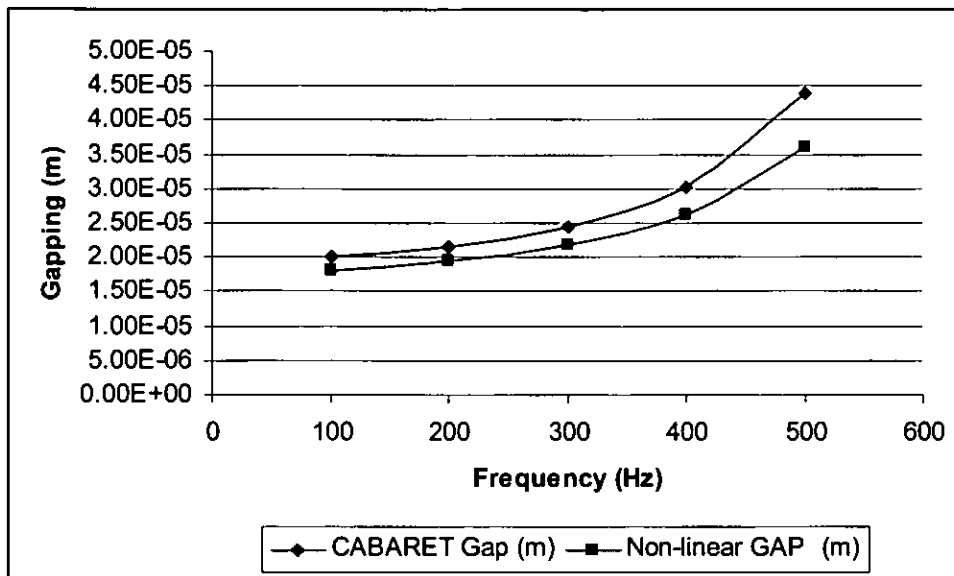


Figure 4.4 Gapping prediction for 5-ball complement at 25g

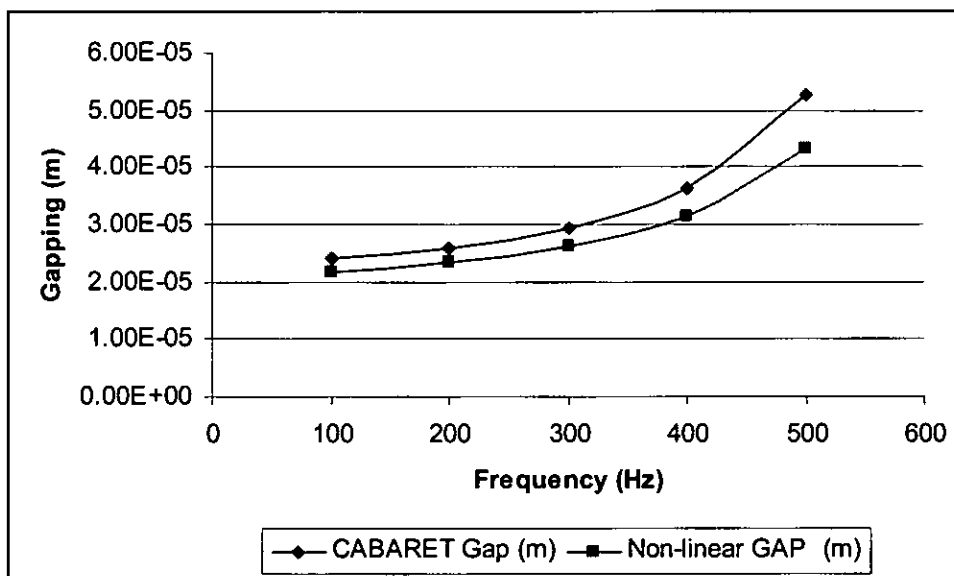


Figure 4.5 Gapping prediction for 5-ball complement at 30g

The above results are practically impossible to justify, although used here to show comparison between the methods. In general gapping occurs, not exceeding that of the deformation of the most loaded ball, when a reasonable preload is used. (Rahnejat et al, 1985)

4.3.2 9-ball complement

The following figures show the gapping prediction results obtained for 5-ball complement angular contact bearing pair.

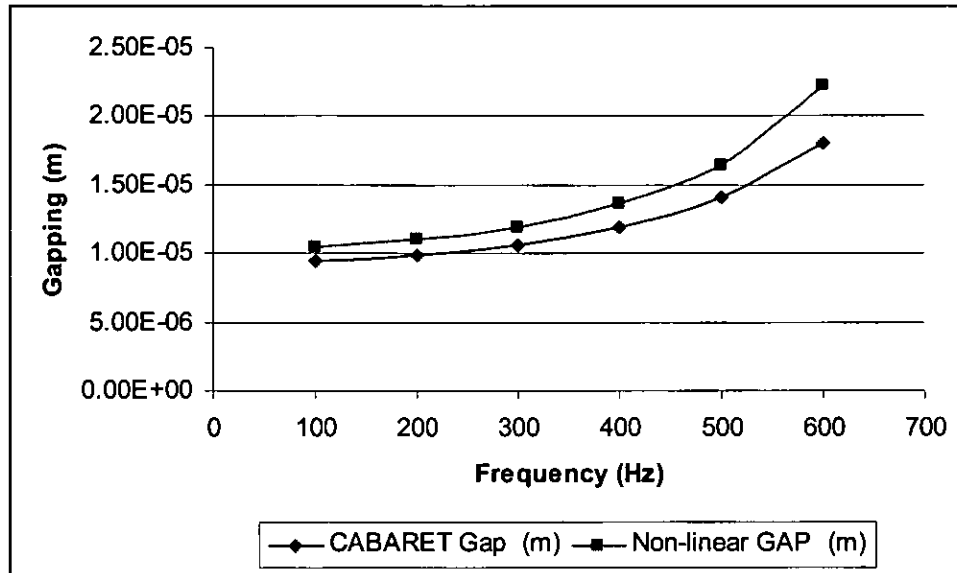


Figure 4.6 Gapping prediction for 9-ball complement at 20g

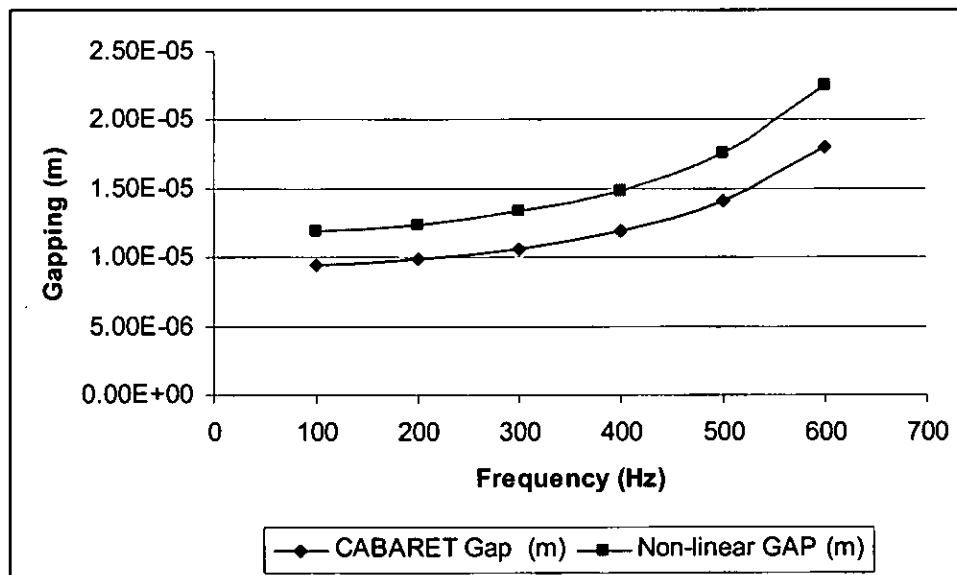


Figure 4.7 Gapping prediction for 9-ball complement at 25g

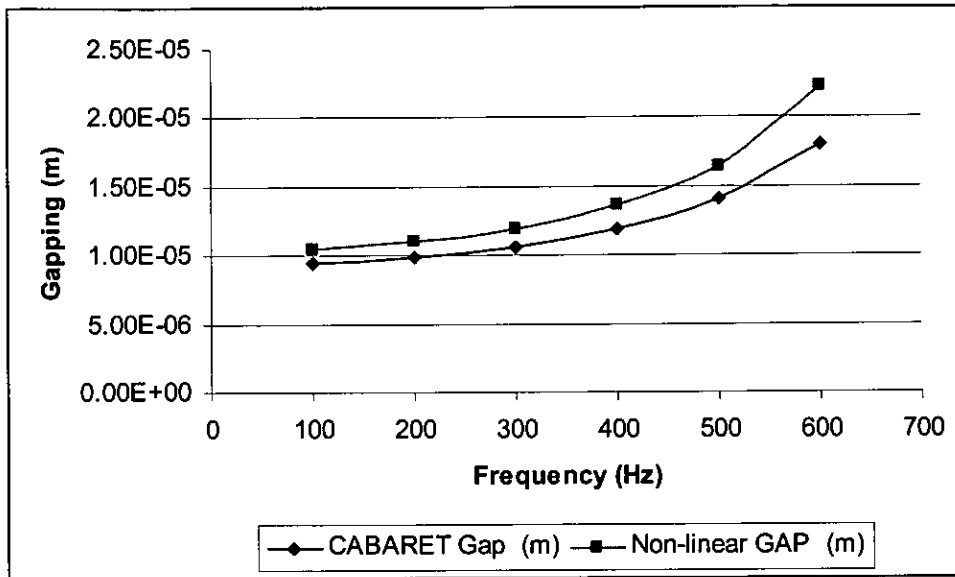


Figure 4.8 Gapping prediction for 9-ball complement at 30g

4.3.3 14-ball complement

The following figures show the gapping prediction results obtained for 5-ball complement angular contact bearing pair.

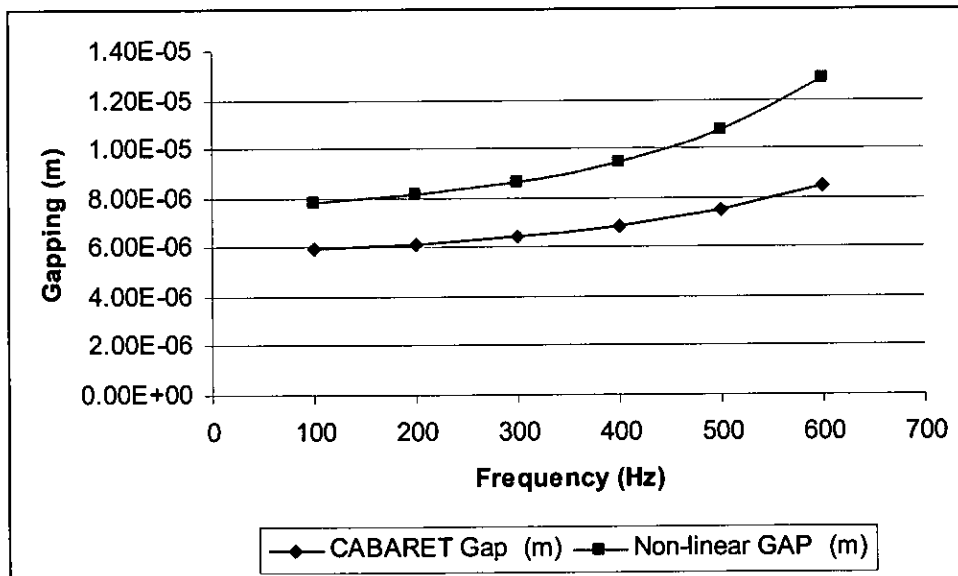


Figure 4.9 Gapping prediction for 14-ball complement at 20g

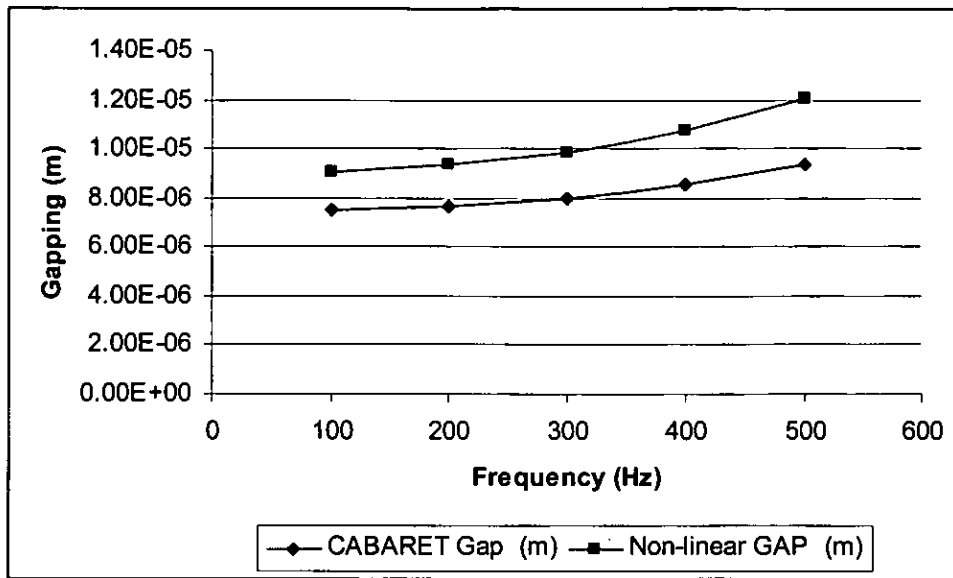


Figure 4.10 Gapping prediction for 14-ball complement at 25g

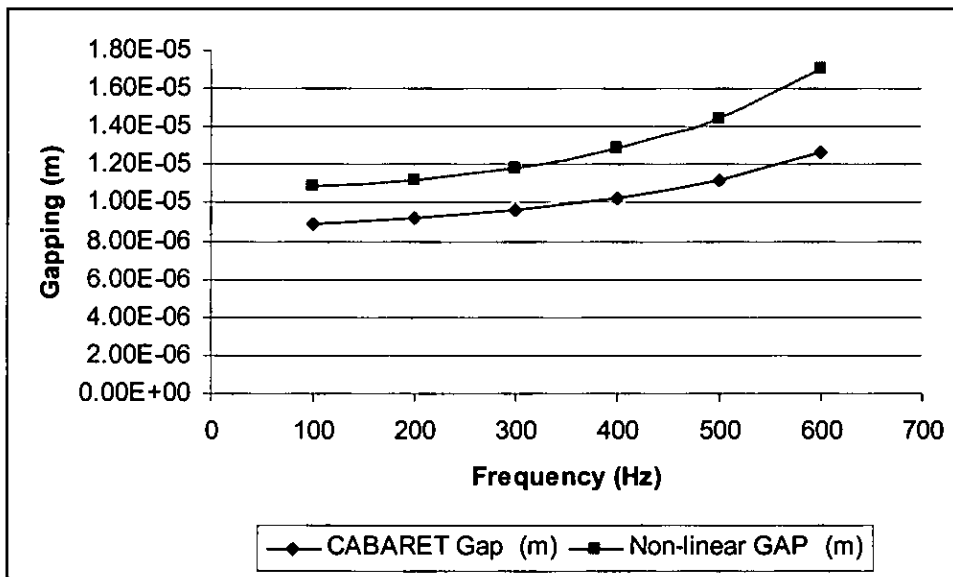


Figure 4.11 Gapping prediction for 14-ball complement at 30g

4.4 Gapping prediction for constant 500 Hz frequency

The gapping prediction results for input acceleration range from 5g to 100g at 500, 1500 and 2000 Hz frequency presented in this section. The frequency range around 1000 Hz avoided because the graph presents gapping levels at certain acceleration values tending to

infinity. This is due to lack of the gapping formula when the condition $1.8\omega^2 = k$ applies as explained on the previous chapter.

CABARET predictions

This section provides the gapping prediction results for 5, 9 and 14 ball complement using CABARET stiffness. Each graph has three lines denoted with squares, triangles and rhombi for 5, 9 and 14-ball respectively.

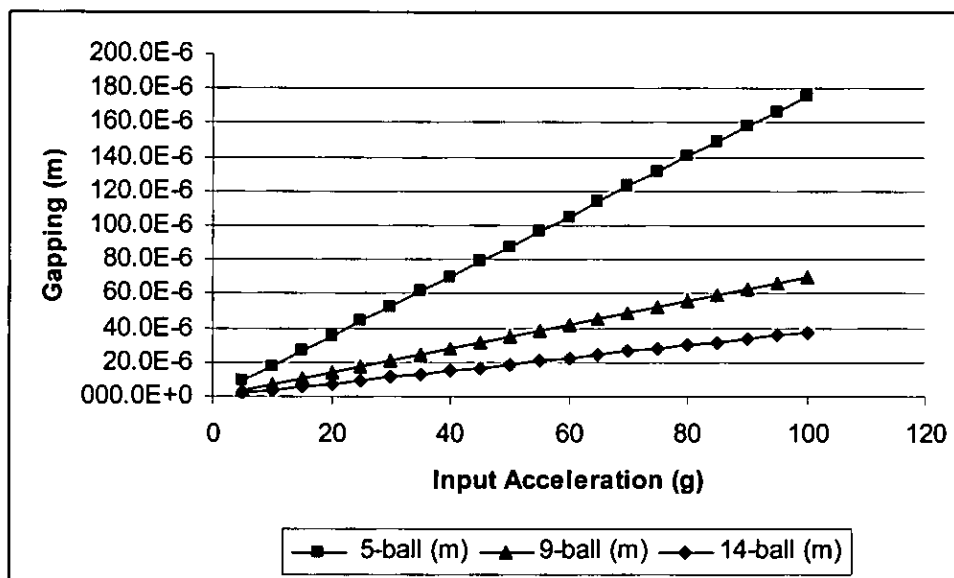


Figure 4.12 Input acceleration – Gapping prediction (using CABARET stiffness) at 500 Hz

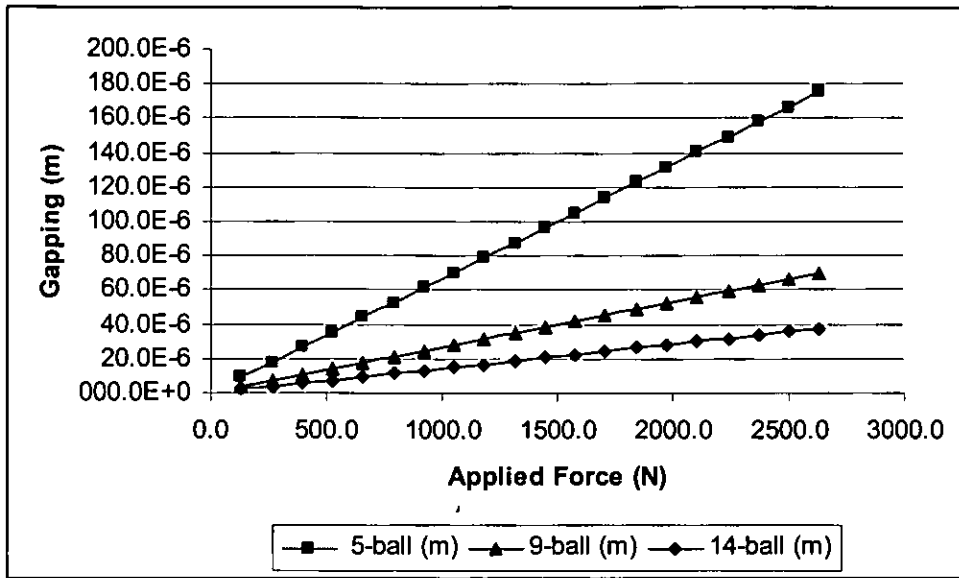


Figure 4.13 Applied Force – Gapping prediction (using CABARET stiffness) at 500 Hz

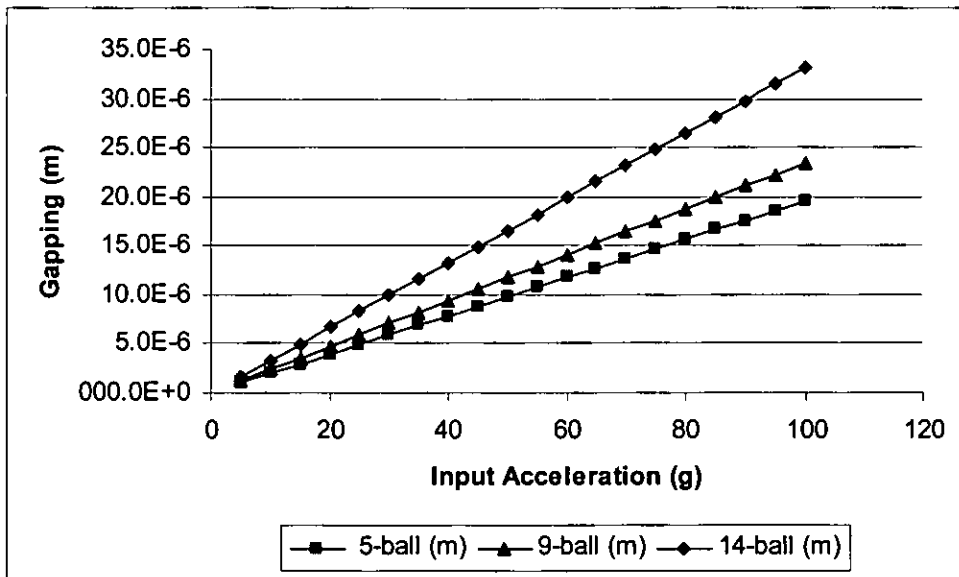


Figure 4.14 Input acceleration – Gapping prediction (using CABARET stiffness) at 1500 Hz

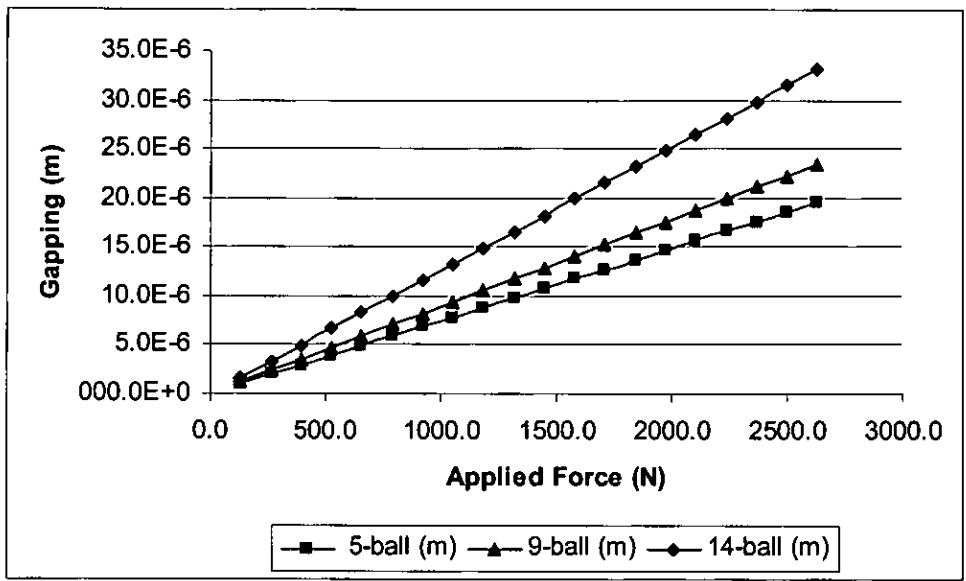


Figure 4.15 Applied Force – Gapping prediction (using CABARET stiffness) at 1500 Hz

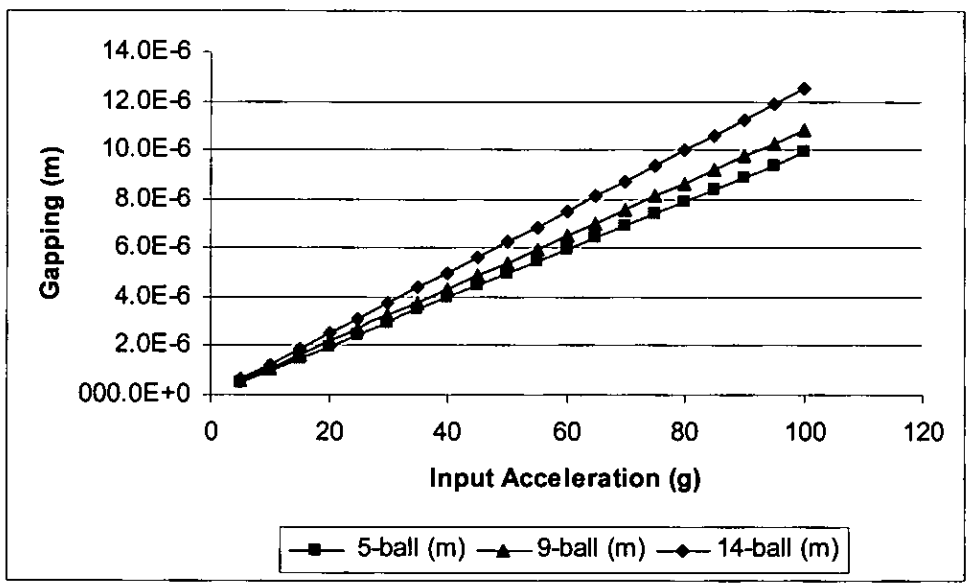


Figure 4.16 Input acceleration – Gapping prediction (using CABARET stiffness) at 2000 Hz

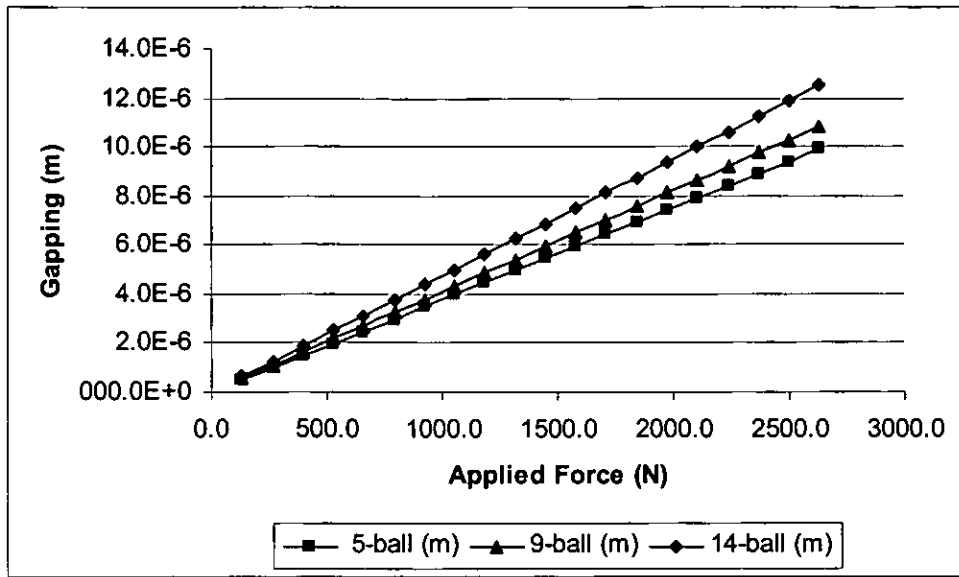
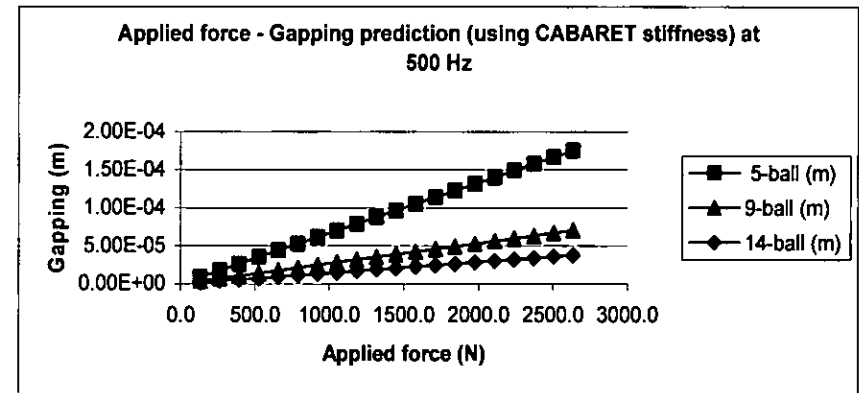
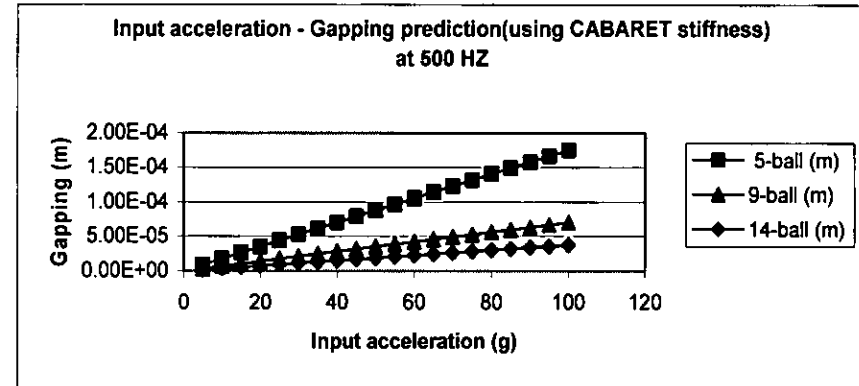


Figure 4.17 Applied Force – Gapping prediction (using CABARET stiffness) at 2000 Hz

Title: Gapping prediction at 500Hz using CABARET stiffness
 Author: PAPAKONSTANTINOUS ANTONIOS

Acceleration a (g)	Applied force F (N)	5-ball (m)	9-ball (m)	14-ball (m)
5	131.6	8.76E-06	3.51E-06	1.87E-06
10	263.2	1.75E-05	7.03E-06	3.74E-06
15	394.8	2.63E-05	1.05E-05	5.61E-06
20	526.4	3.51E-05	1.41E-05	7.48E-06
25	658.0	4.38E-05	1.76E-05	9.35E-06
30	789.6	5.26E-05	2.11E-05	1.12E-05
35	921.2	6.13E-05	2.46E-05	1.31E-05
40	1052.8	7.01E-05	2.81E-05	1.50E-05
45	1184.4	7.89E-05	3.16E-05	1.68E-05
50	1316.0	8.76E-05	3.51E-05	1.87E-05
55	1447.6	9.64E-05	3.86E-05	2.06E-05
60	1579.2	1.05E-04	4.22E-05	2.24E-05
65	1710.8	1.14E-04	4.57E-05	2.43E-05
70	1842.4	1.23E-04	4.92E-05	2.62E-05
75	1974.0	1.31E-04	5.27E-05	2.81E-05
80	2105.6	1.40E-04	5.62E-05	2.99E-05
85	2237.2	1.49E-04	5.97E-05	3.18E-05
90	2368.8	1.58E-04	6.32E-05	3.37E-05
95	2500.4	1.66E-04	6.67E-05	3.55E-05
100	2632.0	1.75E-04	7.03E-05	3.74E-05



4.4.1 Non-linear predictions

In this section the gapping prediction results using non-linear stiffness are presented. Again each graph has three lines denoted with squares, triangles and rhombi for 5, 9 and 14-ball respectively.

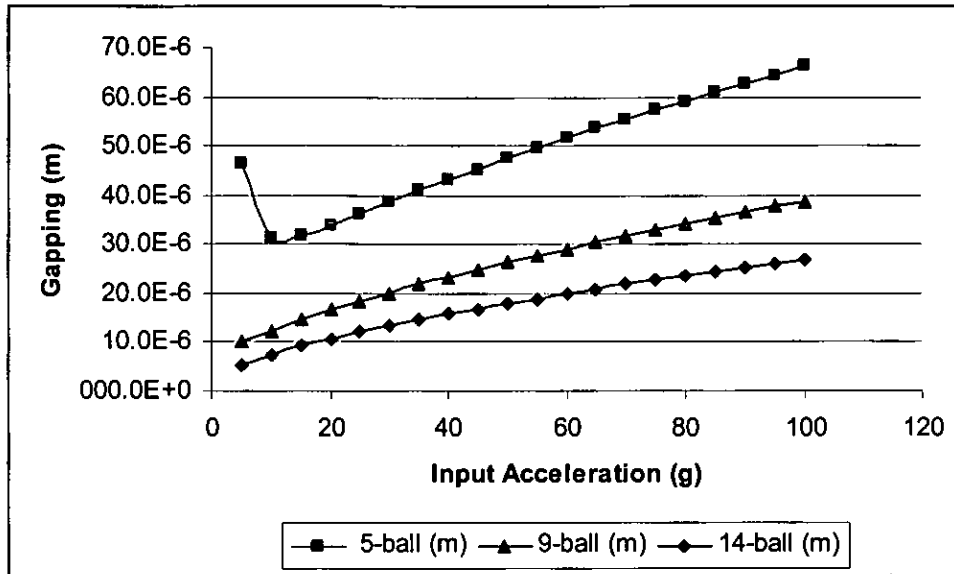


Figure 4.18 Input acceleration – Gapping prediction (using non-linear stiffness) at 500 Hz

The 5-ball complement is physically in free flight in unloaded region.

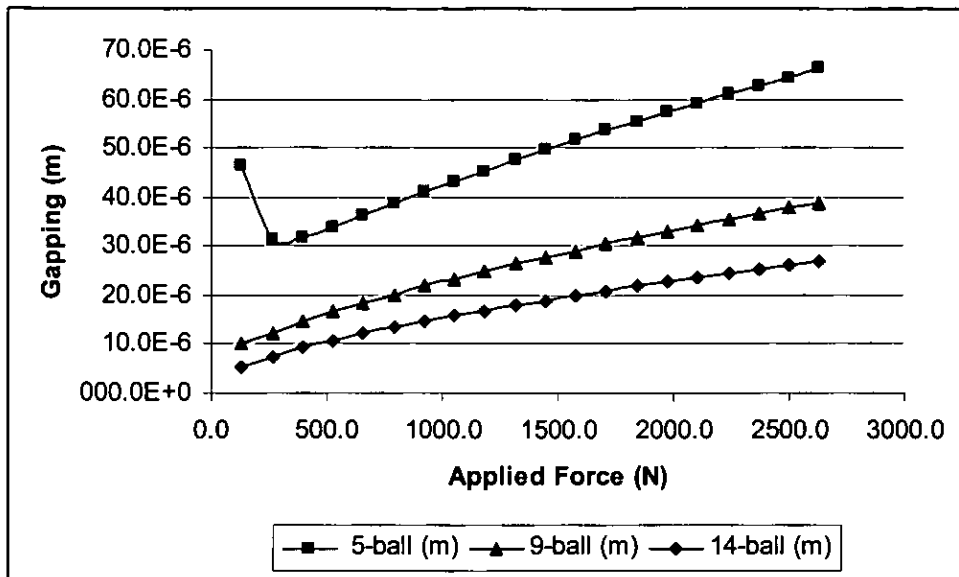


Figure 4.19 Applied Force – Gapping prediction (using non-linear stiffness) at 500 Hz

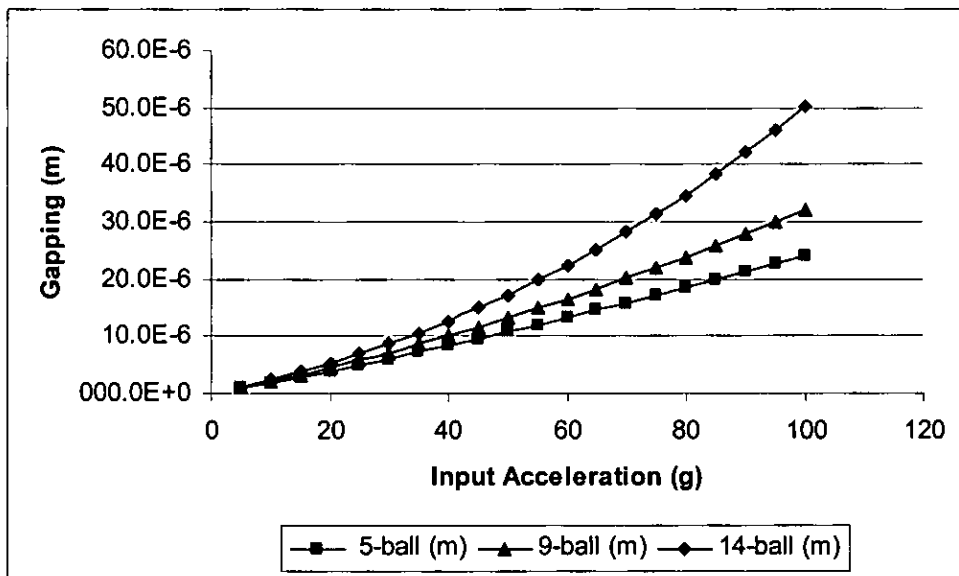


Figure 4.20 Input acceleration – Gapping prediction (using non-linear stiffness) at 1500 Hz

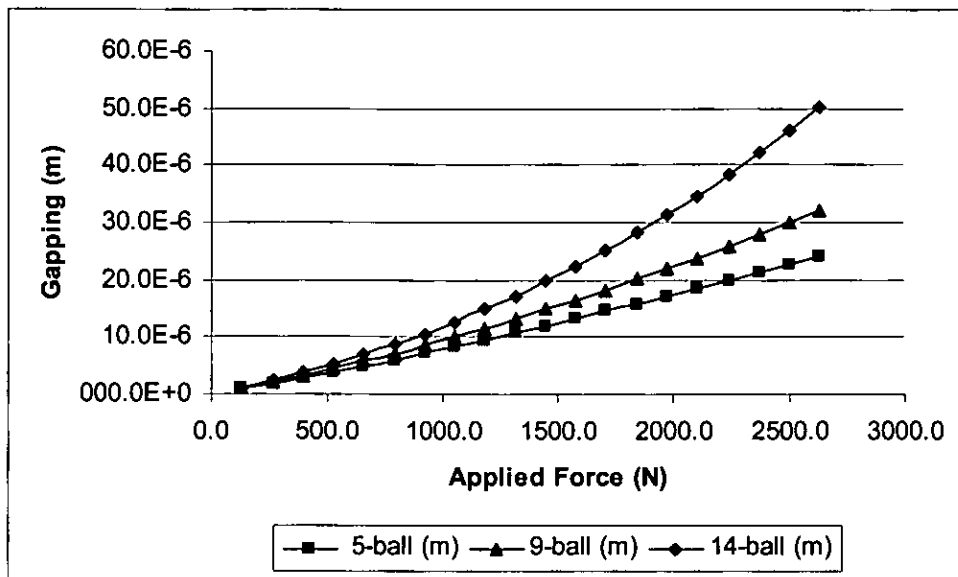


Figure 4.21 Applied Force – Gapping prediction (using non-linear stiffness) at 1500 Hz

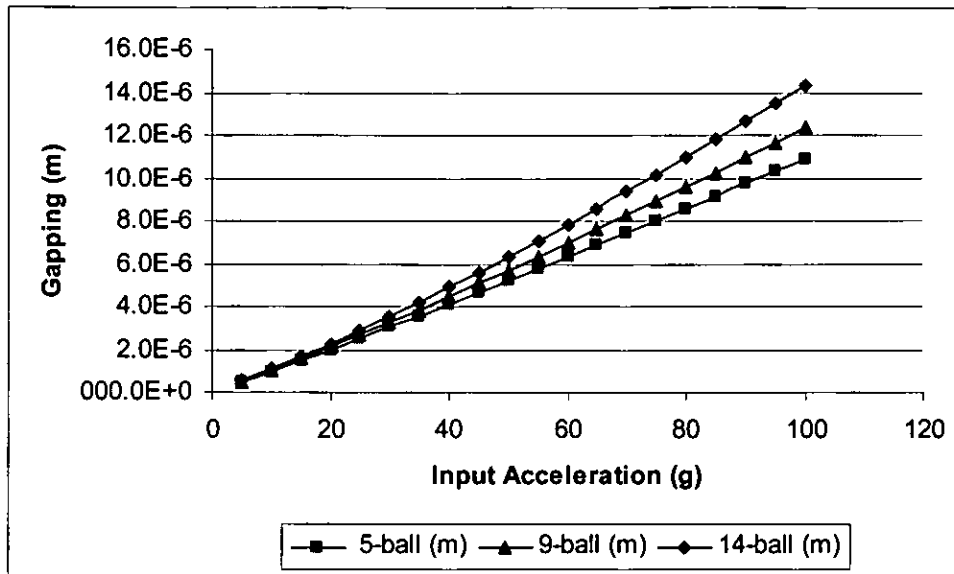


Figure 4.22 Input acceleration – Gapping prediction (using non-linear stiffness) at 2000 Hz

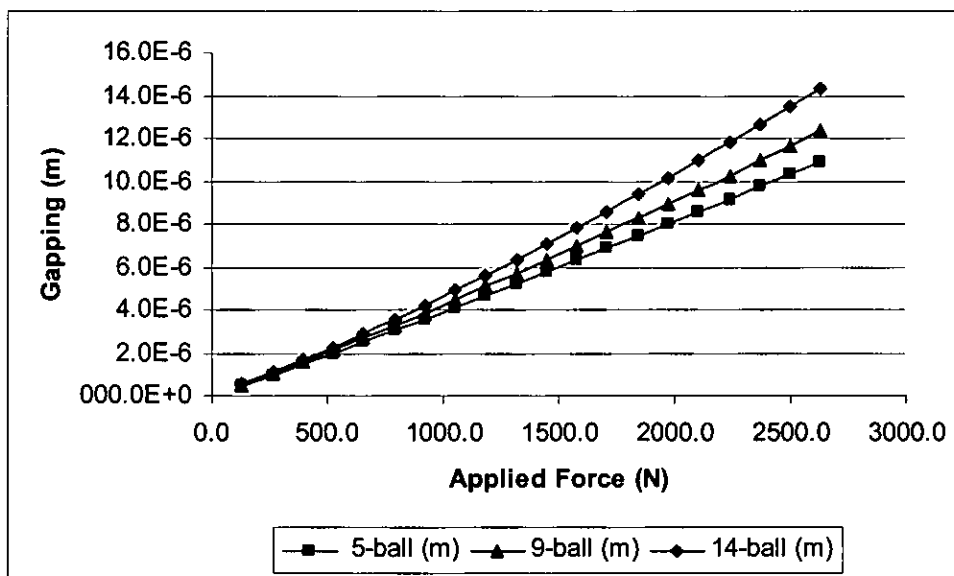


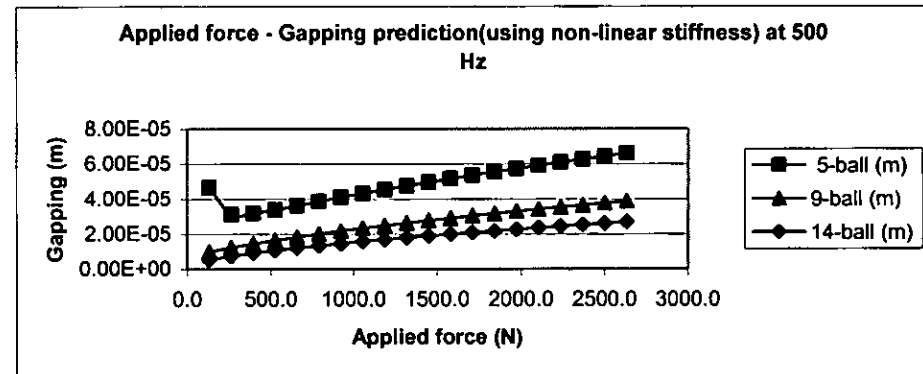
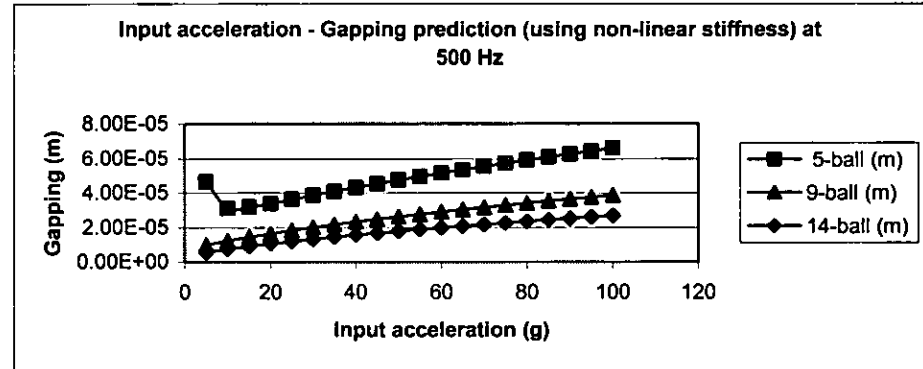
Figure 4.23 Applied Force – Gapping prediction (using non-linear stiffness) at 2000 Hz

Title: Gapping prediction at 500Hz using non-linear stiffness

Author: PAPAKONSTANTINOU ANTONIOS

Date: 5-7-2004

Acceleratio pplied forc	5-ball	9-ball	14-ball	
a (g)	F (N)	(m)	(m)	(m)
5	131.6	4.65E-05	9.99E-06	5.46E-06
10	263.2	3.12E-05	1.23E-05	7.47E-06
15	394.8	3.19E-05	1.45E-05	9.17E-06
20	526.4	3.40E-05	1.65E-05	1.07E-05
25	658.0	3.63E-05	1.84E-05	1.21E-05
30	789.6	3.86E-05	2.01E-05	1.34E-05
35	921.2	4.09E-05	2.18E-05	1.46E-05
40	1052.8	4.32E-05	2.34E-05	1.57E-05
45	1184.4	4.54E-05	2.49E-05	1.68E-05
50	1316.0	4.75E-05	2.63E-05	1.79E-05
55	1447.6	4.95E-05	2.77E-05	1.89E-05
60	1579.2	5.16E-05	2.91E-05	1.99E-05
65	1710.8	5.35E-05	3.04E-05	2.09E-05
70	1842.4	5.54E-05	3.17E-05	2.18E-05
75	1974.0	5.73E-05	3.29E-05	2.27E-05
80	2105.6	5.91E-05	3.41E-05	2.36E-05
85	2237.2	6.09E-05	3.53E-05	2.45E-05
90	2368.8	6.27E-05	3.65E-05	2.53E-05
95	2500.4	6.44E-05	3.77E-05	2.62E-05
100	2632.0	6.61E-05	3.88E-05	2.70E-05



4.5 Ball movement between the rings

In this section the results of the relative movement of the balls and the rings are presented. The results cover the specifications of the SAE-65 SNFA angular contact bearing with reduced ball complement to 5, 9 and 14 at 500 Hz frequency. Section 4.5.1 presents the distances S_1 and S_2 , representing the distance covered by the inner and outer rings respectively from their maximum displacement (gapping) to the point of collision. On the following sections the results for 5, 9 and 14-ball complements are presented for the closing velocity, collision acceleration and the impact force. The results presented considering:

- a) Movement of the inner ring along with the ball towards the outer ring
- b) Movement of the outer ring along with the ball towards the inner ring
- c) Movement of a ball of equivalent mass covering the total distance (gapping) towards a flat surface.

Only one of the three methods is necessary in order to obtain the value of the Impact Force, which will be used for the evaluation of the maximum Hertzian Pressure, as by following either a, b or c the same result for the impact force would be expected. The reason that all three have been presented is for verification purposes.

4.5.1 Covered distances

In this section the distances covered by the inner and outer ring from the point of maximum gapping to the point of collision are presented. Each graph presents the two covered distances for the respective ball complement. S_1 which is denoted with squares on the graph represents the distance covered by the inner ring and the ball from the point of maximum gapping to the point of collision with the outer ring, while S_2 which is denoted with triangles represents the distance covered by the outer ring from the point of maximum gapping to the point of collision with the inner ring.

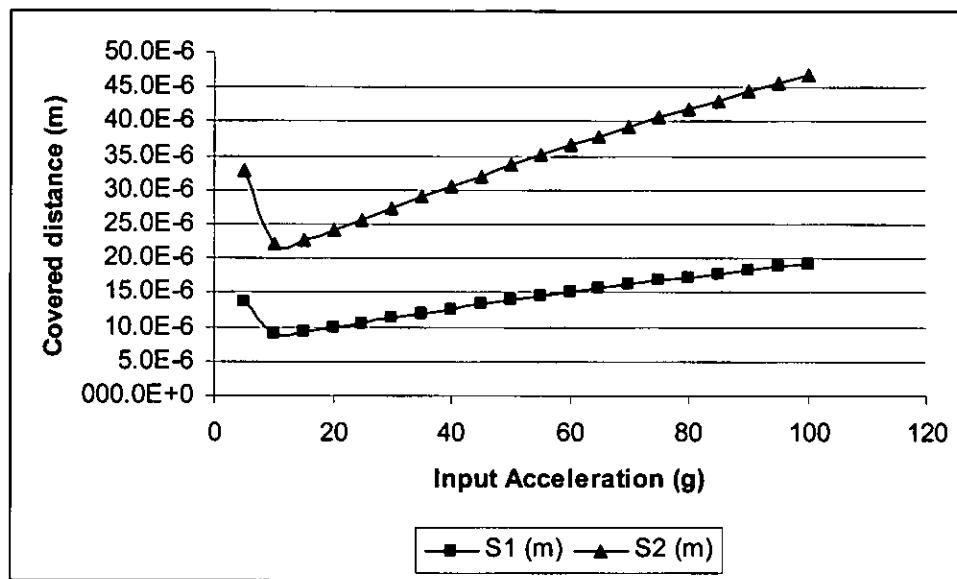


Figure 4.24 Inner and outer ring covered distances for 5-ball complement

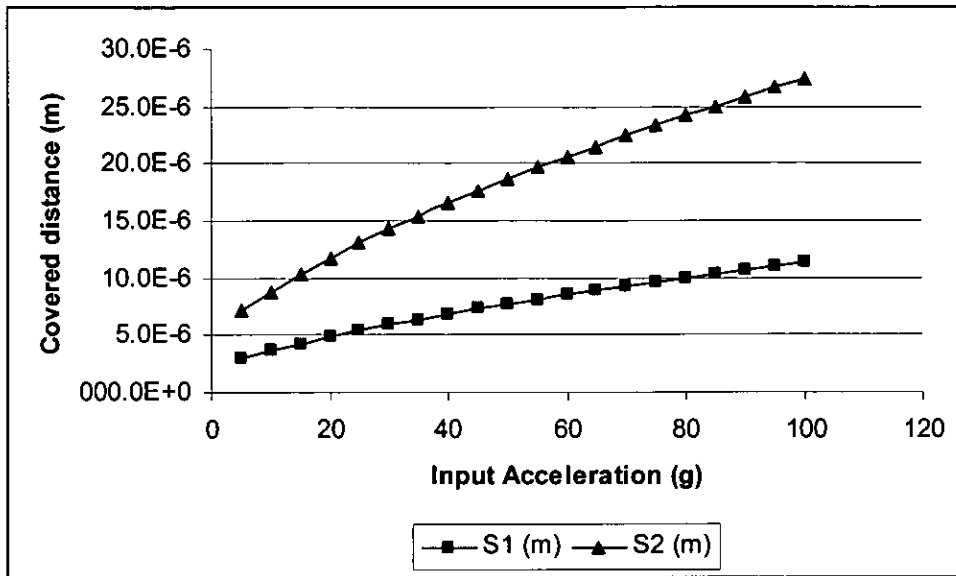


Figure 4.25 Inner and outer ring covered distances for 9-ball complement

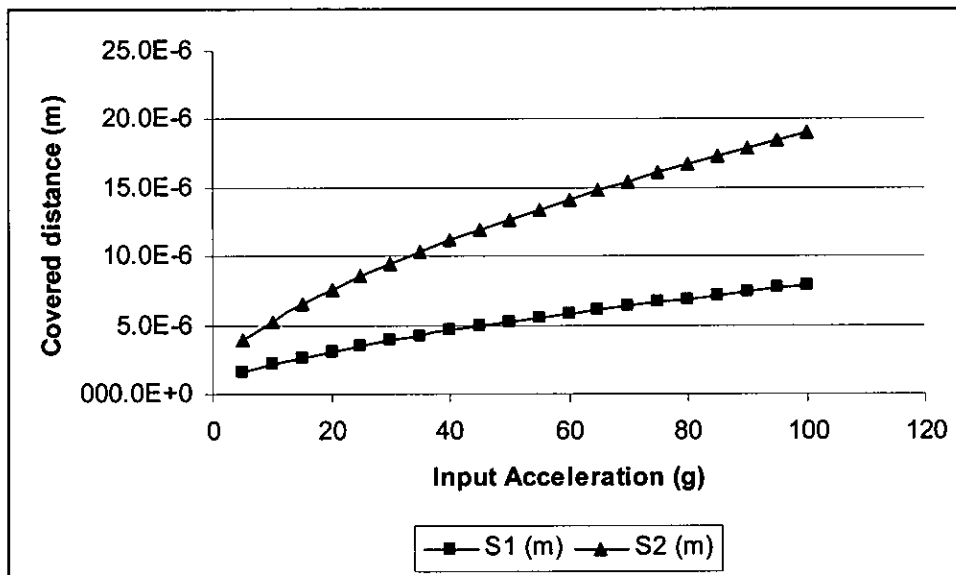


Figure 4.26 Inner and outer ring covered distances for 14-ball complement

Closing velocity

The results for the closing velocity are presented in this section. On each graph there are three lines. Squares denote the closing velocity of the inner ring; triangles denote the

closing velocity of the outer ring, while rhombi denote the closing velocity of the equivalent body.

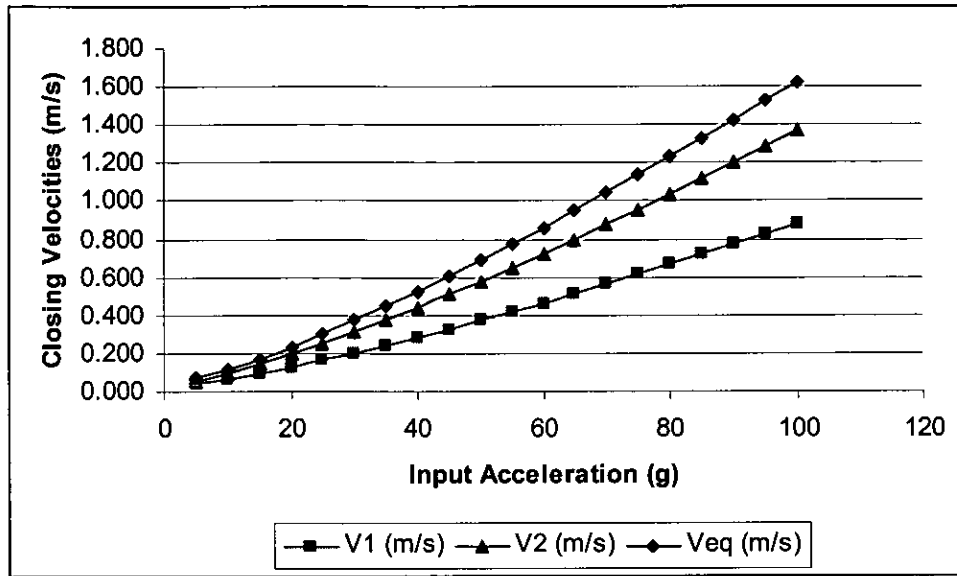


Figure 4.27 Closing velocities for 5-ball complement

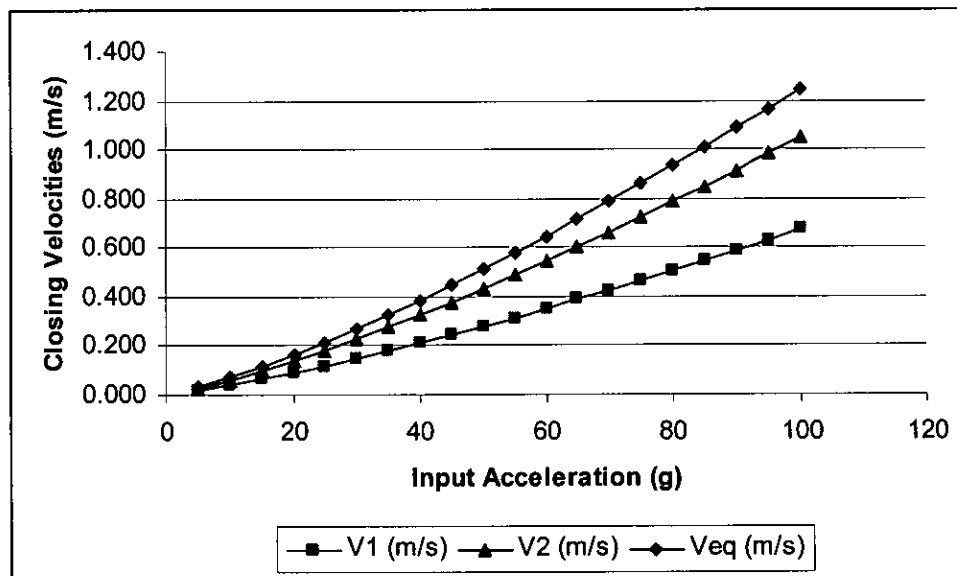


Figure 4.28 Closing velocities for 14-ball complement

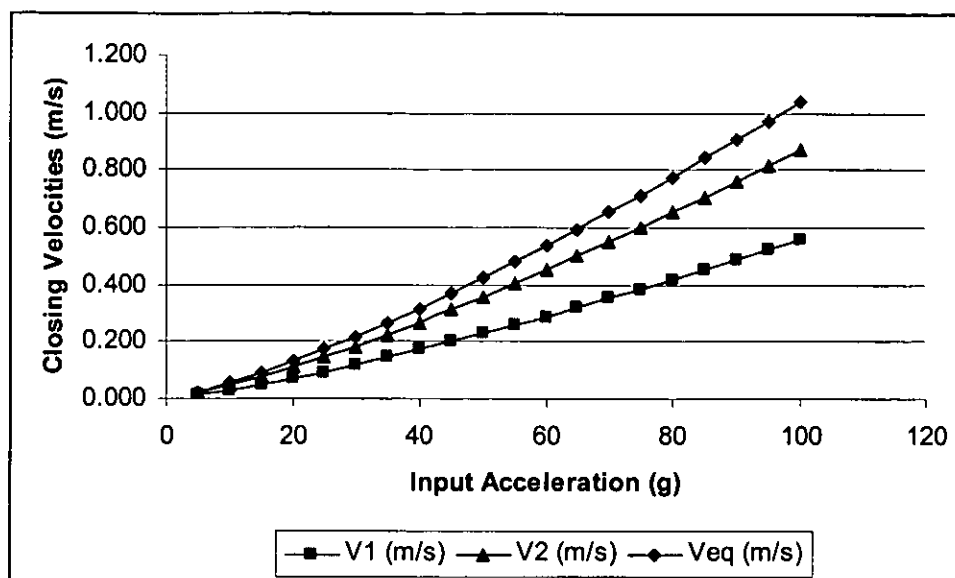


Figure 4.29 Closing velocities for 14-ball complement

4.5.2 Collision Acceleration

This section provides the results for collision acceleration. Note for even are presented having positive acceleration in reality the acceleration is negative i.e. in reality is deceleration. In the first three graphs there are present three lines again. Squares denote the acceleration of the inner ring, triangles the acceleration of the outer ring, and rhombi denote the acceleration of the equivalent body. The last graph of this section shows the proportionality of closing velocity and collision acceleration.

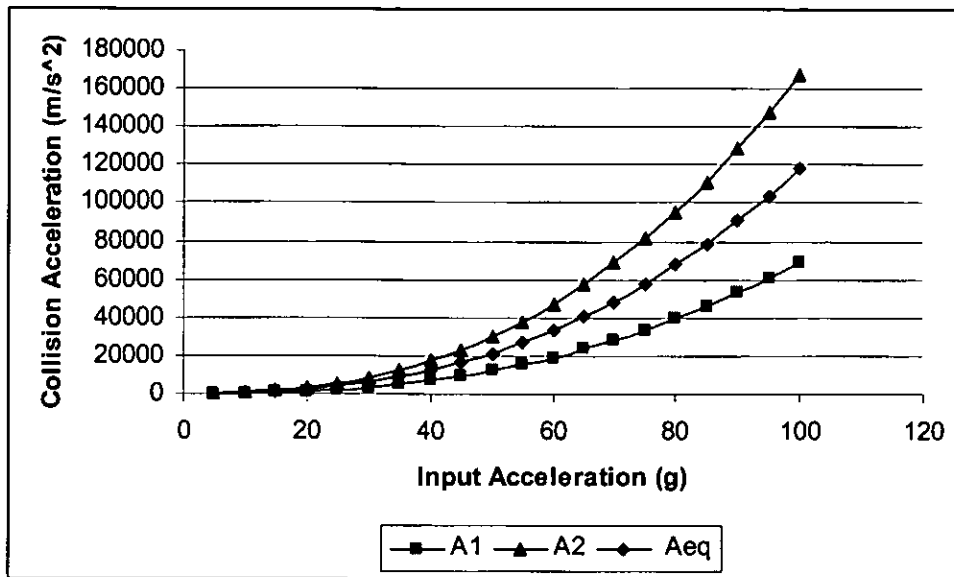


Figure 4.30 Collision Accelerations for 5-ball complement

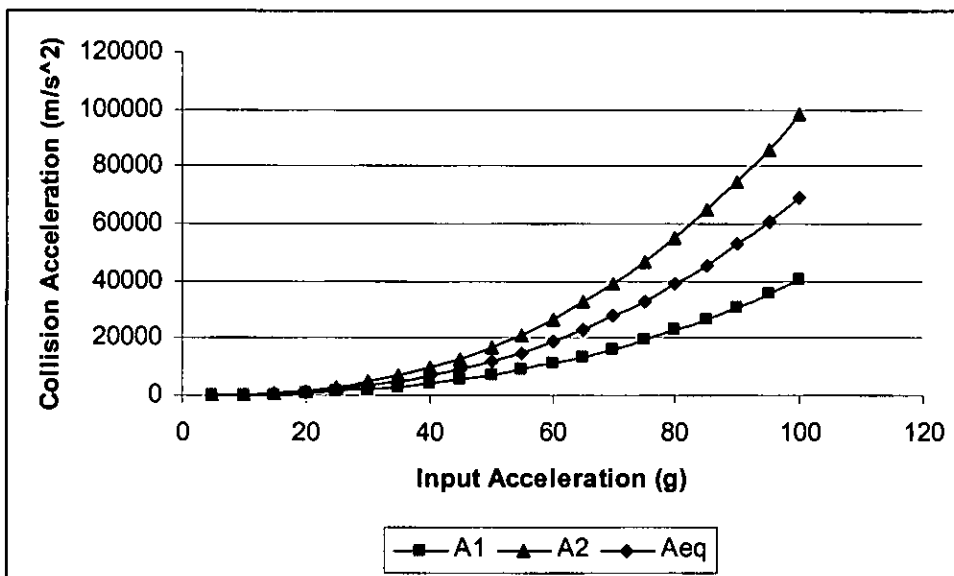


Figure 4.31 Collision Accelerations for 9-ball complement

Since

$$ma = F_1 = K\delta^{3/2} \quad [3.16]$$

a is proportional to $\delta^{3/2}$

so, the shape of the graph explained since the acceleration follows the 3/2 rule

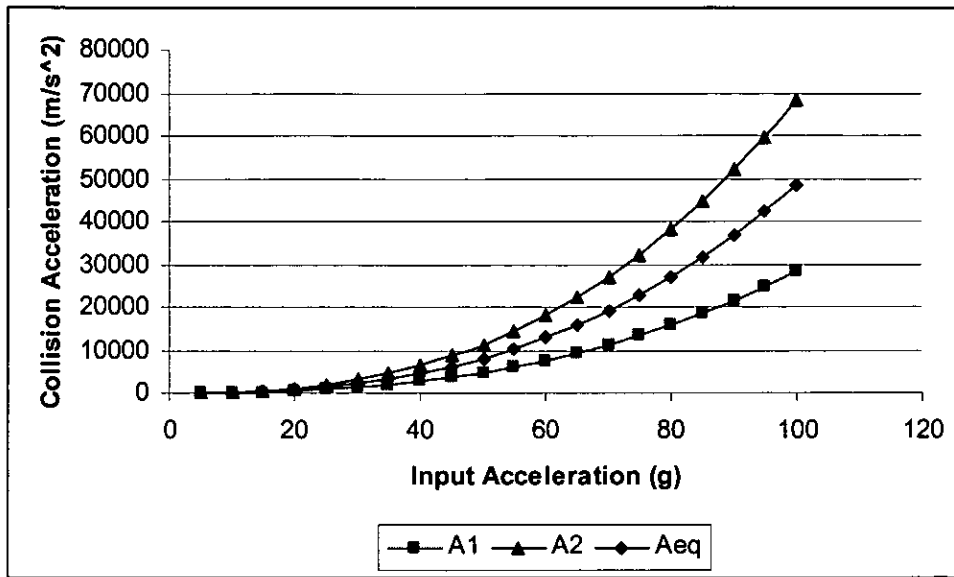


Figure 4.32 Collision Accelerations for 14-ball complement

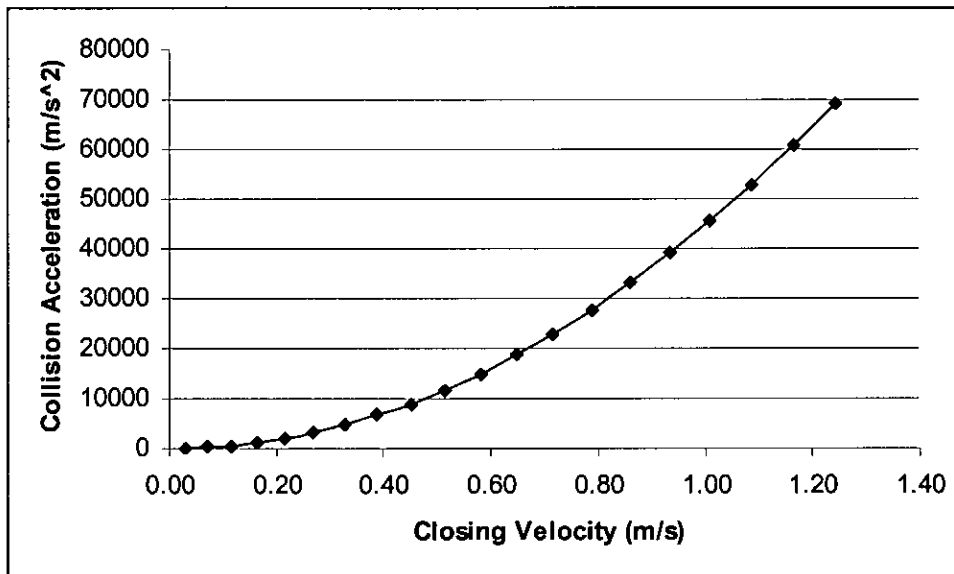


Figure 4.33 Equivalent Closing velocity – Equivalent Collision Acceleration for 9-ball complement

4.5.3 Impact Force

The following graphs present the Impact Force for the different ball complements. The graphs obtained by using the equivalent acceleration. The reason that the graphs for the

Impact Force produced by using the Collision Accelerations obtained considering the movements of the inner and outer rings, is that they give almost identical graphs with those presented. That it can be seen on the spreadsheet following. On figures 4.34 and 4.35 squares, triangles and rhombi denote the obtained results for 5, 9, and 14-ball complement respectively. Figures 4.37 and 4.38 shows the proportionality of collision acceleration and closing velocity to the impact force. The values at 90g and above are excessively high due to the reduced ball complement and the assumption of 2.8 μ m nominal approach.

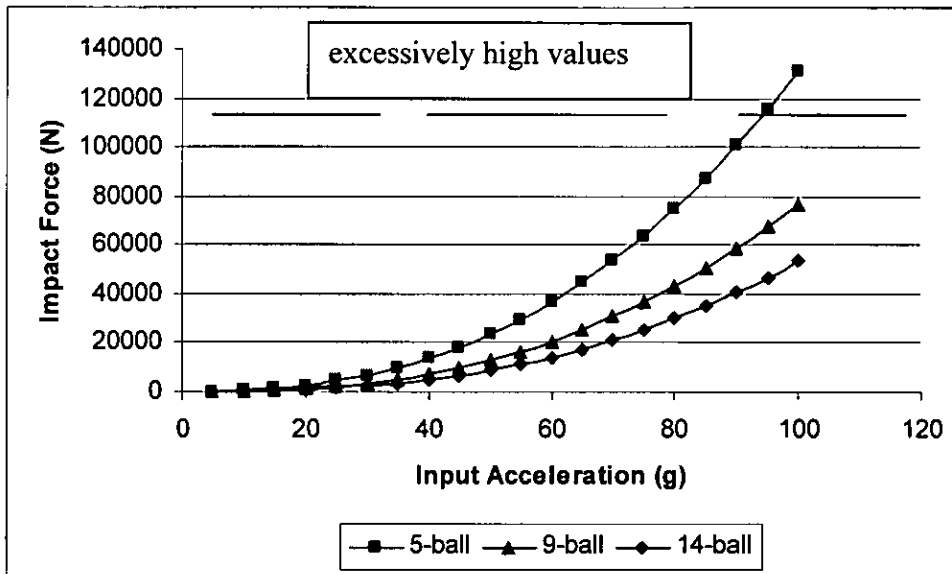


Figure 4.34 Input acceleration – Impact force graph for 5, 9 and 14-ball complement

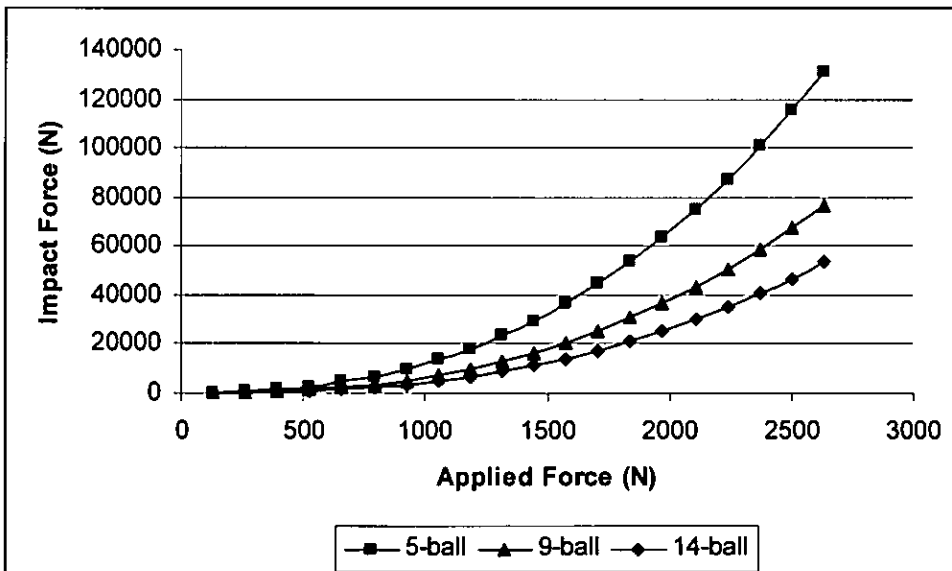


Figure 4.35 Applied Force – Impact force graph for 5, 9 and 14-ball complement

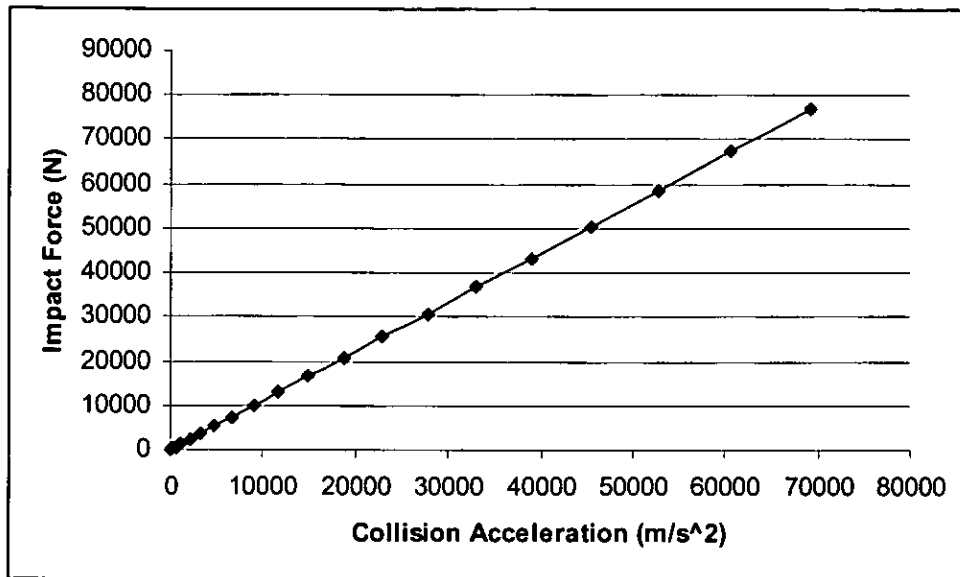


Figure 4.36 Equivalent Collision Acceleration – Impact force for 9-ball complement

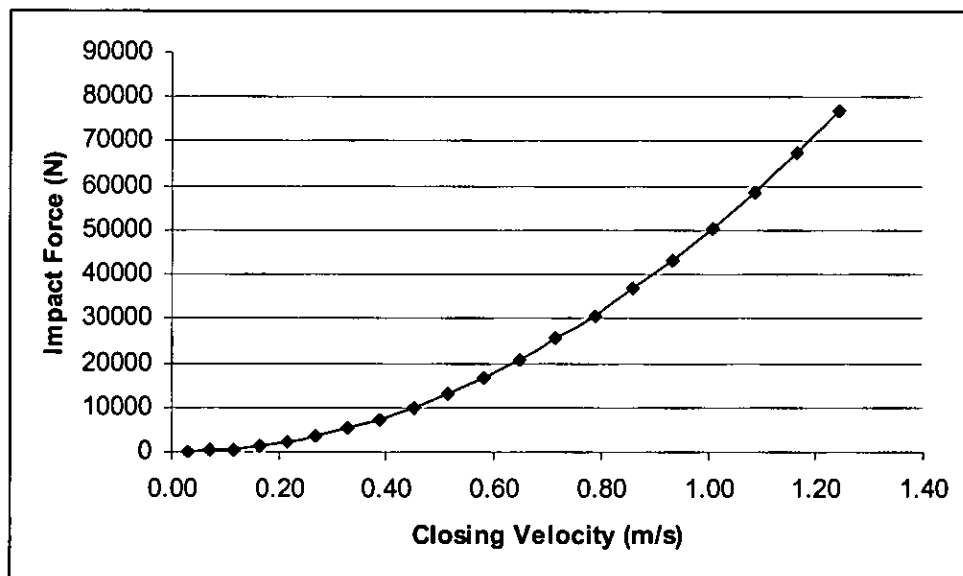


Figure 4.37 Equivalent Closing Velocity – Impact force for 9-ball complement

4.5.4 Hertzian stress

The results for the Hertzian contact stress presented in this section for the different ball complements. At the first two graphs squares, triangles and rhombi denote the obtained results for 5, 9, and 14-ball complement respectively. The last two graphs show the

proportionality of the impact force and collision acceleration to the maximum Hertzian contact stress.

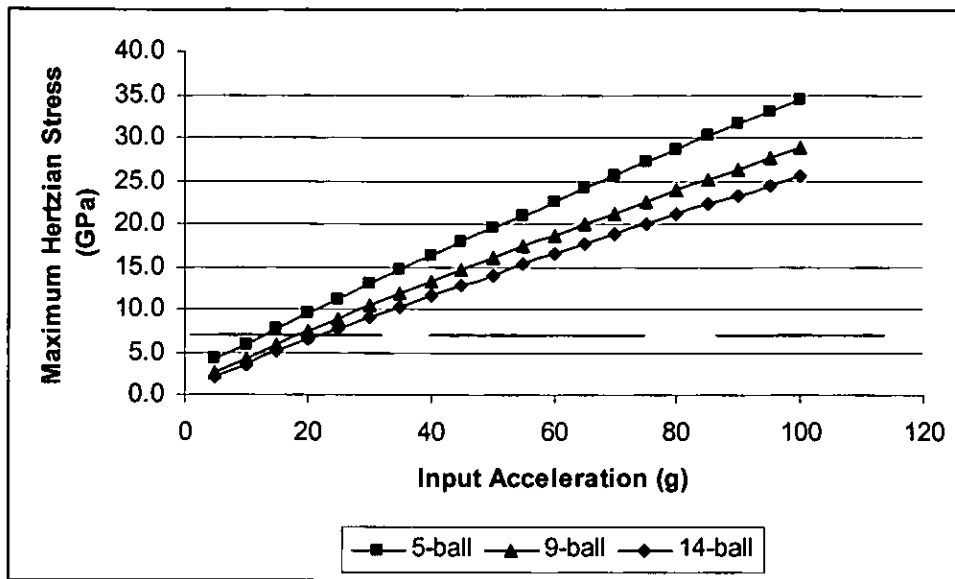


Figure 4.38 Input Acceleration – Maximum Hertzian Stress

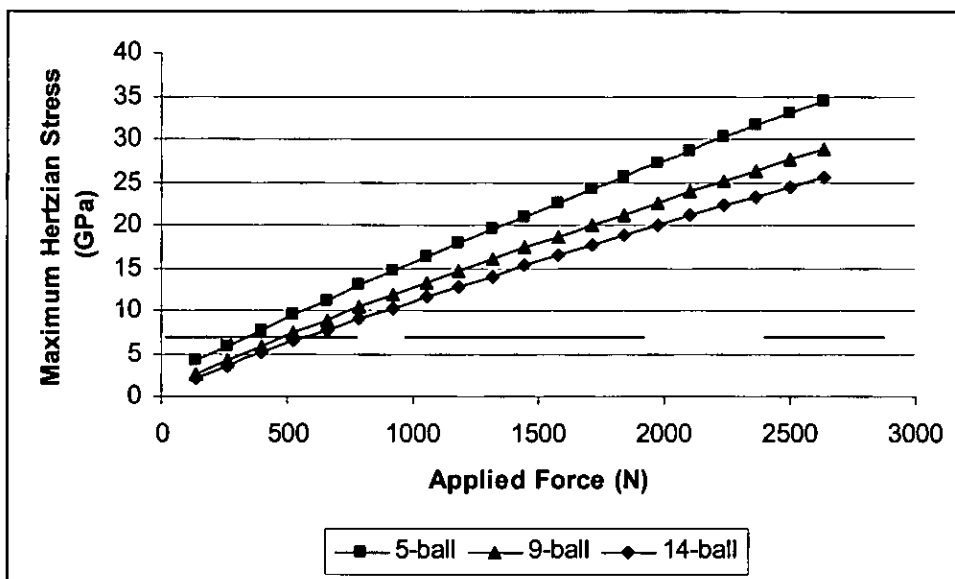


Figure 4.39 Applied Force – Maximum Hertzian Stress

The values of the maximum stress for higher input values cannot be expected in real conditions, and occurred here due to the reduced ball complement and the assumptions followed on the method.

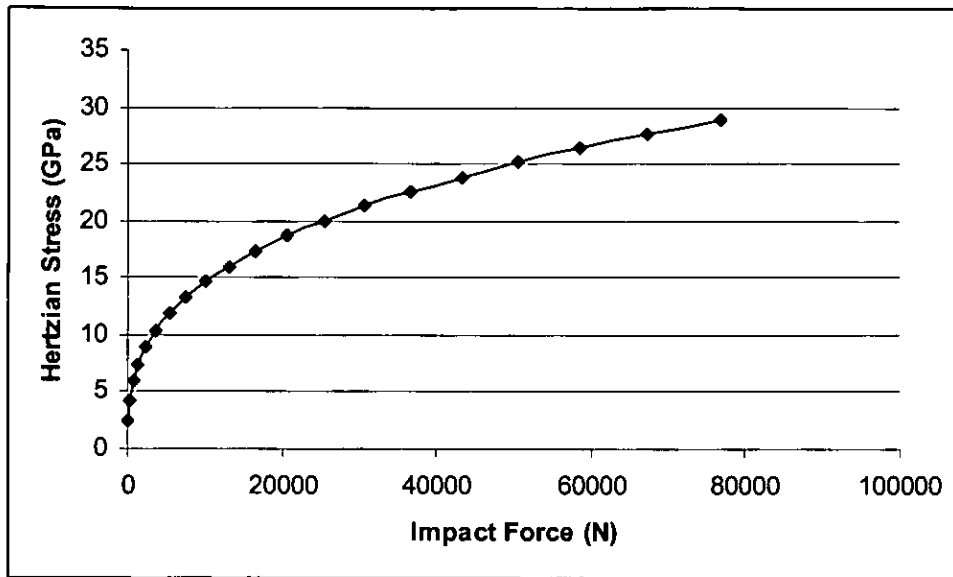


Figure 4.40 Impact Force- Maximum Hertzian Stress for 9-ball Complement

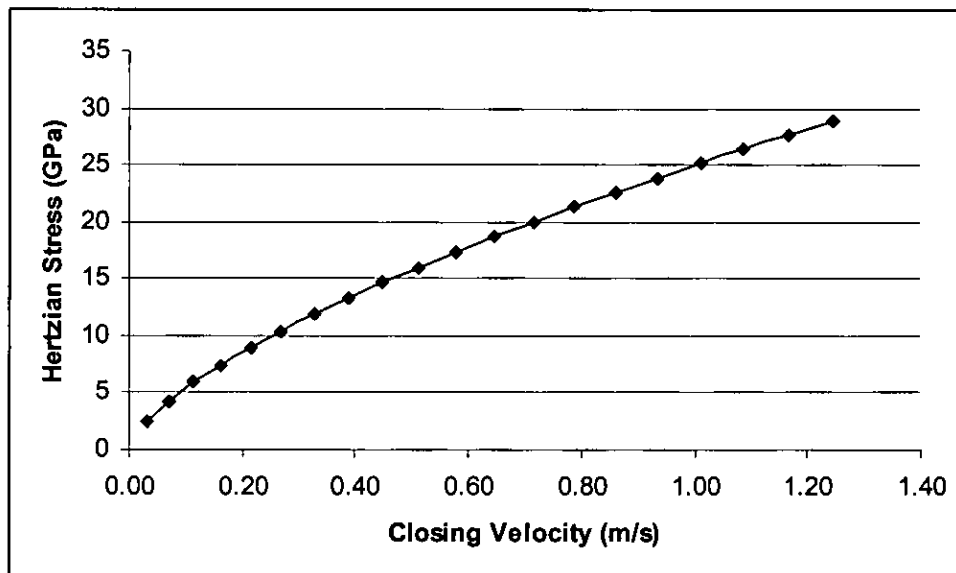


Figure 4.41 Equivalent Closing Velocity – Maximum Hertzian Stress for 9-ball complement

Chapter 5

5 Discussion

This Chapter is a discussion on the results presented on the previous chapter. The theoretical gapping results compared with measured values obtained in previous studies and the comparisons show the validity of the CABARET and non-linear gapping predictions. Also experimental investigations of indentation damage from previous studies used to verify the Hertzian stress calculations and therefore the method used to describe the impact Force between balls and rings.

5.1 Gapping prediction comparison

5.1.1 Constant load

In this section the results presented on the previous chapter for constant loads, compared with the measurement values obtained on previous program of studies as stated on the third chapter. Rhombi on the graphs denote the CABARET gapping prediction, squares the non-linear gapping prediction and triangles the measured values. The mean measured gap is the average of the two measurements. Note that the line on the measured values is only for clarification purposes. Also the measurements around the natural frequency present significant difference in comparison with the other frequencies. The natural frequency for 5-ball complement is 270Hz, for 9-ball is 356 Hz, and for 14-ball is 444Hz.

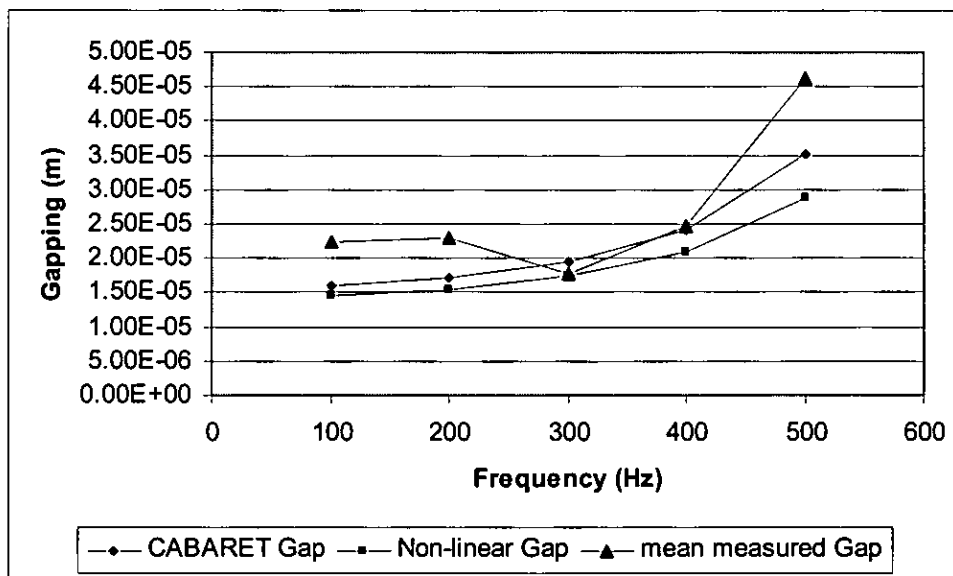


Figure 5.1 Gapping comparison for 5-ball complement at 20g

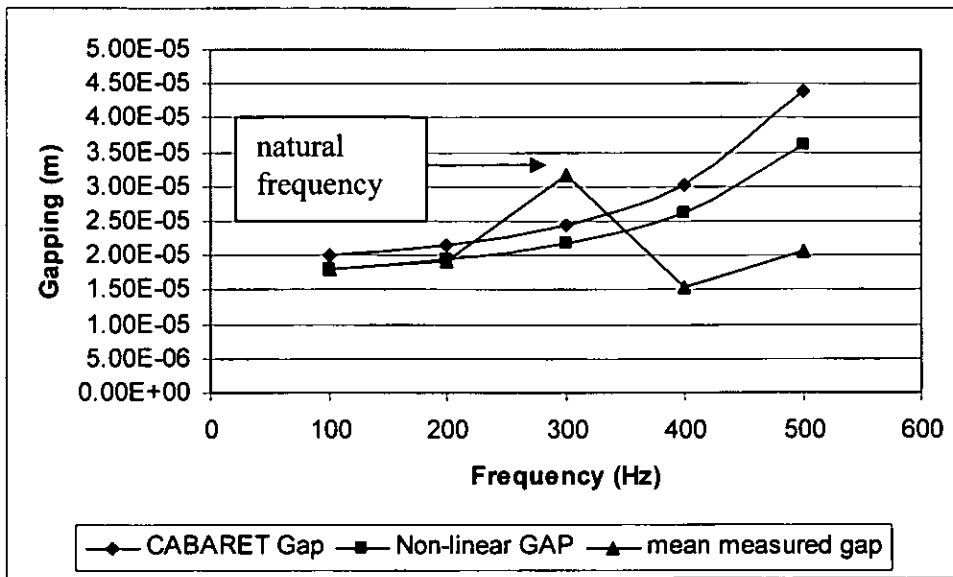


Figure 5.2 Gapping comparison for 5-ball complement at 25g

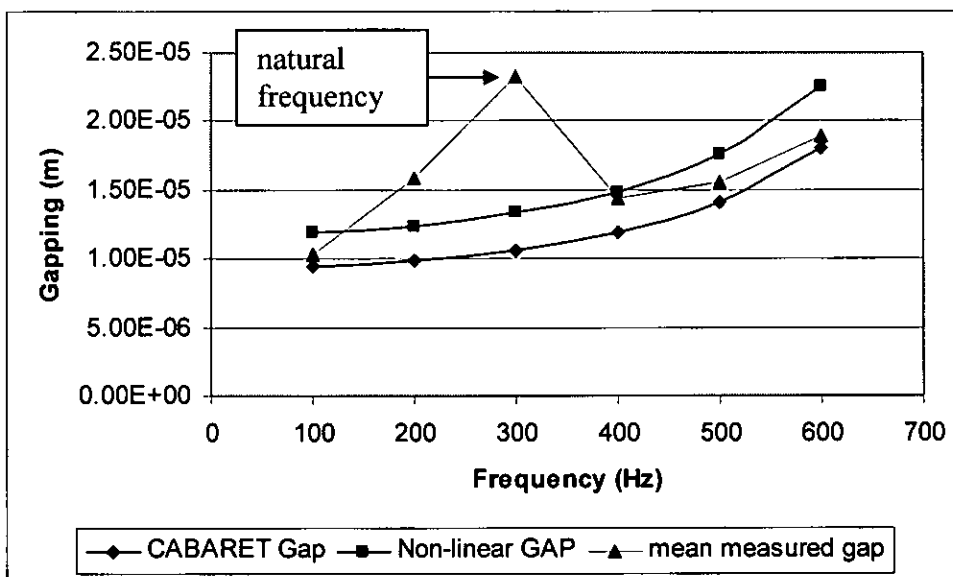


Figure 5.3 Gapping comparison for 9-ball complement at 25g

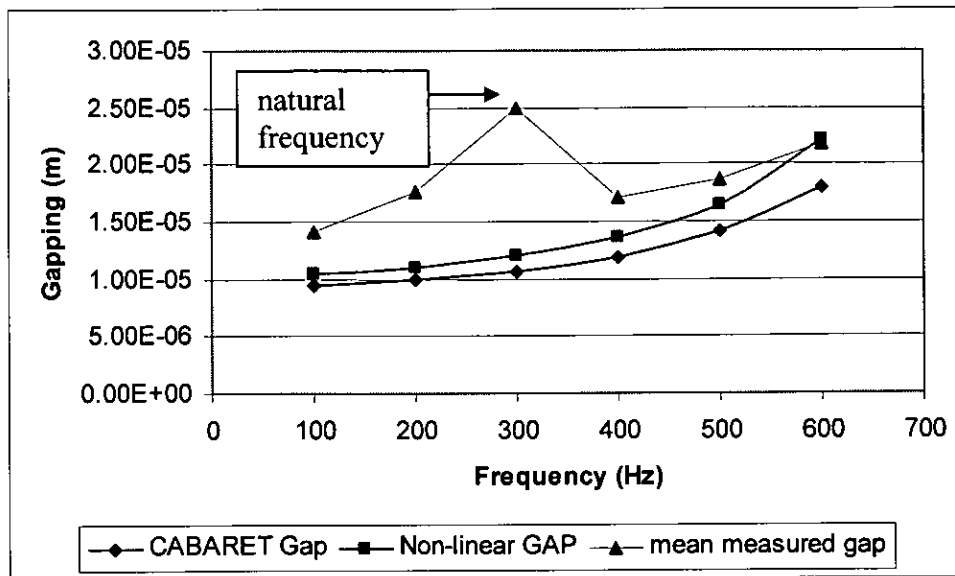


Figure 5.4 Gapping comparison for 9-ball complement at 30g

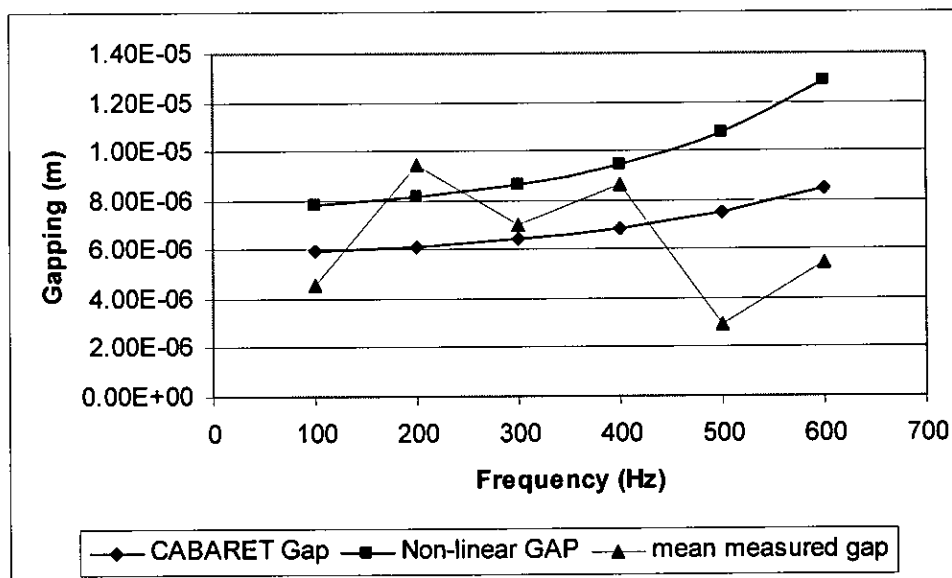


Figure 5.5 Gapping comparison for 14-ball complement at 20g

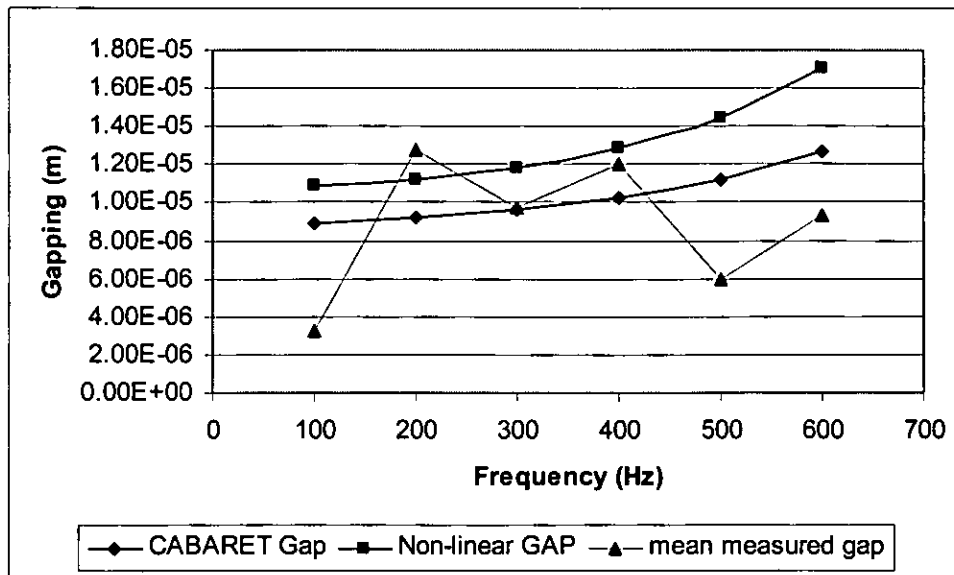


Figure 5.6 Gapping comparison for 14-ball complement at 30g

From the above graphs no safe conclusion could be extracted, on whether the CABARET or the non-linear stiffness produces more accurate gapping predictions. At the test frequencies from 100 to 600 Hz for input acceleration of 20, 25 and 30g they seem to provide results of similar accuracy.

5.1.2 Constant Frequency

5.1.2.1 500 Hz Frequency

This section compares the obtained results between the prediction using CABARET and the one using non-linear stiffness. Since measured results exist only for 9-ball complement, the comparison of the two predictions for 5 and 14 ball complement is on the basis of observing the relative behaviour of the graphs. For the 9-ball complement where measured results are available, the comparison of the predictions is with respect to the measured values.

5.1.2.1.1 5-ball complement

The two predictions (using CABARET and non-linear stiffness) presented on graph

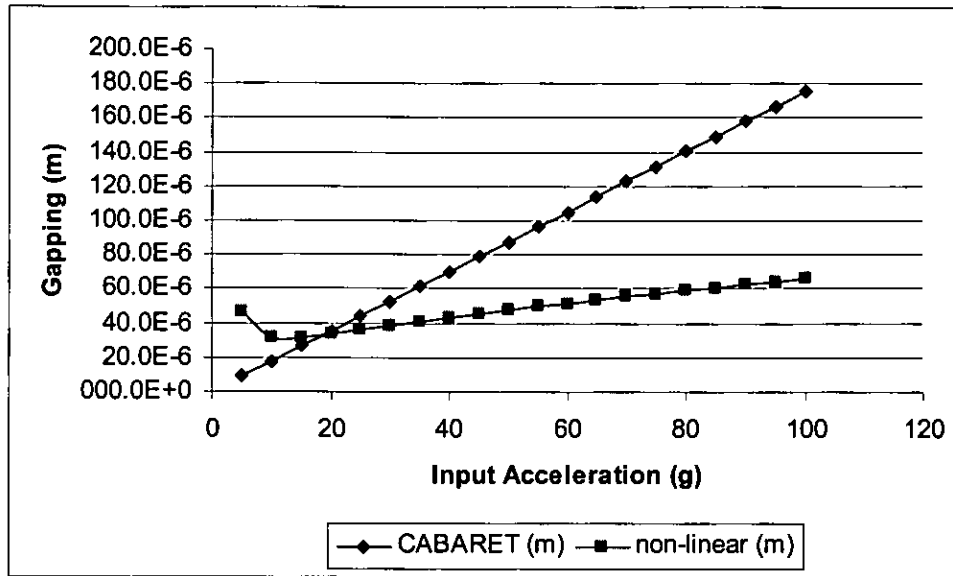


Figure 5.7 Input Acceleration – Gapping Prediction Graph for 5-ball complement at 500 Hz

By the observation of the graph it can be seen that at low acceleration levels the prediction using non-linear stiffness provides higher gapping levels than the prediction using CABARET stiffness, the two predictions matching on acceleration levels around 25g and for higher acceleration levels the non-linear prediction provides significantly lower gapping levels than CABARET.

5.1.2.1.2 14-ball complement

The two predictions (using CABARET and non-linear stiffness) presented on graph

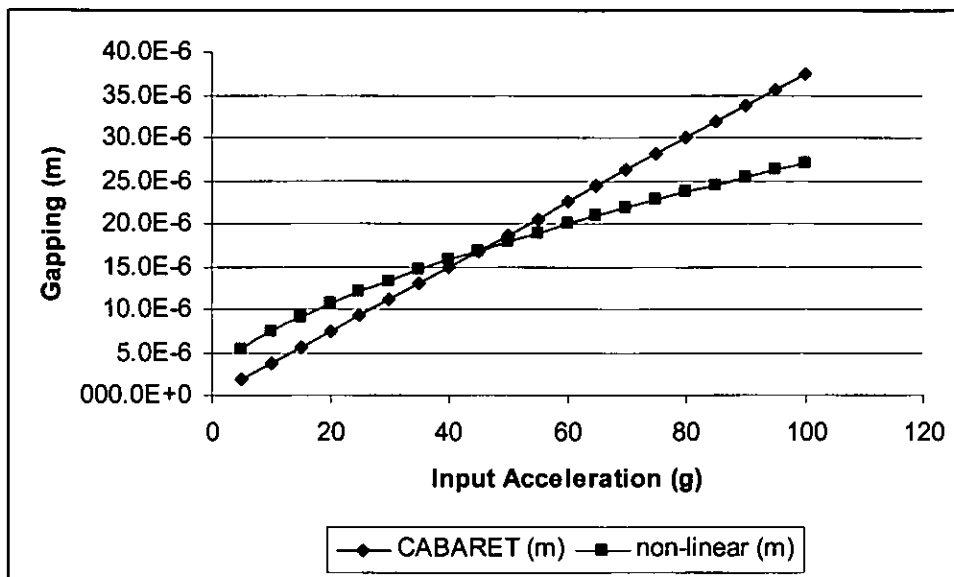


Figure 5.8 Input Acceleration – Gapping Prediction Graph for 14-ball complement at 500 Hz

The observation of the graph leads to the same conclusions as with the 5-ball complement. The difference is that the acceleration level that the two predictions matching is around 45g. Below that acceleration level Non-linear predictions are higher while above that level CABARET predictions are higher.

5.1.2.1.3 9-ball complement

The investigation of the 9-ball case is the most interesting, because measured results are available and therefore can be compared with the predicted values.

Table 5.1 shows the two series of measurements along with their mean value.

Input acceleration (g)	Measured Gap 1 (m)	Measured Gap 1 (m)	Mean Measured Gap (m)
1	5.30E-07	9.00E-07	7.15E-07
8	9.26E-06	7.05E-06	8.16E-06
15	1.09E-05	1.27E-05	1.18E-05
30	2.07E-05	2.10E-05	2.09E-05
45	2.82E-05	3.14E-05	2.98E-05
50	2.80E-05		2.80E-05
57		3.03E-05	3.03E-05
85	3.95E-05	3.55E-05	3.75E-05
100	4.85E-05	4.04E-05	4.45E-05

Table 5-1 Measured gapping for 500 Hz frequency

Figure 5.9 shows the Non-linear and CABARET gapping predictions along with the two sets of measured values.

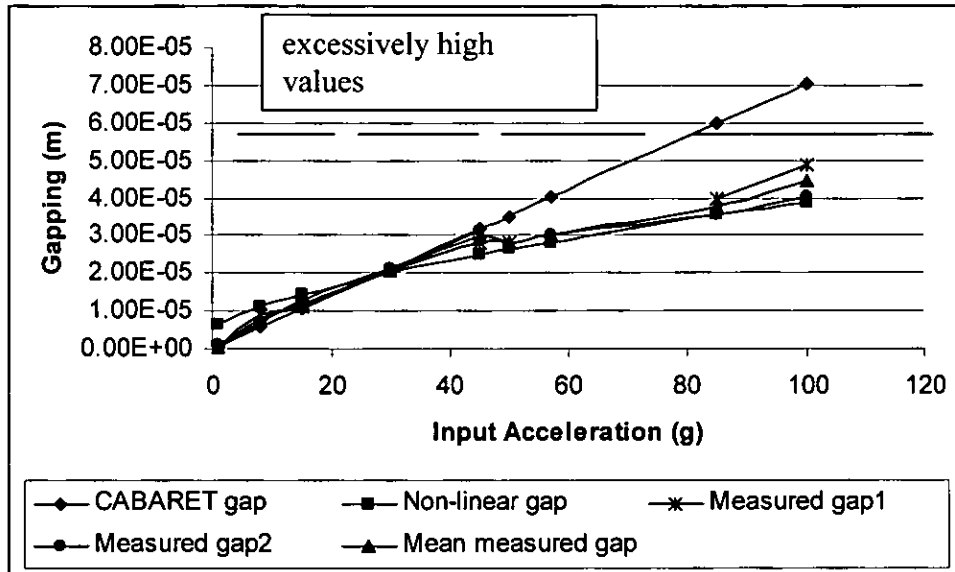


Figure 5.9 Gapping comparison for 9-ball complement at 500 Hz

Figure 5.10 shows the Non-linear and CABARET gapping predictions along with the mean measured values.

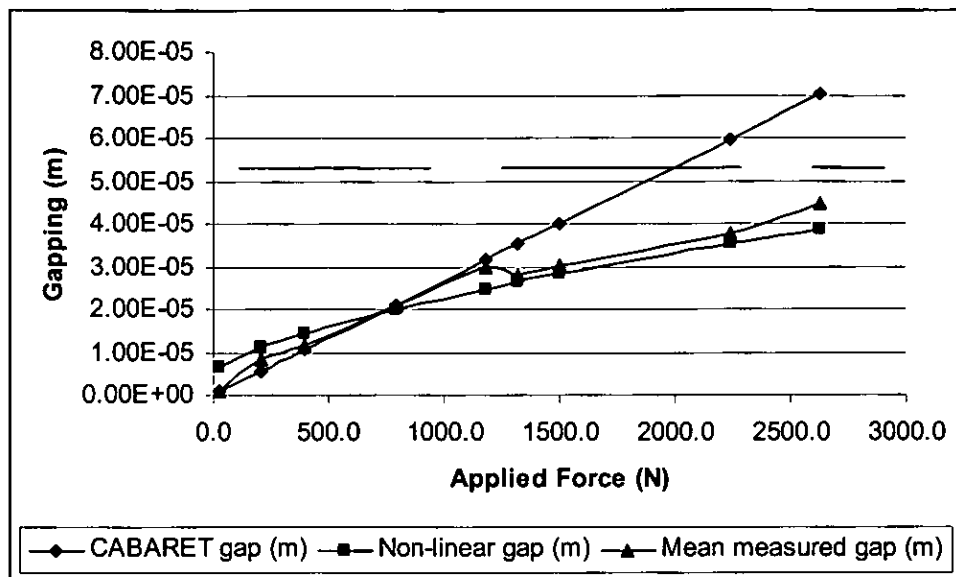


Figure 5.10 Gapping comparison for 9-ball complement at 500 Hz (mean measured gap values)

From the previous two graphs it can be seen that the non-linear prediction is clearly more accurate through the test range. This can be seen even more clearly in the following graphs. Graphs show the absolute error between the CABARET and the Non-linear prediction with the measured results. With the term absolute error meant the absolute difference between Predicted and measured values. Rhombi denote the absolute error between CABARET gapping prediction and the measurement series values, while the squares denote the absolute error between the non-linear gapping prediction and the measurement series values.

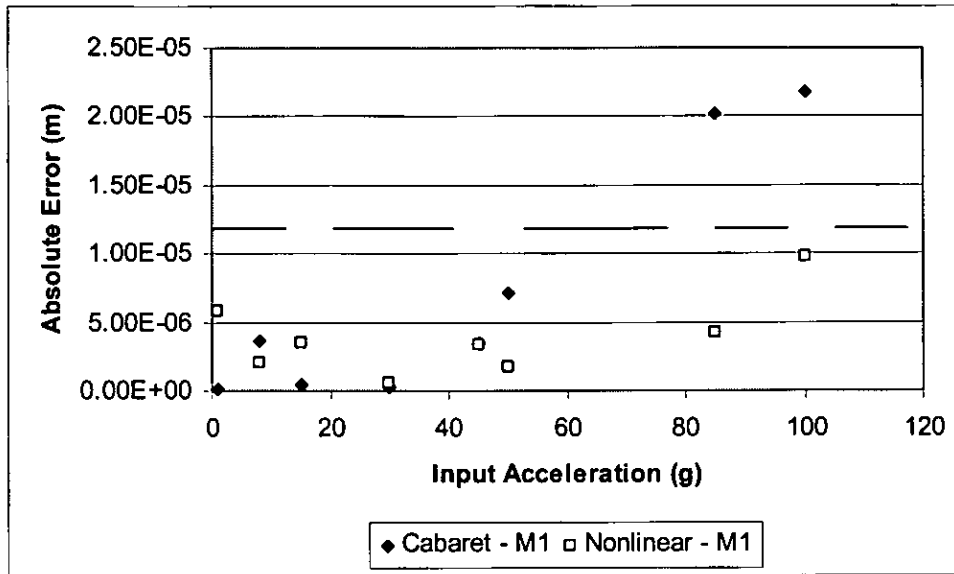


Figure 5.11 Absolute error between predicted values and test results of measurement 1

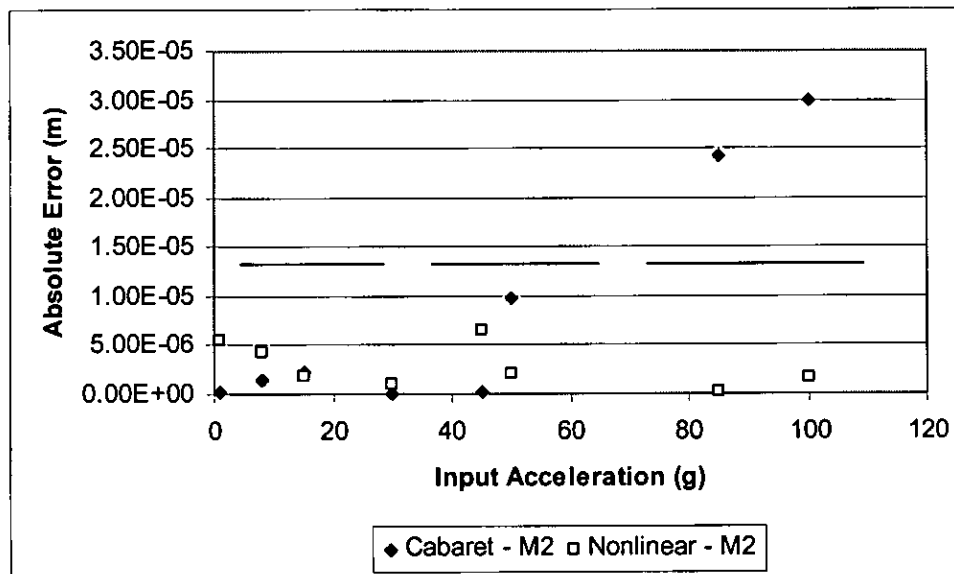


Figure 5.12 Absolute error between predicted values and test results of measurement 2

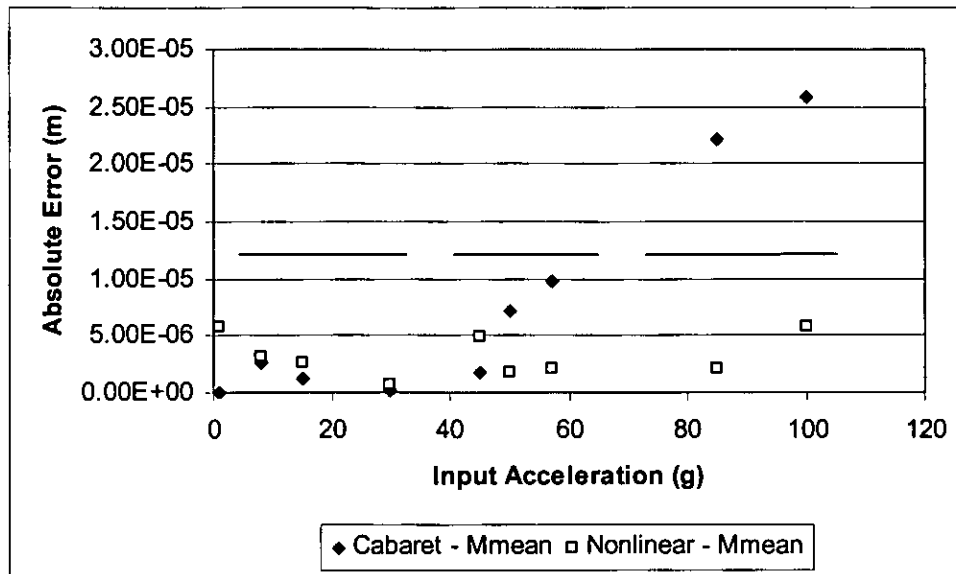


Figure 5.13 Absolute error between predicted values and mean value of the two measurements

The following graphs show the percentage error of the predictions. The error is calculated by:

$$\%error = \frac{theoretical - measured}{theoretical} \times 100$$

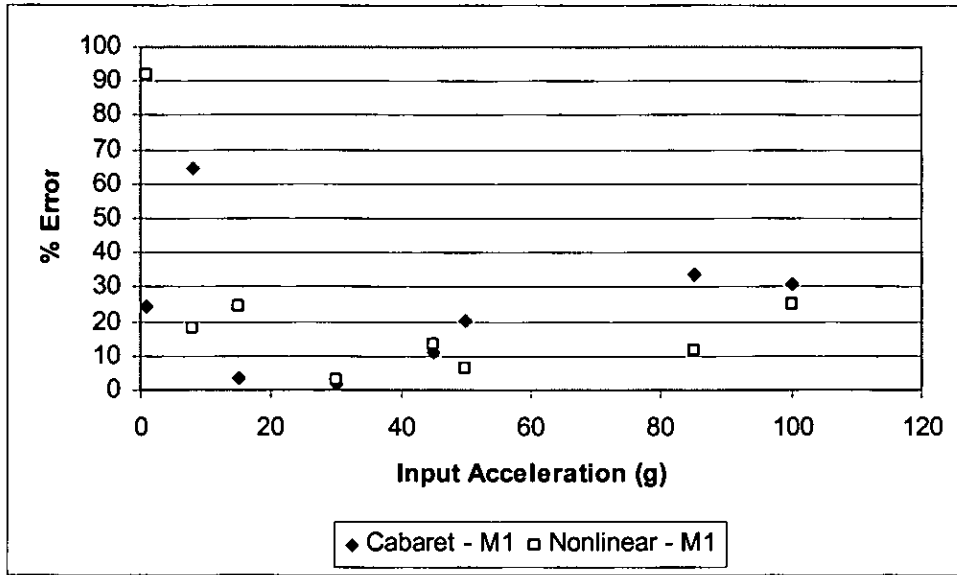


Figure 5.14 %Error between predicted values and test results of measurement 1

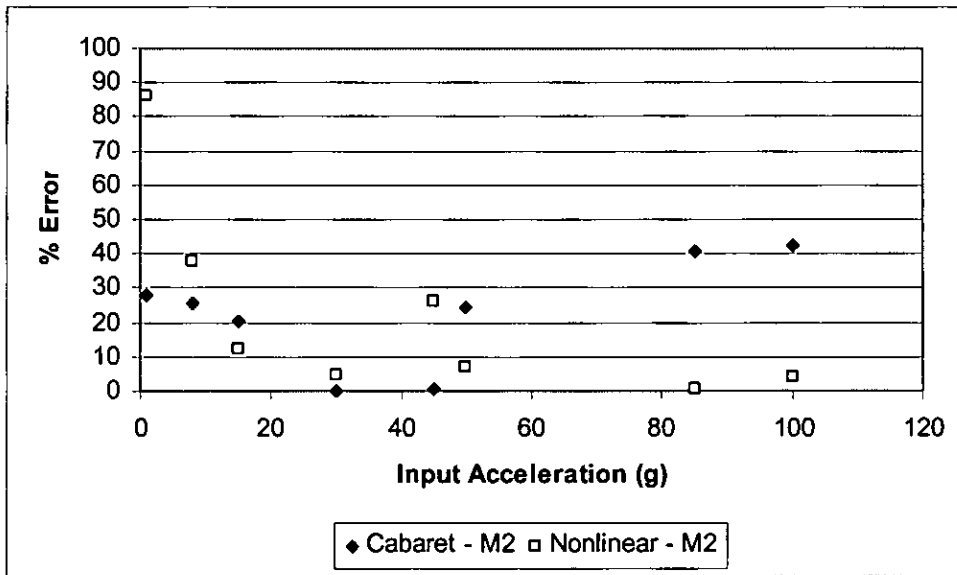


Figure 5.15 %Error between predicted values and test results of measurement 2

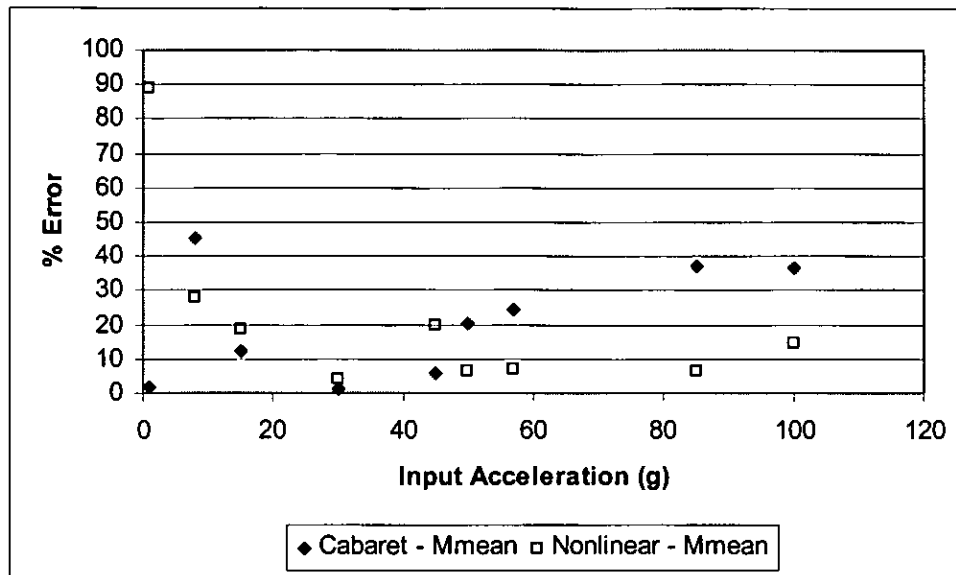


Figure 5.16%Error between predicted values and mean value of the two measurements

From the above graphs it is clear that the non-linear prediction is significantly more accurate than the CABARET prediction. The only acceleration value, where the non-linear prediction is totally inaccurate is for the input acceleration level of 1g. But this is not very important since the gapping levels at that low acceleration levels are very low too. In high acceleration levels (i.e. high load levels) where high gapping levels occur the non-linear prediction finds satisfactory accuracy, much better than the CABARET prediction previously used. Between the acceleration levels of 8g and 45g both predictions find similar accuracy. This explains why no conclusion could be made in previous section of this chapter where the two methods compared at 20g, 25g and 30g with measured results in a frequency range of 100 to 600 Hz.

5.1.3 1500 Hz Frequency

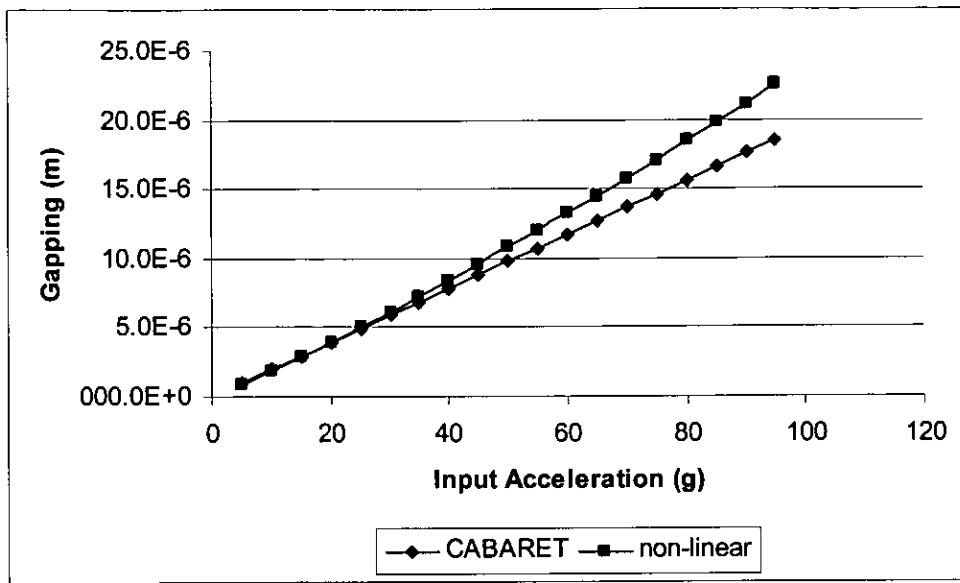


Figure 5.17 Input Acceleration – Gapping prediction graph for 5-ball complement at 1500 Hz

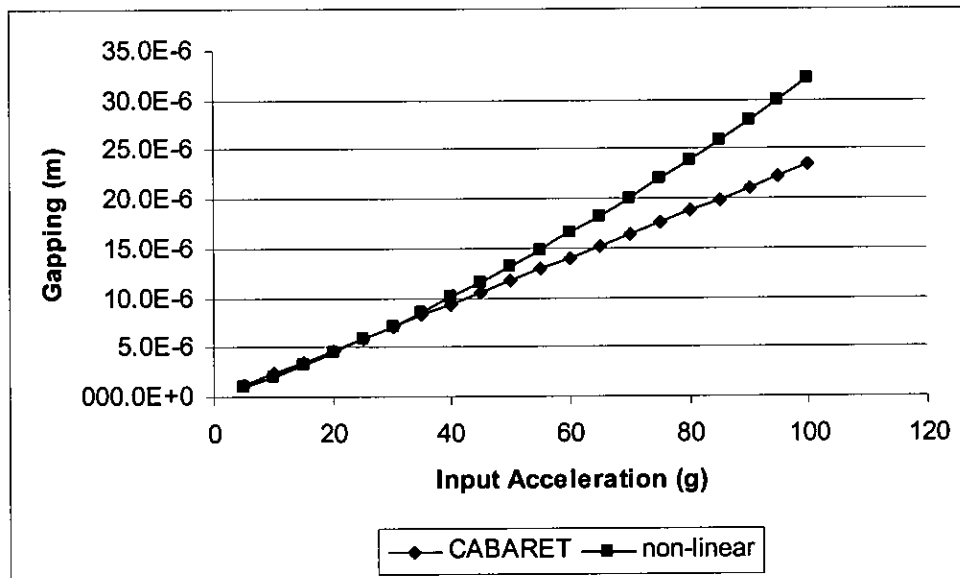


Figure 5.18 Input Acceleration – Gapping prediction graph for 9-ball complement at 1500 Hz

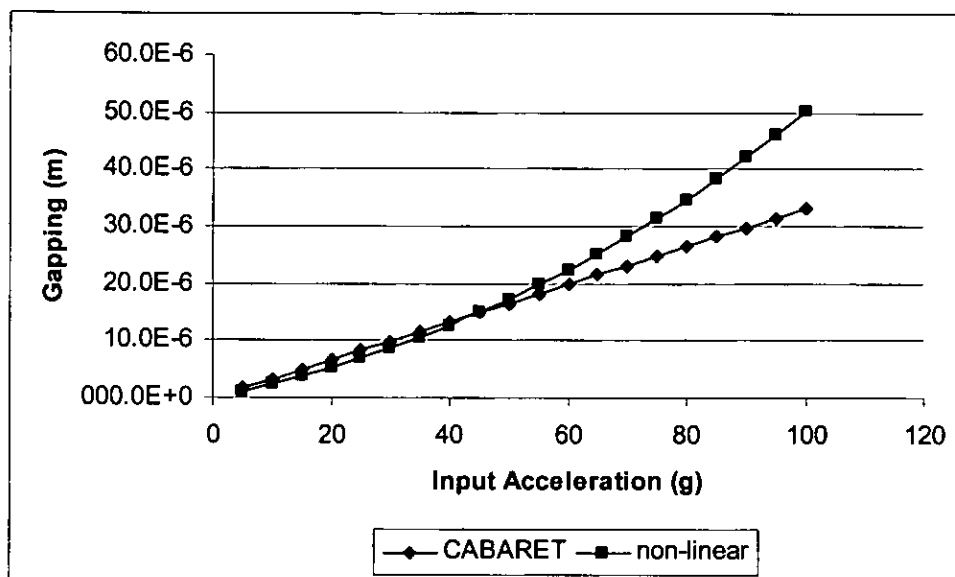


Figure 5.19 Input Acceleration – Gapping prediction graph for 14-ball complement at 1500 Hz

5.1.4 2000 Hertz frequency

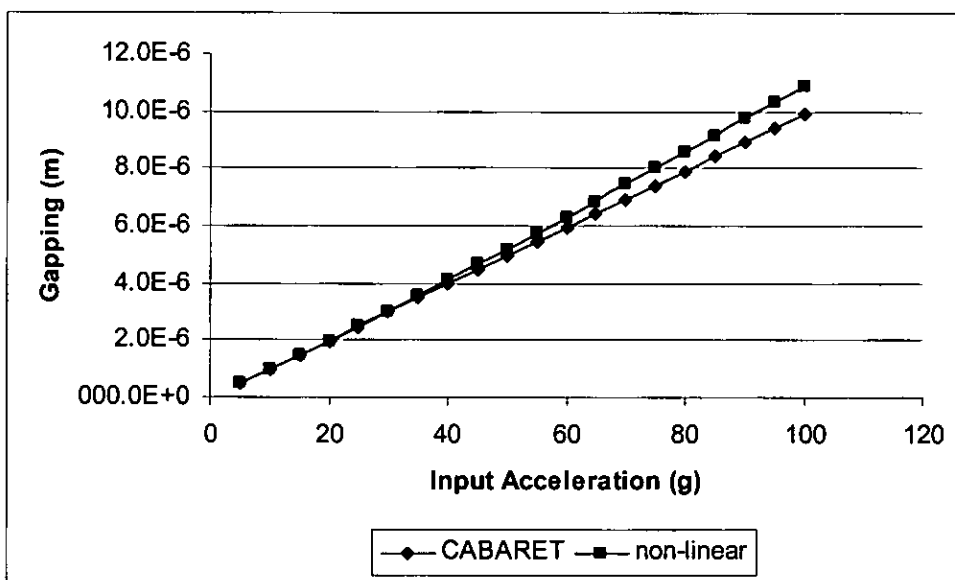


Figure 5.20 Input Acceleration – Gapping prediction graph for 5-ball complement at 2000 Hz

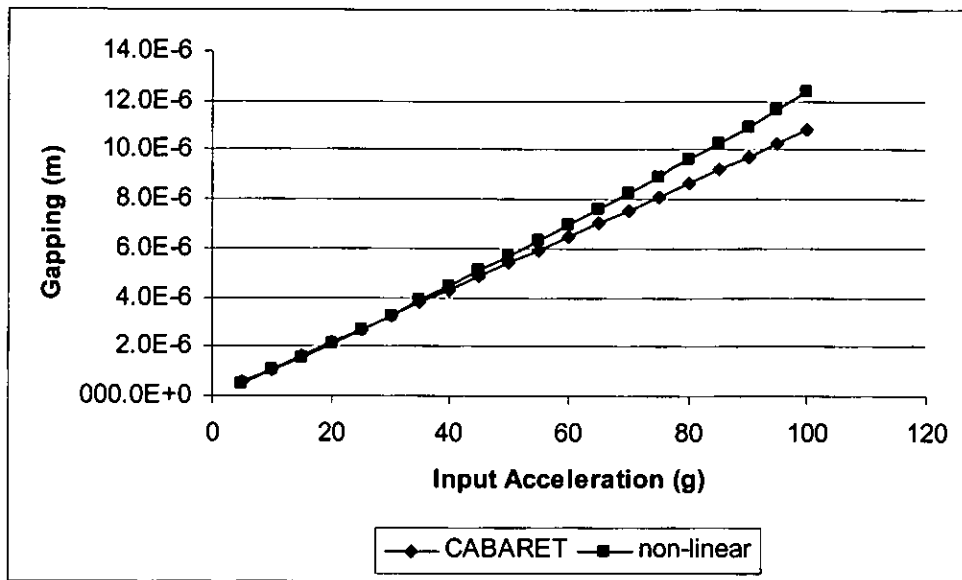


Figure 5.21 Input Acceleration – Gapping prediction graph for 9-ball complement at 2000 Hz

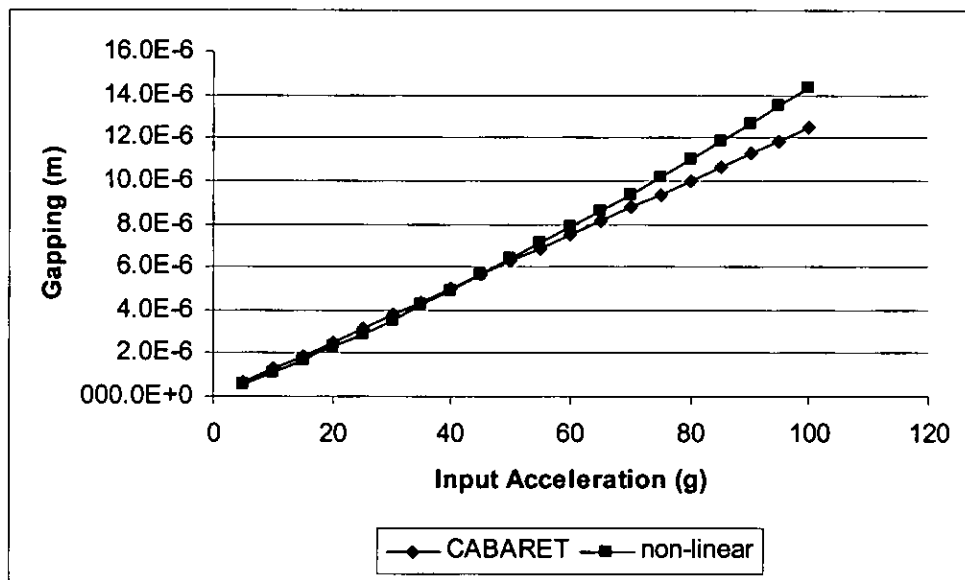


Figure 5.22 Input Acceleration – Gapping prediction graph for 14-ball complement at 2000 Hz

By observing the above graphs it can be seen that at 1500 and 2000Hz the predictions up to accelerations of 50 g, matching well. After reaching this acceleration value the prediction using the non-linear stiffness provides clearly higher gapping levels. That applies for all

three ball complements examined. The second observation also examining figures 4.20 to 4.23 (previous chapter) is that unlike for 500 Hz frequency where larger ball complement implies lower gapping levels, at 1500 and 2000 Hz larger number of balls mean higher gapping levels.

The question which arises from a designer's point of view is how many balls should be selected in a particular bearing. The analysis up to 500 Hz shows that the maximum number of balls that can be used will contribute to low gapping levels. But the analysis of the results for high frequency levels reverses the conclusions. Therefore, the selection of the maximum ball complement seems not to be the ideal solution. The ideal solution lay somewhere in the middle between the maximum and minimum ball complement could be used. That is what can be derived from the available gapping predictions, but since there are experimental results only for 500 Hz, experimental data needed for higher frequencies to verify these observations.

5.2 Collision between ball and rings

The movement of the two rings could be described accurately by the use of an equivalent object covering a distance equal to the sum of the distance covered by the inner and outer rings. This conclusion arises from the fact that the method of the equivalent object produces identical results for the Impact Force with the method of working with the movement of one cage. The whole method is based on the conservation of mechanical energy and the laws of motion. Of course the assumptions include no mechanical energy loss, something that is not true in any real condition, but it is believed that the general approach is satisfactory.

Analysing the results it is clear that the Impact Force is proportional to the closing velocity as it can be seen on figure 4.37. That implies the Impact force is proportional to the gapping level, something expected from equation [3.16].

The calculation of the Hertzian stress showed that the Hertzian stress is higher for lower ball complements. That is true for the 500 Hz where lower ball complements lead to higher gapping levels. The acceleration levels where each ball-complement exceeds the limit of 4.2 GPa where indentation is present are 5g for the 5-ball complement, 10g for the 9-ball complement, and 12g for the 14 ball complement.

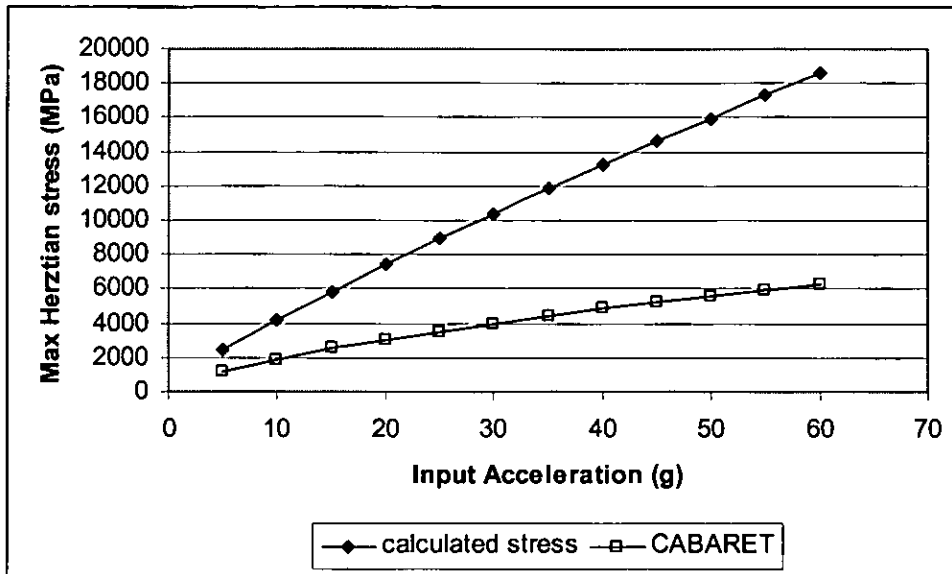


Figure 5.23 Calculated and CABARET maximum Hertzian stress for 9-ball complement at 500 Hz

Figure 5.23 shows the calculated stress along with the CABARET stress for 9-ball complement. The CABARET values presented on the graph are the only values available therefore the comparison is based on these values. As it can be seen the maximum stress calculated is much greater than the CABARET stress, and the difference increasing with the increase of input acceleration.

Investigations made by Lewis in a previous program of studies, as mentioned in chapter 3, showed that indentations caused at acceleration levels lower than 45 g where according to CABARET the Hertz stress reaches the value of 5.2 GPa. A reasonable assumption is that these indentations resulted from vibration at 30 g (Sochting et al, 2004). Having in mind that the indentations are visible for stresses greater than 5.5-6 GPa it is clear that the calculated on chapter 4 stress is more realistic than CABARET stress which is underestimated, at least for the input accelerations used on the mentioned tests.

Chapter 6

6 Conclusions and recommendations

This chapter contains the conclusions of the thesis, as for the work completion , identifies possible sources of error and provides recommendations for further work.

6.1 Summary of the work completed

As stated in the introductory chapter of the thesis the aims of the current project were:

- To introduce of non-linear stiffness into the existing 2-DOF model in order to predict gapping
- To develop a method that evaluates the Impact Force generated between the ball and the rings in an angular contact bearing, in order to calculate the Hertzian contact stress.

The first aim was completed as the non-linear stiffness was introduced into an existing 2-DOF model. The gapping predictions made using the non-linear stiffness proved more accurate than the method used previously (gapping predictions using CABARET stiffness), when compared with the existing measured gapping values, for the test data range. Therefore the initial assumption that the introduction of the non-linear stiffness into the prediction model would optimize the gapping predictions, proved to be correct.

The second aim to evaluate Hertzian contact stress was completed by the use of the conservation of energy laws and Newton's laws of motion. That implies the analysis of the bearing rings, with evaluation of the velocity with which they collide with each other, and the deceleration from the point of collision to the maximum deformation. A model of an equivalent body that simulates the movement of the two rings worked out, and the results showed that it was successful.

The Impact Force results were then used to calculate the maximum Hertzian stress using appropriate formulae for elliptical contacts. The comparison with CABARET stress showed that the stress evaluated by the author was more accurate than CABARET stress, when compared with experimental investigations, for the range of the experimental data.

6.2 Identifying sources of error

On the analysis used on the present thesis a number of assumptions were made. Each assumption is a potential source of error. More specifically:

The bearing is assumed to be subjected to purely axial load. That applies in both the bearing stiffness calculation as well as in the gapping prediction formula. The results then compared to measured values. The test was made in conditions in order to achieve purely axial load but this is not possible and a very small radial load is always present. Therefore the predicted results for purely axial load are compared with measured values of almost purely axial load.

- The 2-DOF model is considered as undamped. Even though in reality it is more likely to be lightly damped. The sources of damping are: the material strain, the friction between sliding surfaces, and the resistance of the fluid. (Sarafin, 1995)
- The contact angle which assumed constant as on the unload condition. This is not true since the contact angle increases with the load.
- The Impact Force evaluation considers no energy loss, even though there are energy losses.
- The conditions are considered to be Hertzian, thus the results do not apply to thin coated solids or lubricated contacts.

6.3 Recommendations for further work

The recommendations for further work divided into two categories. First are the recommendations for the theoretical part and second are the recommendations for experimental work.

Theoretical work

The 2-DOF model proved to provide gapping predictions that have very good agreement with the measured results, since the % error does not exceed the 20 % of the average of the measured values. A further improvement of the model that involves damping could result to even more accurate predictions. Also the introduction of a second spring and the pivotal motion could be examined as factors that could provide further improvement of the model.

The equation used for the gapping prediction is not valid when $1.8\omega^2 = k$ since then the denominator of the formula is zero. Therefore, predictions for such values are not possible. Rearranging the formula for the range of “problematic” values could solve the problem.

One factor that can possibly improve the bearing stiffness calculation is the contact angle. If the change in contact angle considered it may lead to more accurate bearing stiffness values.

On the evaluation of impact force assumed no energy loss. A possible evaluation of the energy losses will result to more accurate values for the impact force.

The calculation of the maximum Hertzian stress is based on the method suggested by Greenwood in 1983, for elliptical contacts. The use of other suggested methods is recommended since a comparison between them may lead to improved accuracy.

6.3.1 Experimental work

Modern science is based on the fact that the theoretical knowledge must be verified experimentally. Therefore, the validity of every theoretical method depends on the

experimental verification. The experimental verification has difficulties since is dependent on the experimental capacity of the instruments.

A large part of the present thesis has been verified by experimental work made by another investigator. For part of theoretically investigated there are no experimental data. Therefore, this part verification cannot yet be accepted as valid since there are not sufficient experimental data for verification.

The gapping measurements for constant input acceleration i.e. constant applied load. Experimental results exist only for frequencies up to 600 Hz and input acceleration of 30g. Gapping measurements for constant frequency exist only for the frequency of 500 Hz. Therefore, the validity of the method is verified only for that data range. Gapping measurements for frequencies up to 2 MHz where is the maximum vibration frequency in space applications and input acceleration up to 100g would be valuable as they would permit verification of the method for a broad range of the conditions expected in space applications.

References

- Arnell, R.D., Davies, P.B., Halling, J. & Whomes, T.L. (1991) Tribology - Principles and Design Applications, MacMillan Education, 1st edition*
- Bhushan, B., Gupta, B.K. (1991) Handbook of Tribology - Materials, Coatings, and Surface Treatments, MacGraw-Hill*
- ESTL, (1996) Tribology for spacecraft, Lecture*
- ESTL, (1997), Space Tribology Handbook, AEA Technology*
- Fusaro R.L., (1991), Tribology Needs for Future Space and Aeronautical Systems, NASA TM 104525*
- Fusaro R.L., (1994), Lubrication of Space Systems, NASA TM 106392*
- Greenwood J.A., (1985), Formulas for moderately elliptical Hertzian contacts, Journal of tribology, October 1985, vol 107, pages 501-504*
- Greenwood J.A., (1997) Analysis of elliptical Hertzian Contact, Tribology International, Volume 30, Issue3, March1997,Pages235-237*
- Haltner A.J, Flom D.G., (1983), Lubrication in space, CRC handbook of lubrication : (theory and practice of tribology). Vol.1, CRC Press*
- Harris T.A, (1966), Rolling Bearing Analysis, Wiley, 1st edition*
- Johnson K.L, (1989), Contact Mechanics, Cambridge University Press, First paperback reprinted edition*
- Lewis S. D., Sochting S., Effects of axial vibration-induced gapping on angular contact bearing torque performance, (2002), ESA-ESTL-TM 0006*

Miyoshi K, (1999), Aerospace mechanisms and tribology technology case study, Tribology International Volume 32, Issue 11, November 1999, Pages 673-685

Nishimura M, Suzuki M., (1999), Solid-lubricated bearings for use in vacuum-state of the art, Tribology International, Volume 32, Issue 11, November 1999, Pages 637-647

Palmgren A, (1946), Ball and roller bearing engineering, Philadelphia SKF Industries, 2nd edition

Parssinen N, (1998) Hertzian contact vibrations under random external excitation and surface roughness, Editorial, Journal of Sound and Vibration (1998), 214 (4), pp 779 - 783

Rahnejat H, Gohar R, (1985), The vibrations of radial ball bearings, Proc Inst Mech Engrs Vol 199, No C3, pp 181 - 193

Roberts E.W., (1990), Thin Solid Lubricant Films in Space, Tribology International Volume 23, Issue 2, April 1990, Pages 95-104

Takano A, (1999), Tribology related space mechanism anomalies and the newly constructed high-vacuum mechanism test facilities in NASDA, Tribology International Volume 32, Issue 11, November 1999, Pages 661-671

Sanders J.H., Cutler, J. N., Miller J. A. and Zabinski J. S., (1999) In vacuo tribological investigations of metal, ceramic and hybrid interfaces for high-speed spacecraft bearing applications, Tribology International Volume 32, Issue 11, November 1999, Pages 649-659

Sarafin, T.P., (1995) Spacecraft structures and mechanisms- From concept to launch, Kluwer Academic Publishers , 1st edition

Shapiro W , (1995), Space mechanisms lessons learned study, vol 1: summary, NASA TM 107046

Sochting S, Sherington I., Lewis S. D., Roberts E.W,(submitted 2004), An evaluation of simulated launch vibration on the friction performance and lubrication of ball bearings for space applications, Submitted to Wear, not published yet

Todd M.J., (1990), Modelling of Ball Bearings in Spacecraft, Tribology International Volume 23, Issue 2, April 1990, Pages 123-128

www.sti.nasa.gov

www.skf.com

APPENDIX

Title: BEARING STIFFNESS at 2000Hz
Author: PAPAKONSTANTINOY ANTONIOS
Date: 5-7-2004

Input data

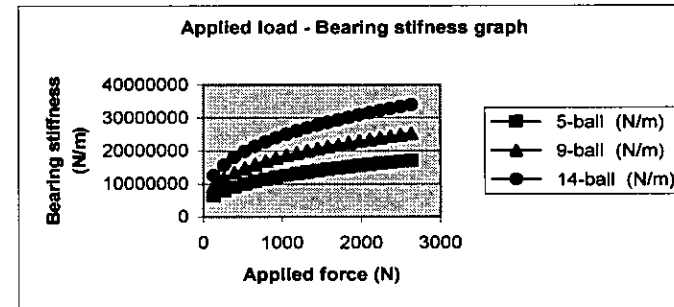
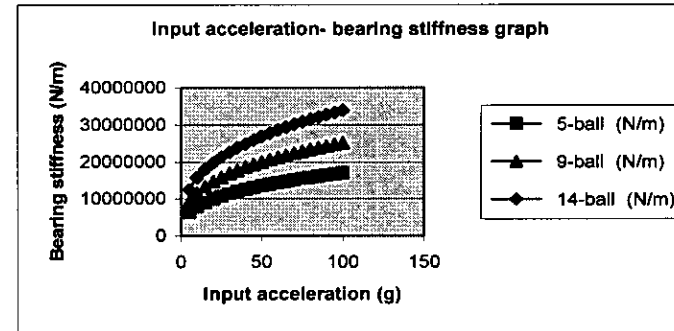
Shaft assembly mass total (m_1)	1.9	kg		
Outer housing assembly mass	0.783	kg		
Ball complement Z	5	9	14	
Ball diameter (D)	0.005555	m		
Frequency	2000	Hz		
Angular acceleration ω	12560	rad/s		
CABARET stiffness	9.85E+06	1.64E+07	2.60E+07	

FORMULAE

$$F = (m_1 + m_2)a$$

$$\text{Stiffness} = 2.27 * 10^7 * Z^{2/3} * F^{1/3} * D^{1/3} * \sin^{2/3} \alpha$$

Acceleration a (g)	Applied load F (N)	Contact angle (degrees)	Calculated Bearing Stiffness		
			5-ball (N/m)	9-ball (N/m)	14-ball (N/m)
5	131.6	15	6.29E+06	9.31E+06	1.25E+07
10	263.2	15	7.93E+06	1.17E+07	1.57E+07
15	394.8	15	9.08E+06	1.34E+07	1.80E+07
20	526.4	15	9.99E+06	1.48E+07	1.98E+07
25	658.0	15	1.08E+07	1.59E+07	2.14E+07
30	789.6	15	1.14E+07	1.69E+07	2.27E+07
35	921.2	15	1.20E+07	1.78E+07	2.39E+07
40	1052.8	15	1.26E+07	1.86E+07	2.50E+07
45	1184.4	15	1.31E+07	1.94E+07	2.60E+07
50	1316.0	15	1.36E+07	2.01E+07	2.69E+07
55	1447.6	15	1.40E+07	2.07E+07	2.78E+07
60	1579.2	15	1.44E+07	2.13E+07	2.86E+07
65	1710.8	15	1.48E+07	2.19E+07	2.94E+07
70	1842.4	15	1.52E+07	2.24E+07	3.01E+07
75	1974.0	15	1.55E+07	2.30E+07	3.08E+07
80	2105.6	15	1.59E+07	2.35E+07	3.15E+07
85	2237.2	15	1.62E+07	2.39E+07	3.21E+07
90	2368.8	15	1.65E+07	2.44E+07	3.28E+07
95	2500.4	15	1.68E+07	2.48E+07	3.34E+07
100	2632.0	15	1.71E+07	2.53E+07	3.39E+07

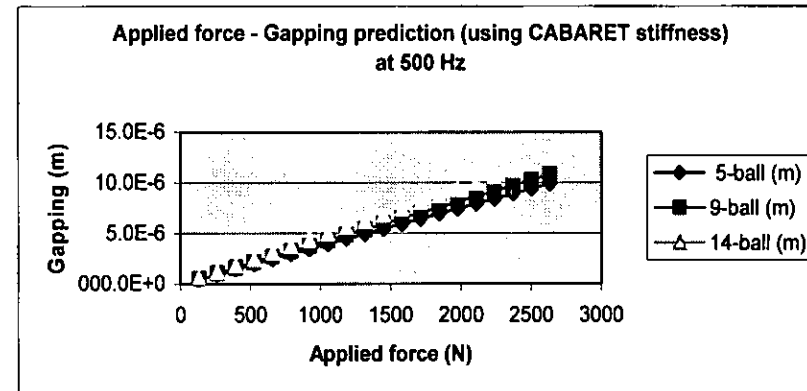
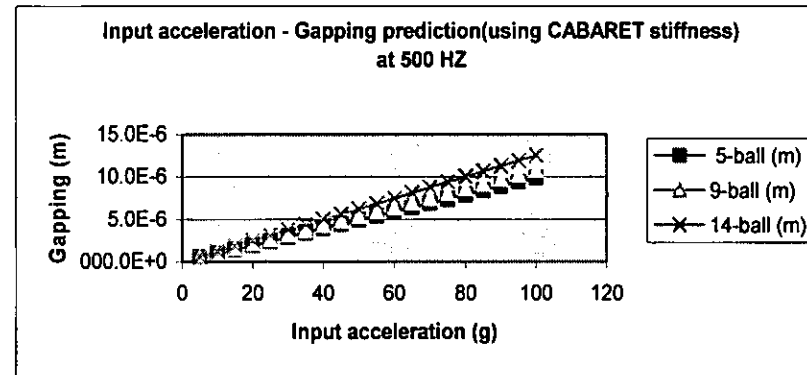


Title: Gapping prediction at 2000Hz using CABARET stiffness

Author: PAPAKONSTANTINOU ANTONIOS

Date: 5-7-2004

Acceleration a (g)	Applied force F (N)	5-ball (m)	9-ball (m)	14-ball (m)
5	131.6	494.8E-9	540.4E-9	624.8E-9
10	263.2	989.6E-9	1.1E-6	1.2E-6
15	394.8	1.5E-6	1.6E-6	1.9E-6
20	526.4	2.0E-6	2.2E-6	2.5E-6
25	658.0	2.5E-6	2.7E-6	3.1E-6
30	789.6	3.0E-6	3.2E-6	3.7E-6
35	921.2	3.5E-6	3.8E-6	4.4E-6
40	1052.8	4.0E-6	4.3E-6	5.0E-6
45	1184.4	4.5E-6	4.9E-6	5.6E-6
50	1316.0	4.9E-6	5.4E-6	6.2E-6
55	1447.6	5.4E-6	5.9E-6	6.9E-6
60	1579.2	5.9E-6	6.5E-6	7.5E-6
65	1710.8	6.4E-6	7.0E-6	8.1E-6
70	1842.4	6.9E-6	7.6E-6	8.7E-6
75	1974.0	7.4E-6	8.1E-6	9.4E-6
80	2105.6	7.9E-6	8.6E-6	10.0E-6
85	2237.2	8.4E-6	9.2E-6	10.6E-6
90	2368.8	8.9E-6	9.7E-6	11.2E-6
95	2500.4	9.4E-6	10.3E-6	11.9E-6
100	2632.0	9.9E-6	10.8E-6	12.5E-6

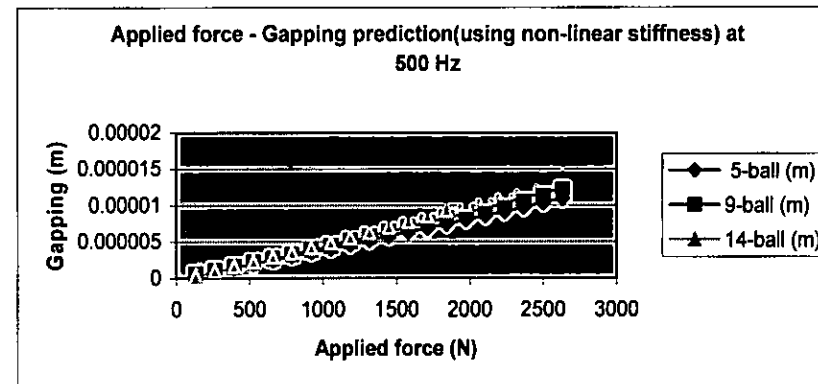
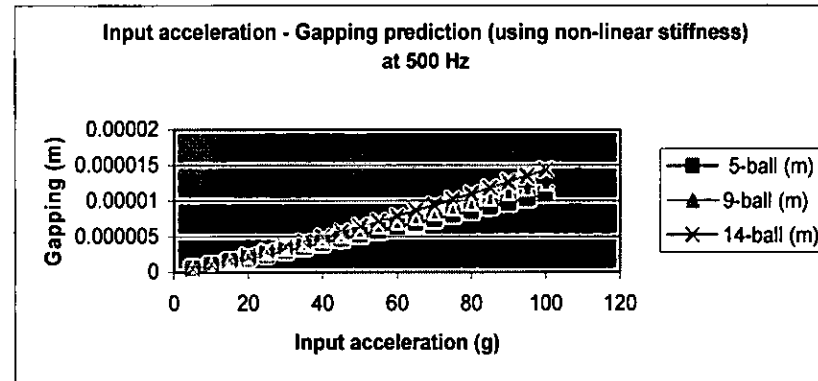


Title: Gapping prediction at 2000Hz using non-linear stiffness

Author: PAPAKONSTANTINOU ANTONIOS

Date: 5-7-2004

Acceleration a (g)	Applied force F (N)	5-ball (m)	9-ball (m)	14-ball (m)
5	131.6	473.1E-9	491.4E-9	512.3E-9
10	263.2	965.6E-9	1.0E-6	1.1E-6
15	394.8	1.5E-6	1.6E-6	1.7E-6
20	526.4	2.0E-6	2.1E-6	2.3E-6
25	658.0	2.5E-6	2.7E-6	2.9E-6
30	789.6	3.0E-6	3.3E-6	3.6E-6
35	921.2	3.6E-6	3.9E-6	4.2E-6
40	1052.8	4.1E-6	4.5E-6	4.9E-6
45	1184.4	4.6E-6	5.1E-6	5.6E-6
50	1316.0	5.2E-6	5.7E-6	6.3E-6
55	1447.6	5.7E-6	6.3E-6	7.1E-6
60	1579.2	6.3E-6	7.0E-6	7.8E-6
65	1710.8	6.9E-6	7.6E-6	8.6E-6
70	1842.4	7.4E-6	8.3E-6	9.4E-6
75	1974.0	8.0E-6	8.9E-6	10.2E-6
80	2105.6	8.6E-6	9.6E-6	11.0E-6
85	2237.2	9.2E-6	10.3E-6	11.8E-6
90	2368.8	9.7E-6	11.0E-6	12.6E-6
95	2500.4	10.3E-6	11.7E-6	13.5E-6
100	2632.0	10.9E-6	12.3E-6	14.3E-6



Title: BEARING STIFFNESS at 1500Hz
Author: PAPAKONSTANTINOU ANTONIOS
Date: 5-7-2004

Input data

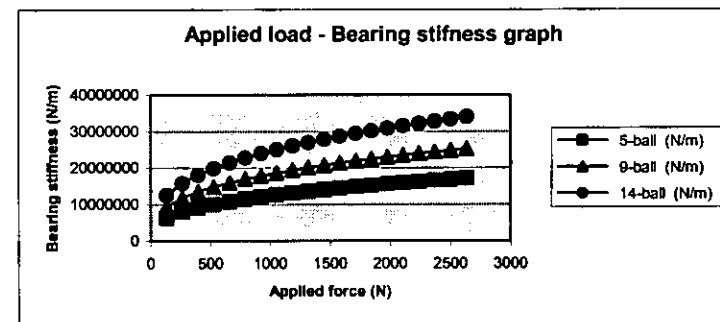
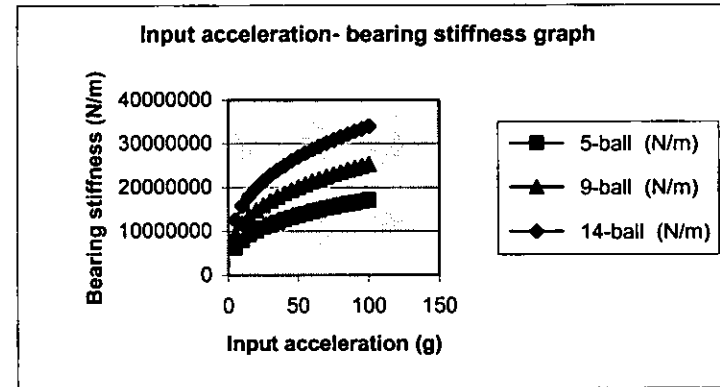
Shaft assembly mass total (m_1)	1.9	kg		
Outer housing assembly mass	0.783	kg		
Ball complement Z	5	9	14	
Ball diameter (D)	0.005555	m		
Frequency	1500	Hz		
Angular acceleration ω	9420	rad/s		
CABARET stiffness	9.85E+06	1.64E+07	2.60E+07	

FORMULAE

$$F = (m_1 + m_2)a$$

$$\text{Stiffness} = 2.27 * 10^7 * Z^{2/3} * F^{1/3} * D^{1/3} * \sin^{2/3} \alpha$$

Acceleration a (g)	Applied load F (N)	Contact angle (degrees)	Calculated Bearing Stiffness		
			5-ball (N/m)	9-ball (N/m)	14-ball (N/m)
5	131.6	15	6.29E+06	9.31E+06	1.25E+07
10	263.2	15	7.93E+06	1.17E+07	1.57E+07
15	394.8	15	9.08E+06	1.34E+07	1.80E+07
20	526.4	15	9.99E+06	1.48E+07	1.98E+07
25	658.0	15	1.08E+07	1.59E+07	2.14E+07
30	789.6	15	1.14E+07	1.69E+07	2.27E+07
35	921.2	15	1.20E+07	1.78E+07	2.39E+07
40	1052.8	15	1.26E+07	1.86E+07	2.50E+07
45	1184.4	15	1.31E+07	1.94E+07	2.60E+07
50	1316.0	15	1.36E+07	2.01E+07	2.69E+07
55	1447.6	15	1.40E+07	2.07E+07	2.78E+07
60	1579.2	15	1.44E+07	2.13E+07	2.86E+07
65	1710.8	15	1.48E+07	2.19E+07	2.94E+07
70	1842.4	15	1.52E+07	2.24E+07	3.01E+07
75	1974.0	15	1.55E+07	2.30E+07	3.08E+07
80	2105.6	15	1.59E+07	2.35E+07	3.15E+07
85	2237.2	15	1.62E+07	2.39E+07	3.21E+07
90	2368.8	15	1.65E+07	2.44E+07	3.28E+07
95	2500.4	15	1.68E+07	2.48E+07	3.34E+07
100	2632.0	15	1.71E+07	2.53E+07	3.39E+07

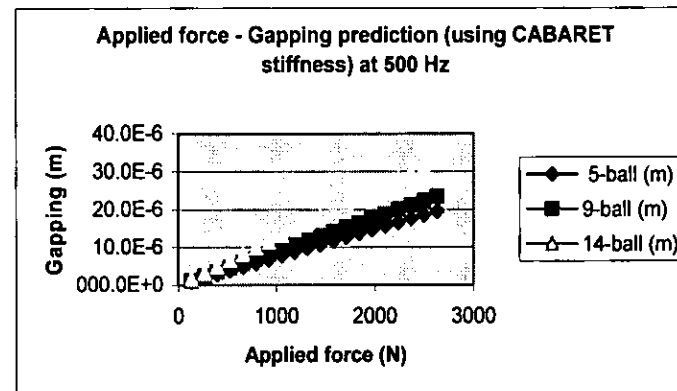
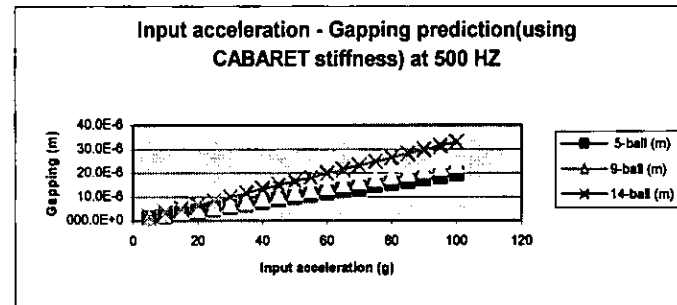


Title: Gapping prediction at 1500Hz using CABARET stiffness

Author: PAPAKONSTANTINOU ANTONIOS

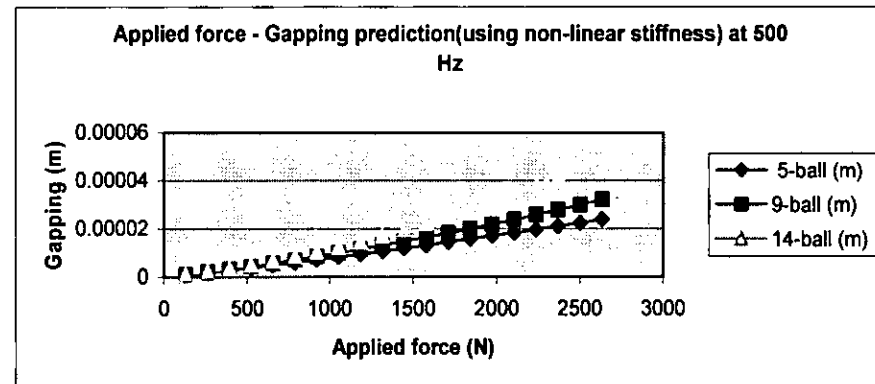
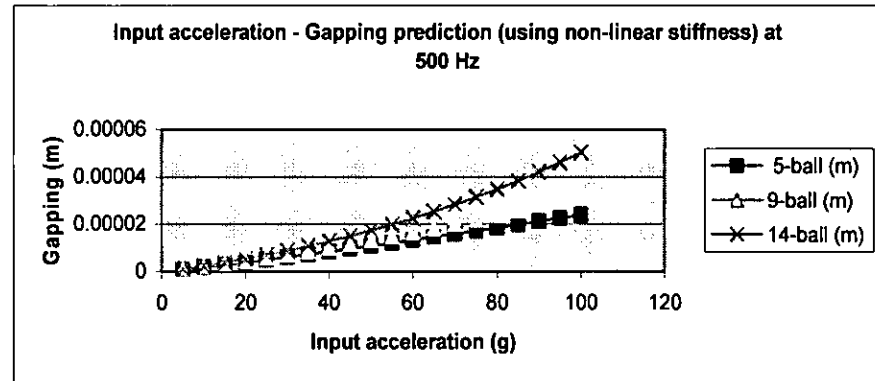
Date: 5-7-2004

Acceleration a (g)	Applied force F (N)	5-ball (m)	9-ball (m)	14-ball (m)
5	131.6	975.9E-9	1.2E-6	1.7E-6
10	263.2	2.0E-6	2.3E-6	3.3E-6
15	394.8	2.9E-6	3.5E-6	5.0E-6
20	526.4	3.9E-6	4.7E-6	6.6E-6
25	658.0	4.9E-6	5.9E-6	8.3E-6
30	789.6	5.9E-6	7.0E-6	9.9E-6
35	921.2	6.8E-6	8.2E-6	11.6E-6
40	1052.8	7.8E-6	9.4E-6	13.2E-6
45	1184.4	8.8E-6	10.5E-6	14.9E-6
50	1316.0	9.8E-6	11.7E-6	16.6E-6
55	1447.6	10.7E-6	12.9E-6	18.2E-6
60	1579.2	11.7E-6	14.0E-6	19.9E-6
65	1710.8	12.7E-6	15.2E-6	21.5E-6
70	1842.4	13.7E-6	16.4E-6	23.2E-6
75	1974.0	14.6E-6	17.6E-6	24.8E-6
80	2105.6	15.6E-6	18.7E-6	26.5E-6
85	2237.2	16.6E-6	19.9E-6	28.1E-6
90	2368.8	17.6E-6	21.1E-6	29.8E-6
95	2500.4	18.5E-6	22.2E-6	31.4E-6
100	2632.0	19.5E-6	23.4E-6	33.1E-6



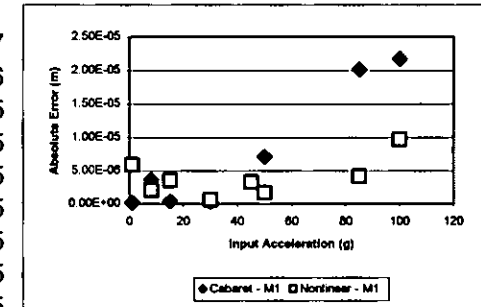
Title: Gapping prediction at 1500Hz using non-linear stiffness
 Author: PAPAKONSTANTINOUS ANTONIOS
 Date: 5-7-2004

Acceleration a (g)	Applied force F (N)	5-ball (m)	9-ball (m)	14-ball (m)
5	131.6	895.0E-9	962.7E-9	1.0E-6
10	263.2	1.9E-6	2.0E-6	2.3E-6
15	394.8	2.9E-6	3.2E-6	3.7E-6
20	526.4	3.9E-6	4.5E-6	5.2E-6
25	658.0	5.0E-6	5.8E-6	6.9E-6
30	789.6	6.1E-6	7.1E-6	8.7E-6
35	921.2	7.2E-6	8.6E-6	10.6E-6
40	1052.8	8.4E-6	10.0E-6	12.7E-6
45	1184.4	9.6E-6	11.6E-6	14.9E-6
50	1316.0	10.8E-6	13.2E-6	17.2E-6
55	1447.6	12.0E-6	14.8E-6	19.7E-6
60	1579.2	13.2E-6	16.5E-6	22.4E-6
65	1710.8	14.5E-6	18.3E-6	25.2E-6
70	1842.4	15.8E-6	20.1E-6	28.2E-6
75	1974.0	17.1E-6	22.0E-6	31.4E-6
80	2105.6	18.4E-6	23.9E-6	34.7E-6
85	2237.2	19.8E-6	25.8E-6	38.3E-6
90	2368.8	21.1E-6	27.9E-6	42.0E-6
95	2500.4	22.5E-6	30.0E-6	46.0E-6
100	2632.0	23.9E-6	32.1E-6	50.3E-6

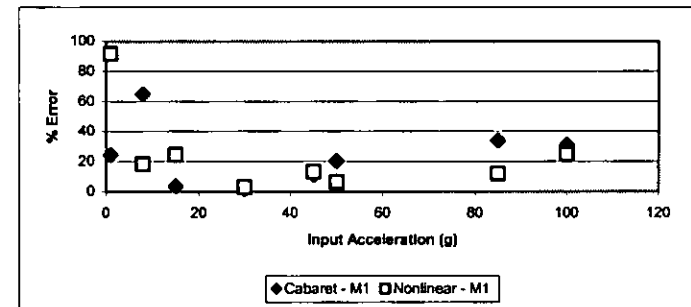


Title: Gapping Prediction Error Comparrison
Author: PAPAKONSTANTINOI ANTONIOS

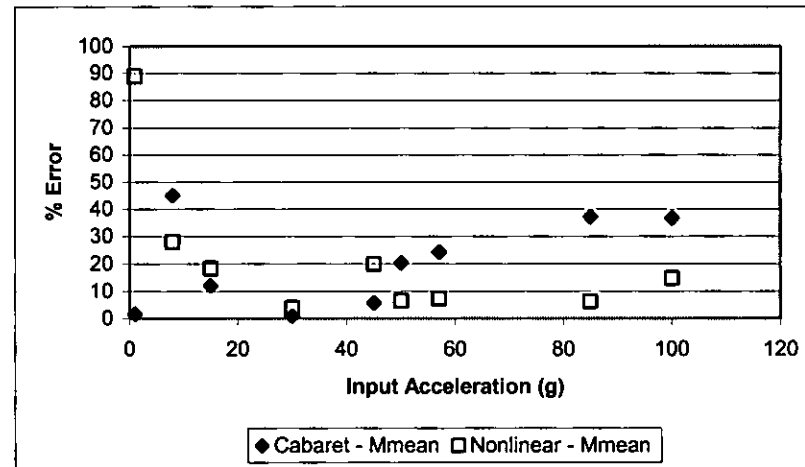
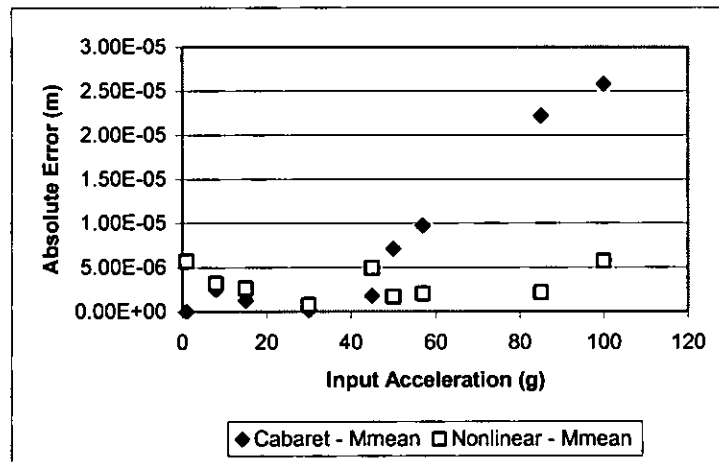
Acceleration a (g)	CABARET gap (m)	Non-linear gap (m)	Measured gap1 (m)	Measured gap2 (m)	Mean measured gap (m)
1	7.03E-07	6.40E-06	5.30E-07	9.00E-07	7.15E-07
8	5.62E-06	1.13E-05	9.26E-06	7.05E-06	8.16E-06
15	1.05E-05	1.45E-05	1.09E-05	1.27E-05	1.18E-05
30	2.11E-05	2.01E-05	2.07E-05	2.10E-05	2.09E-05
45	3.16E-05	2.49E-05	2.82E-05	3.14E-05	2.98E-05
50	3.51E-05	2.63E-05	2.80E-05		2.80E-05
57	4.00E-05	2.83E-05		3.03E-05	3.03E-05
85	5.97E-05	3.53E-05	3.95E-05	3.55E-05	3.75E-05
100	7.03E-05	3.88E-05	4.85E-05	4.04E-05	4.45E-05



Acceleration	Absolute error comparisson		Theoretical to measured ratio	
	Cabaret - M1	Nonlinear - M1	Cabaret - M1	Nonlinear - M1
1	1.73E-07	5.87E-06	25	92
8	3.64E-06	2.07E-06	65	18
15	3.81E-07	3.55E-06	4	25
30	3.37E-07	6.19E-07	2	3
45	3.45E-06	3.30E-06	11	13
50	7.12E-06	1.69E-06	20	6
85	2.02E-05	4.19E-06	34	12
100	2.18E-05	9.70E-06	31	25

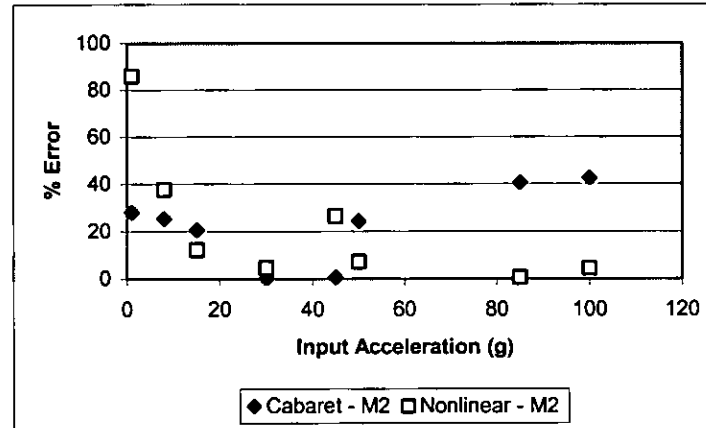
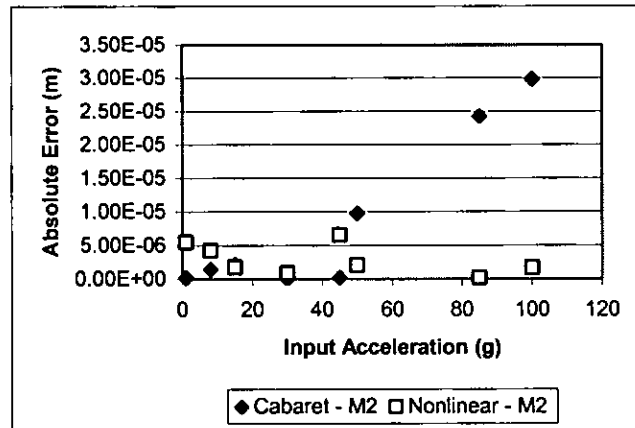


Absolute error comparisson			% error comparisson _	
Acceleration	Cabaret - Mmean	Nonlinear - Mmean	Cabaret - Mmean	Nonlinear - Mmean
1	1.24231E-08	5.68409E-06	1.768216595	88.82653117
8	2.53438E-06	3.17574E-06	45.09087523	28.02765701
15	1.27635E-06	2.65624E-06	12.11109362	18.35531709
30	1.87308E-07	7.6865E-07	0.888669247	3.820074214
45	1.81596E-06	4.93421E-06	5.743811825	19.84336601
50	7.11885E-06	1.69203E-06	20.26495813	6.429187408
57	9.73688E-06	2.04228E-06	24.31371255	7.224769251
85	2.2199E-05	2.17903E-06	37.17246423	6.165736872
100	2.57977E-05	5.68E-06	36.71867259	14.64672511



Absolute error comp: Theoretical to measured ratio
Acceleratio Cabaret - I Nonlinear Cabaret - I Nonlinear - M2

1	1.97E-07	5.50E-06	28	86
8	1.43E-06	4.28E-06	25	38
15	2.17E-06	1.76E-06	21	12
30	3.73E-08	9.19E-07	0	5
45	1.86E-07	6.56E-06	1	26
50	9.74E-06	2.04E-06	24	7
85	2.42E-05	1.69E-07	41	0
100	2.98E-05	1.66E-06	42	4



Title: Gapping Prediction Comparison for 9-ball complement at 500Hz

Author: PAPAKONSTANTINOU ANTONIOS

Input data

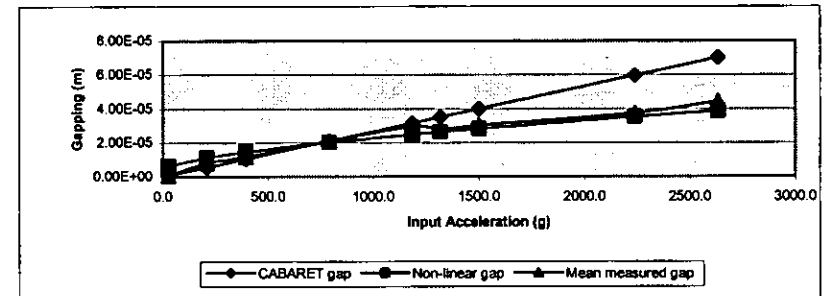
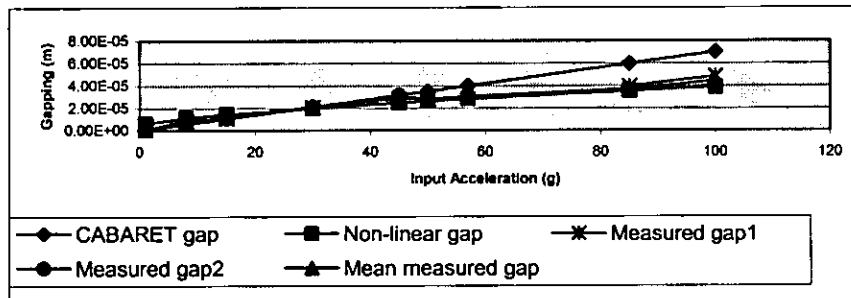
Shaft assembly mass total (m_1)	1.9	kg
Outer housing assembly mass m_2	0.783	kg
Ball complement Z	9	
Contact angle (α)	15.0	
Ball diameter (D)	0.005555	m
Frequency	500	Hz
Angular acceleration ω	3140	rad/s
CABARET stiffness	1.64E+07	N/m
Preload	22	N

FORMULAE

$$F = (m_1 + m_2)a$$

$$Stiffness = 2.27 * 10^7 * F^{1/3} * D^{1/3} * \sin^{5/3} \alpha$$

Acceleration	Applied force	Stiffness	CABARET gap	Non-linear gap	Measured gap1	Measured gap2	Mean measured gap
1	26.3	6.67E+06	7.03E-07	6.40E-06	5.30E-07	9.00E-07	7.15E-07
8	210.6	1.09E+07	5.62E-06	1.13E-05	9.26E-06	7.05E-06	8.16E-06
15	394.8	1.34E+07	1.05E-05	1.45E-05	1.09E-05	1.27E-05	1.18E-05
30	789.6	1.69E+07	2.11E-05	2.01E-05	2.07E-05	2.10E-05	2.09E-05
45	1184.4	1.94E+07	3.16E-05	2.49E-05	2.82E-05	3.14E-05	2.98E-05
50	1316.0	2.01E+07	3.51E-05	2.63E-05	2.80E-05		2.80E-05
57	1500.3	2.10E+07	4.00E-05	2.83E-05		3.03E-05	3.03E-05
85	2237.2	2.39E+07	5.97E-05	3.53E-05	3.95E-05	3.55E-05	3.75E-05
100	2632.0	2.53E+07	7.03E-05	3.88E-05	4.85E-05	4.04E-05	4.45E-05



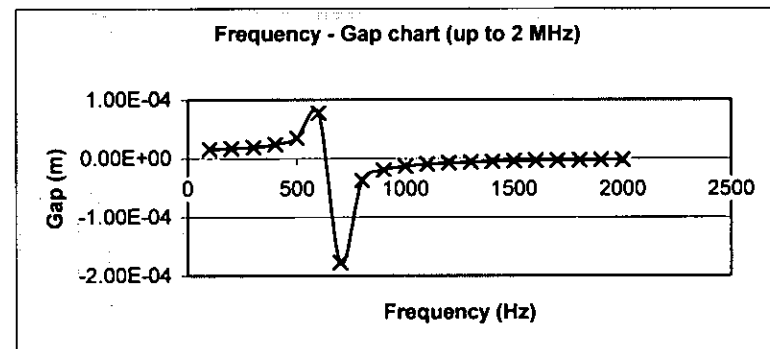
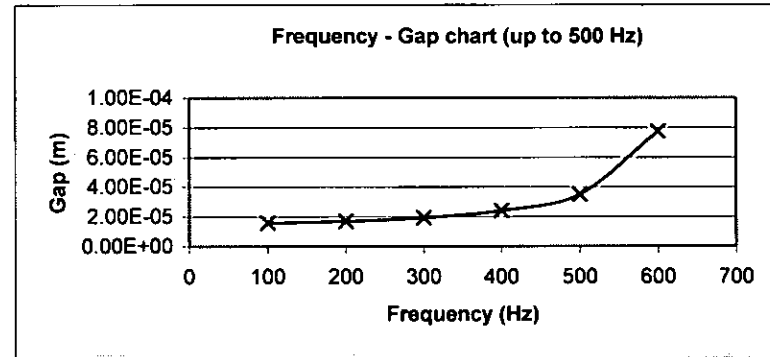
Title: GAP PREDICTION FOR 5-BALL COMPLEMENT (using CABARET stiffness) at 20g acceleration

Author: PAPAKONSTANTINOU ANTONIOS

Input data

Shaft assembly mass total (m_1)	1.9	kg
Outer housing assembly mass total (m_2)	0.783	kg
Input acceleration (α)	196.2	m/s^2
Input force (F)	526.4	N
Stiffness (k)	9850000	N/m

frequency f (Hz)	angular velocity ω (rad / s)	amplitude A_1 (m)	amplitude A_2 (m)	Gap D (m)
100	628	-4.93E-04	-5.09E-04	1.60E-05
200	1256	-1.19E-04	-1.36E-04	1.71E-05
300	1884	-4.96E-05	-6.91E-05	1.95E-05
400	2512	-2.40E-05	-4.82E-05	2.42E-05
500	3140	-9.67E-06	-4.47E-05	3.51E-05
600	3768	8.85E-06	-6.88E-05	7.77E-05
700	4396	-6.20E-05	1.16E-04	-1.78E-04
800	5024	-1.86E-05	1.85E-05	-3.71E-05
900	5652	-1.18E-05	7.69E-06	-1.95E-05
1000	6280	-8.71E-06	4.08E-06	-1.28E-05
1100	6908	-6.81E-06	2.44E-06	-9.25E-06
1200	7536	-5.53E-06	1.57E-06	-7.10E-06
1300	8164	-4.60E-06	1.07E-06	-5.67E-06
1400	8792	-3.90E-06	7.57E-07	-4.65E-06
1500	9420	-3.35E-06	5.53E-07	-3.90E-06
1600	10048	-2.92E-06	4.15E-07	-3.33E-06
1700	10676	-2.56E-06	3.18E-07	-2.88E-06
1800	11304	-2.27E-06	2.48E-07	-2.52E-06
1900	11932	-2.03E-06	1.96E-07	-2.22E-06
2000	12560	-1.82E-06	1.58E-07	-1.98E-06



Title: GAP PREDICTION FOR 5-BALL COMPLEMENT (using non-linear stiffness) at 20g acceleration

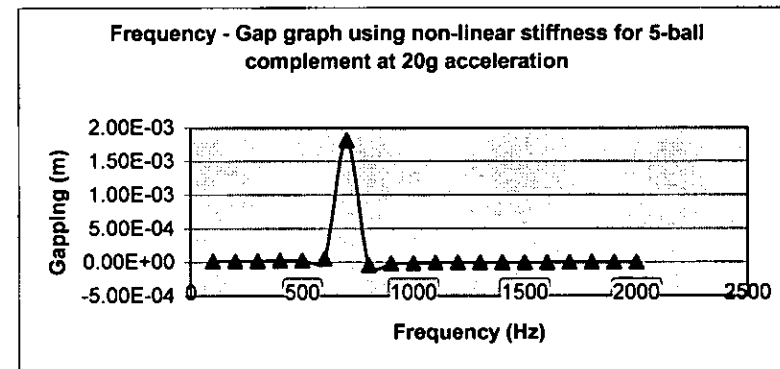
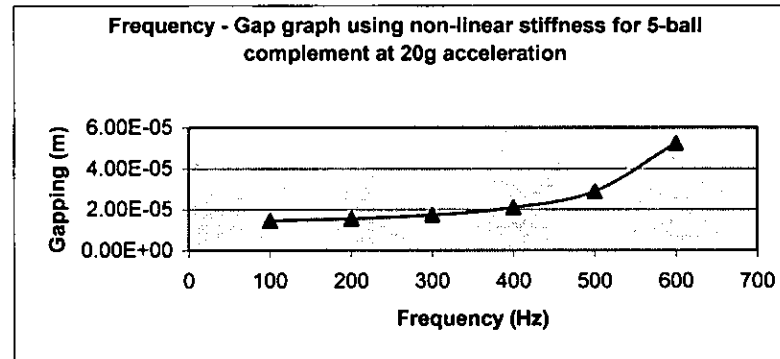
Autor: PAPAKONSTANTINOUS ANTONIOS

Date: 31-10-2003

Input data

Shaft assembly mass total (m_1)	1.9	kg
Outer housing assembly mass total (m_2)	0.783	kg
Input acceleration (α)	196.2	m/s^2
Input force (F)	526.4	N
Stiffness (k)	1.08E+07	N/m

frequency f (Hz)	angular velocity ω (rad / s)	amplitude A_1 (m)	amplitude A_2 (m)	Gap D (m)
100	628	-4.93E-04	-5.08E-04	1.45E-05
200	1256	-1.20E-04	-1.35E-04	1.55E-05
300	1884	-5.02E-05	-6.76E-05	1.74E-05
400	2512	-2.50E-05	-4.60E-05	2.10E-05
500	3140	-1.15E-05	-4.03E-05	2.88E-05
600	3768	1.50E-06	-5.10E-05	5.25E-05
700	4396	5.20E-04	-1.30E-03	1.82E-03
800	5024	-2.18E-05	2.63E-05	-4.81E-05
900	5652	-1.26E-05	9.59E-06	-2.22E-05
1000	6280	-9.03E-06	4.85E-06	-1.39E-05
1100	6908	-6.97E-06	2.84E-06	-9.81E-06
1200	7536	-5.62E-06	1.80E-06	-7.42E-06
1300	8164	-4.66E-06	1.22E-06	-5.87E-06
1400	8792	-3.94E-06	8.55E-07	-4.79E-06
1500	9420	-3.38E-06	6.22E-07	-4.00E-06
1600	10048	-2.94E-06	4.65E-07	-3.40E-06
1700	10676	-2.58E-06	3.55E-07	-2.93E-06
1800	11304	-2.28E-06	2.76E-07	-2.56E-06
1900	11932	-2.04E-06	2.18E-07	-2.25E-06
2000	12560	-1.83E-06	1.75E-07	-2.00E-06



Title: GAP PREDICTION COMPARISSON FOR 5-BALL COMPLEMENT at 20g acceleration

Autor: PPAKONSTANTINO ANTONIOS

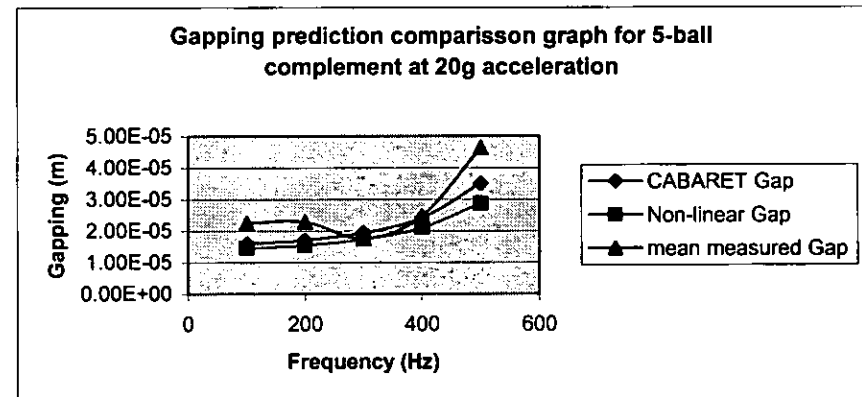
Date: 31-10-2003

Input data

Shaft assembly mass total (m_1)	1.9	kg
Outer housing assembly mass total (m_2)	0.783	kg
Input acceleration (α)	245.25	m/s^2
Input force (F)	658.0	N

frequency	angular velocity	CABARET Gap	Non-linear GAP	measured 1	measured 2	measured 3	mean measured gap
f (Hz)	ω (rad / s)	D (m)	D (m)	D (m)	D (m)	D (m)	D (m)
100	628	1.60E-05	1.45E-05	8.28E-06	1.99E-05	3.93E-05	2.25E-05
200	1256	1.71E-05	1.55E-05	2.19E-05	2.44E-05	2.25E-05	2.29E-05
300	1884	1.95E-05	1.74E-05	2.47E-05	1.44E-05	1.37E-05	1.76E-05
400	2512	2.42E-05	2.10E-05	2.79E-05	2.89E-05	1.74E-05	2.47E-05
500	3140	3.51E-05	2.88E-05	3.59E-05	5.43E-05	4.88E-05	4.63E-05

frequency	CABARET Gap	Non-linear Gap	mean measured Gap
100	1.60E-05	1.45E-05	2.25E-05
200	1.71E-05	1.55E-05	2.29E-05
300	1.95E-05	1.74E-05	1.76E-05
400	2.42E-05	2.10E-05	2.47E-05
500	3.51E-05	2.88E-05	4.63E-05



Title: GAP PREDICTION FOR 5-BALL COMPLEMENT (using CABARET stiffness) at 25g acceleration

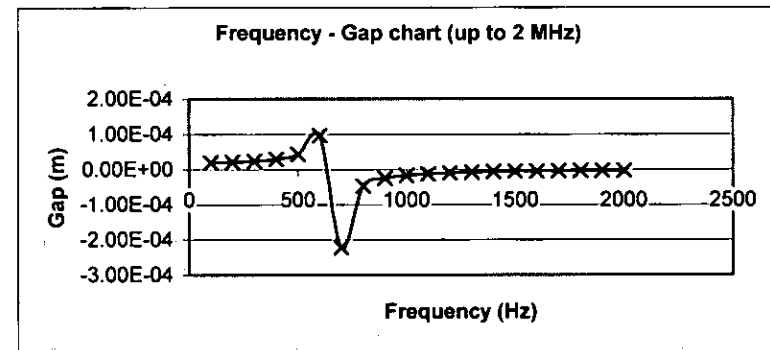
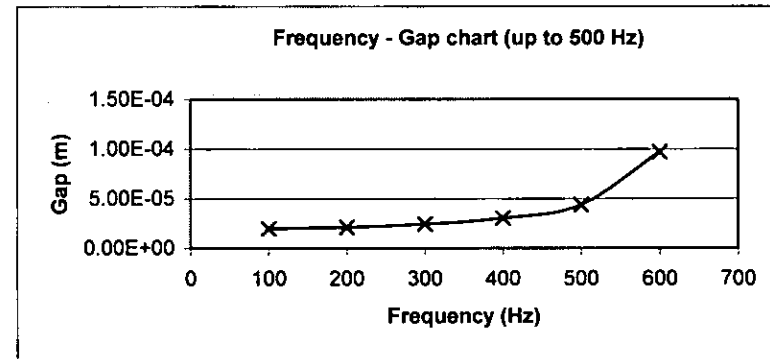
Autor: PAPAKONSTANTINOUS ANTONIOS

Date: 31-10-2003

Input data

Shaft assembly mass total (m_1)	1.9	kg
Outer housing assembly mass total (m_2)	0.783	kg
Input acceleration (α)	245.25	m/s^2
Input force (F)	658.0	N
Stiffness (k)	9850000	N/m

frequency	angular velocity	amplitude	amplitude	Gap
f (Hz)	ω (rad / s)	A_1 (m)	A_2 (m)	D (m)
100	628	-6.16E-04	-6.36E-04	1.99E-05
200	1256	-1.49E-04	-1.71E-04	2.14E-05
300	1884	-6.20E-05	-8.63E-05	2.44E-05
400	2512	-3.00E-05	-6.03E-05	3.02E-05
500	3140	-1.21E-05	-5.59E-05	4.38E-05
600	3768	1.11E-05	-8.60E-05	9.71E-05
700	4396	-7.74E-05	1.44E-04	-2.22E-04
800	5024	-2.32E-05	2.31E-05	-4.63E-05
900	5652	-1.48E-05	9.62E-06	-2.44E-05
1000	6280	-1.09E-05	5.10E-06	-1.60E-05
1100	6908	-8.51E-06	3.05E-06	-1.16E-05
1200	7536	-6.91E-06	1.97E-06	-8.87E-06
1300	8164	-5.75E-06	1.34E-06	-7.08E-06
1400	8792	-4.87E-06	9.47E-07	-5.82E-06
1500	9420	-4.19E-06	6.92E-07	-4.88E-06
1600	10048	-3.64E-06	5.19E-07	-4.16E-06
1700	10676	-3.20E-06	3.97E-07	-3.60E-06
1800	11304	-2.84E-06	3.10E-07	-3.15E-06
1900	11932	-2.53E-06	2.46E-07	-2.78E-06
2000	12560	-2.28E-06	1.97E-07	-2.47E-06



Title: GAP PREDICTION FOR 5-BALL COMPLEMENT (using non-linear stiffness) at 25g acceleration

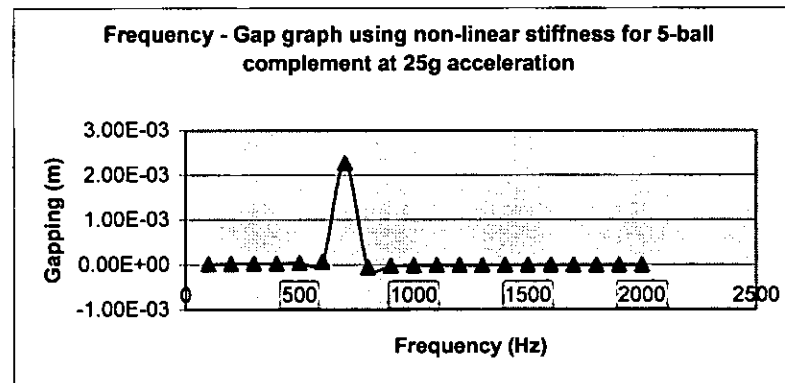
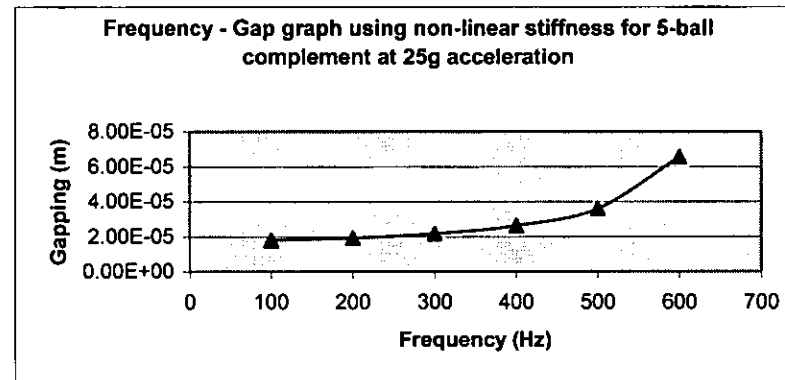
Autor: PAPAKONSTANTINOU ANTONIOS

Date: 31-10-2003

Input data

Shaft assembly mass total (m_1)	1.9	kg
Outer housing assembly mass total (m_2)	0.783	kg
Input acceleration (a)	245.25	m/s^2
Input force (F)	658.0	N
Stiffness (k)	1.08E+07	N/m

frequency f (Hz)	angular velocity ω (rad / s)	amplitude A_1 (m)	amplitude A_2 (m)	Gap D (m)
100	628	-6.17E-04	-6.35E-04	1.81E-05
200	1256	-1.50E-04	-1.69E-04	1.93E-05
300	1884	-6.27E-05	-8.45E-05	2.17E-05
400	2512	-3.12E-05	-5.75E-05	2.63E-05
500	3140	-1.44E-05	-5.04E-05	3.60E-05
600	3768	1.87E-06	-6.37E-05	6.56E-05
700	4396	6.50E-04	-1.62E-03	2.27E-03
800	5024	-2.73E-05	3.28E-05	-6.01E-05
900	5652	-1.58E-05	1.20E-05	-2.78E-05
1000	6280	-1.13E-05	6.07E-06	-1.73E-05
1100	6908	-8.72E-06	3.54E-06	-1.23E-05
1200	7536	-7.03E-06	2.25E-06	-9.28E-06
1300	8164	-5.82E-06	1.52E-06	-7.34E-06
1400	8792	-4.92E-06	1.07E-06	-5.99E-06
1500	9420	-4.22E-06	7.77E-07	-5.00E-06
1600	10048	-3.67E-06	5.81E-07	-4.25E-06
1700	10676	-3.22E-06	4.43E-07	-3.66E-06
1800	11304	-2.85E-06	3.45E-07	-3.20E-06
1900	11932	-2.54E-06	2.73E-07	-2.82E-06
2000	12560	-2.29E-06	2.19E-07	-2.50E-06



Title: GAP PREDICTION COMPARISSON FOR 5-BALL COMPLEMENT at 25g acceleration

Autor: PAPAKONSTANTINOU ANTONIOS

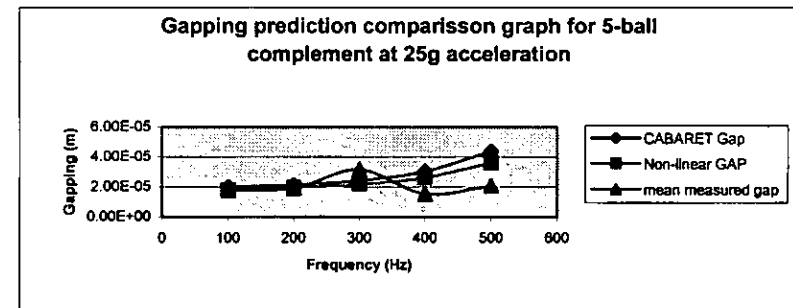
Date: 31-10-2003

Input data

Shaft assembly mass total (m_1)	1.9	kg
Outer housing assembly mass total (m_2)	0.783	kg
Input acceleration (a)	245.25	m/s^2
Input force (F)	658.0	N

frequency f (Hz)	angular velocity ω (rad / s)	CABARET Gap D (m)	Non-linear GAP D (m)	measured 1 D (m)	measured 2 D (m)	measured 3 D (m)	mean measured gap D (m)
100	628	1.99E-05	1.81E-05	2.19E-05	1.26E-05	1.94E-05	1.80E-05
200	1256	2.14E-05	1.93E-05	2.00E-05	2.01E-05	1.73E-05	1.91E-05
300	1884	2.44E-05	2.17E-05	3.14E-05	3.27E-05	3.05E-05	3.16E-05
400	2512	3.02E-05	2.63E-05	1.53E-05	1.56E-05	1.50E-05	1.53E-05
500	3140	4.38E-05	3.60E-05	2.15E-05	2.01E-05	2.02E-05	2.06E-05

frequency	CABARET Gap	Non-linear GAP	mean measured gap
100	1.99E-05	1.81E-05	1.80E-05
200	2.14E-05	1.93E-05	1.91E-05
300	2.44E-05	2.17E-05	3.16E-05
400	3.02E-05	2.63E-05	1.53E-05
500	4.38E-05	3.60E-05	2.06E-05



Title: GAP PREDICTION FOR 9-BALL COMPLEMENT (using CABARET stiffness)

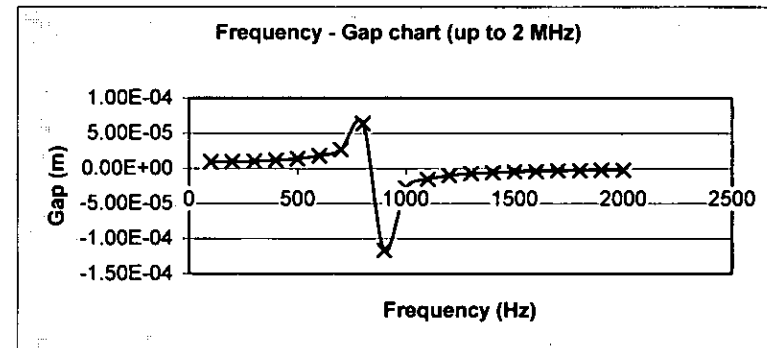
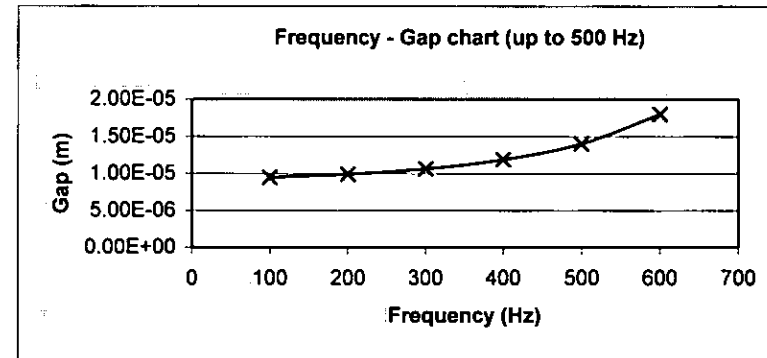
Autor: PAPAKONSTANTINOU ANTONIOS

Date: 31-10-2003

Input data

Shaft assembly mass total (m_1)	1.9	kg
Outer housing assembly mass total (m_2)	0.783	kg
Input acceleration (a)	196.2	m/s^2
Input force (F)	526.4	N
Stiffness (k)	16400000	N/m

frequency	angular velocity	amplitude	amplitude	Gap
f (Hz)	ω (rad / s)	A_1 (m)	A_2 (m)	D (m)
100	628	-4.95E-04	-5.04E-04	9.49E-06
200	1256	-1.21E-04	-1.31E-04	9.90E-06
300	1884	-5.22E-05	-6.28E-05	1.06E-05
400	2512	-2.76E-05	-3.95E-05	1.19E-05
500	3140	-1.58E-05	-2.99E-05	1.41E-05
600	3768	-8.56E-06	-2.66E-05	1.80E-05
700	4396	-2.27E-06	-2.93E-05	2.70E-05
800	5024	1.09E-05	-5.30E-05	6.39E-05
900	5652	-4.03E-05	7.67E-05	-1.17E-04
1000	6280	-1.32E-05	1.49E-05	-2.81E-05
1100	6908	-8.57E-06	6.70E-06	-1.53E-05
1200	7536	-6.43E-06	3.75E-06	-1.02E-05
1300	8164	-5.12E-06	2.35E-06	-7.47E-06
1400	8792	-4.23E-06	1.57E-06	-5.81E-06
1500	9420	-3.58E-06	1.11E-06	-4.68E-06
1600	10048	-3.08E-06	8.05E-07	-3.88E-06
1700	10676	-2.68E-06	6.03E-07	-3.28E-06
1800	11304	-2.36E-06	4.62E-07	-2.82E-06
1900	11932	-2.09E-06	3.61E-07	-2.46E-06
2000	12560	-1.87E-06	2.87E-07	-2.16E-06



Title: GAP PREDICTION FOR 9-BALL COMPLEMENT (using non-linear stiffness)

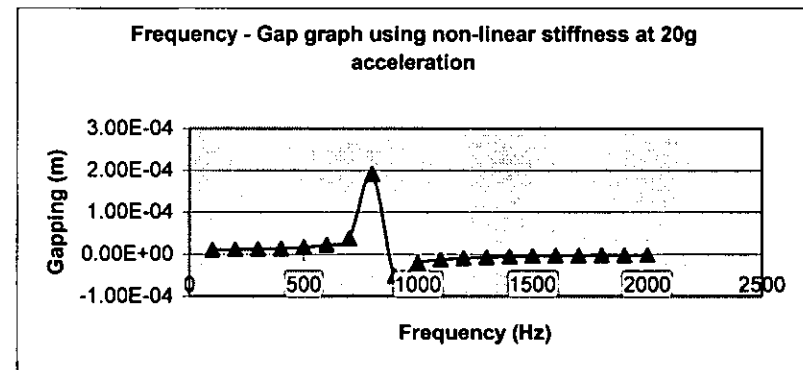
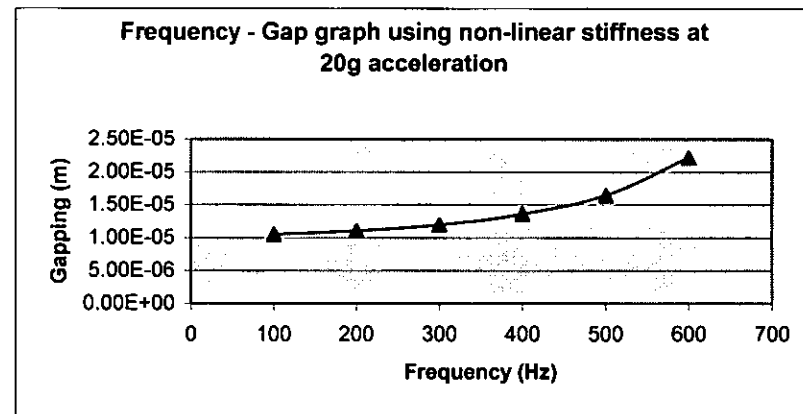
Autor: PAPAKONSTANTINOU ANTONIOS

Date: 31-10-2003

Input data

Shaft assembly mass total (m_1)	1.9	kg
Outer housing assembly mass total (m_2)	0.783	kg
Input acceleration (α)	196.2	m/s^2
Input force (F)	526.4	N
Stiffness (k)	14800000	N/m

frequency	angular velocity	amplitude	amplitude	Gap
f (Hz)	ω (rad / s)	A_1 (m)	A_2 (m)	D (m)
100	628	-4.94E-04	-5.05E-04	1.05E-05
200	1256	-1.21E-04	-1.32E-04	1.10E-05
300	1884	-5.18E-05	-6.38E-05	1.20E-05
400	2512	-2.71E-05	-4.07E-05	1.36E-05
500	3140	-1.51E-05	-3.16E-05	1.65E-05
600	3768	-7.35E-06	-2.95E-05	2.22E-05
700	4396	8.24E-07	-3.68E-05	3.76E-05
800	5024	4.80E-05	-1.43E-04	1.91E-04
900	5652	-2.15E-05	3.12E-05	-5.27E-05
1000	6280	-1.13E-05	1.04E-05	-2.17E-05
1100	6908	-7.96E-06	5.22E-06	-1.32E-05
1200	7536	-6.14E-06	3.06E-06	-9.20E-06
1300	8164	-4.97E-06	1.97E-06	-6.93E-06
1400	8792	-4.14E-06	1.34E-06	-5.47E-06
1500	9420	-3.51E-06	9.51E-07	-4.47E-06
1600	10048	-3.03E-06	6.98E-07	-3.73E-06
1700	10676	-2.65E-06	5.26E-07	-3.17E-06
1800	11304	-2.34E-06	4.05E-07	-2.74E-06
1900	11932	-2.08E-06	3.18E-07	-2.39E-06
2000	12560	-1.86E-06	2.53E-07	-2.11E-06



Title: GAP PREDICTION COMPARISSON FOR 9-BALL COMPLEMENT at 20g acceleration

Autor: PAPAKONSTANTINOUS ANTONIOS

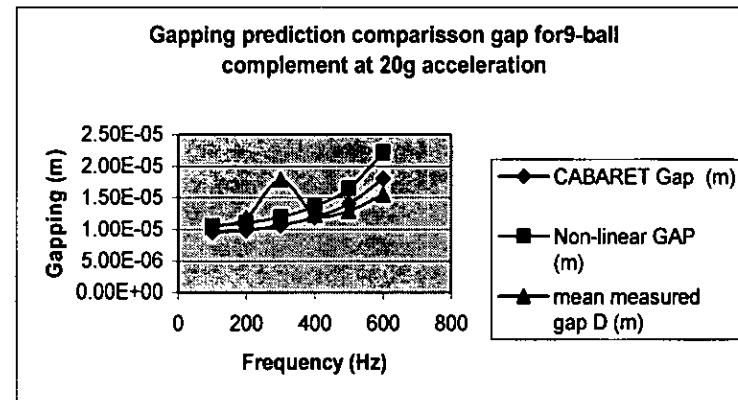
Date: 31-10-2003

Input data

Shaft assembly mass total (m_1)	1.9	kg
Outer housing assembly mass total (m_2)	0.783	kg
Input acceleration (α)	196.2	m/s^2
Input force (F)	526.4	N

frequency	angular velocity	CABARET Gap	Non-linear GAP	measured 1	measured 2	measured 3	mean measured gap
f (Hz)	ω (rad / s)	D (m)	D (m)	D (m)	D (m)	D (m)	D (m)
100	628	9.49E-06	1.05E-05	8.52E-06	1.30E-05	9.73E-06	1.04E-05
200	1256	9.90E-06	1.10E-05	1.17E-05	1.09E-05	1.28E-05	1.18E-05
300	1884	1.06E-05	1.20E-05	1.87E-05	1.69E-05	1.81E-05	1.79E-05
400	2512	1.19E-05	1.36E-05	1.25E-05	1.27E-05	1.18E-05	1.23E-05
500	3140	1.41E-05	1.65E-05	1.27E-05	1.30E-05	1.30E-05	1.29E-05
600	3768	1.80E-05	2.22E-05	1.48E-05	1.61E-05	1.55E-05	1.55E-05

frequency	CABARET Gap	Non-linear GAP	mean measured gap
f (Hz)	(m)	(m)	D (m)
100	9.49E-06	1.05E-05	1.04E-05
200	9.90E-06	1.10E-05	1.18E-05
300	1.06E-05	1.20E-05	1.79E-05
400	1.19E-05	1.36E-05	1.23E-05
500	1.41E-05	1.65E-05	1.29E-05
600	1.80E-05	2.22E-05	1.55E-05



Title: GAP PREDICTION FOR 9-BALL COMPLEMENT (using CABARET stiffness) at 25g acceleration

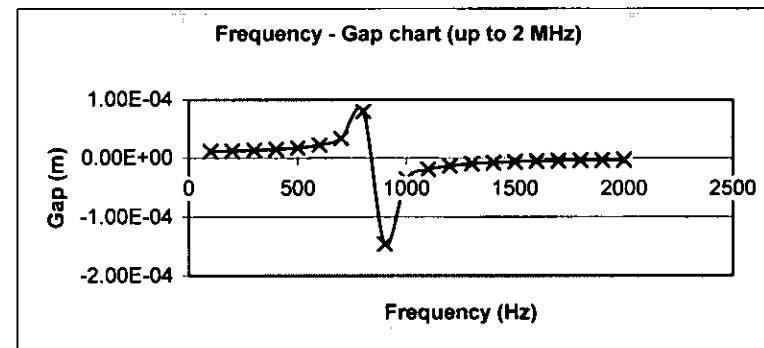
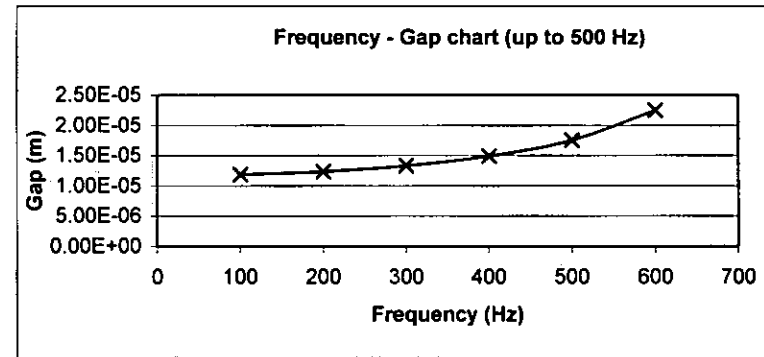
Autor: PAPAKONSTANTINOU ANTONIOS

Date: 31-10-2003

Input data

Shaft assembly mass total (m_1)	1.9	kg
Outer housing assembly mass total (m_2)	0.783	kg
Input acceleration (α)	245.25	m/s^2
Input force (F)	658.0	N
Stiffness (k)	16400000	N/m

frequency	angular velocity	amplitude	amplitude	Gap
f (Hz)	ω (rad / s)	A_1 (m)	A_2 (m)	D (m)
100	628	-6.18E-04	-6.30E-04	1.19E-05
200	1256	-1.52E-04	-1.64E-04	1.24E-05
300	1884	-6.52E-05	-7.85E-05	1.33E-05
400	2512	-3.45E-05	-4.94E-05	1.49E-05
500	3140	-1.97E-05	-3.73E-05	1.76E-05
600	3768	-1.07E-05	-3.32E-05	2.25E-05
700	4396	-2.83E-06	-3.66E-05	3.38E-05
800	5024	1.36E-05	-6.63E-05	7.99E-05
900	5652	-5.04E-05	9.59E-05	-1.46E-04
1000	6280	-1.65E-05	1.87E-05	-3.51E-05
1100	6908	-1.07E-05	8.38E-06	-1.91E-05
1200	7536	-8.03E-06	4.69E-06	-1.27E-05
1300	8164	-6.41E-06	2.94E-06	-9.34E-06
1400	8792	-5.29E-06	1.97E-06	-7.26E-06
1500	9420	-4.47E-06	1.38E-06	-5.85E-06
1600	10048	-3.84E-06	1.01E-06	-4.85E-06
1700	10676	-3.35E-06	7.54E-07	-4.10E-06
1800	11304	-2.95E-06	5.78E-07	-3.53E-06
1900	11932	-2.62E-06	4.52E-07	-3.07E-06
2000	12560	-2.34E-06	3.59E-07	-2.70E-06



Title: GAP PREDICTION FOR 9-BALL COMPLEMENT (using non-linear stiffness) at 25g acceleration

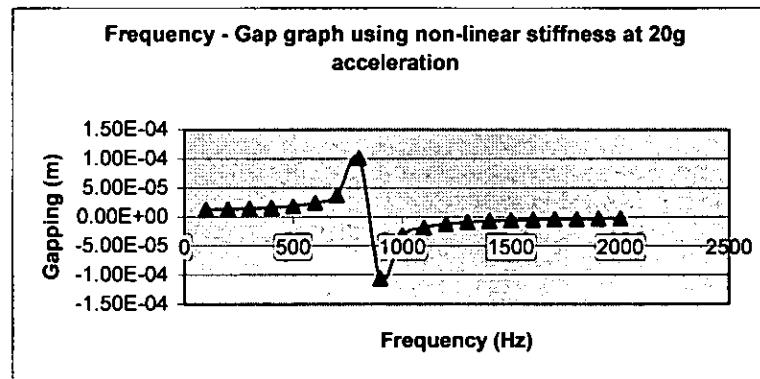
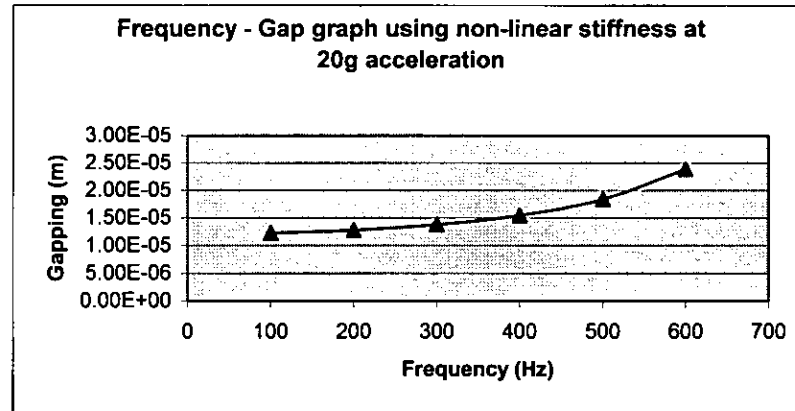
Autor: PAPAKONSTANTINOU ANTONIOS

Date: 31-10-2003

Input data

Shaft assembly mass total (m_1)	1.9	kg
Outer housing assembly mass total (m_2)	0.783	kg
Input acceleration (a)	245.25	m/s^2
Input force (F)	658.0	N
Stiffness (k)	15900000	N/m

frequency	angular velocity	amplitude	amplitude	Gap
f (Hz)	ω (rad / s)	A_1 (m)	A_2 (m)	D (m)
100	628	-6.18E-04	-6.31E-04	1.22E-05
200	1256	-1.52E-04	-1.65E-04	1.28E-05
300	1884	-6.51E-05	-7.89E-05	1.38E-05
400	2512	-3.43E-05	-4.98E-05	1.55E-05
500	3140	-1.95E-05	-3.79E-05	1.84E-05
600	3768	-1.03E-05	-3.42E-05	2.39E-05
700	4396	-1.88E-06	-3.89E-05	3.70E-05
800	5024	1.97E-05	-8.11E-05	1.01E-04
900	5652	-3.86E-05	6.73E-05	-1.06E-04
1000	6280	-1.56E-05	1.66E-05	-3.22E-05
1100	6908	-1.04E-05	7.74E-06	-1.82E-05
1200	7536	-7.91E-06	4.40E-06	-1.23E-05
1300	8164	-6.34E-06	2.78E-06	-9.12E-06
1400	8792	-5.25E-06	1.87E-06	-7.12E-06
1500	9420	-4.45E-06	1.32E-06	-5.77E-06
1600	10048	-3.83E-06	9.64E-07	-4.79E-06
1700	10676	-3.34E-06	7.23E-07	-4.06E-06
1800	11304	-2.94E-06	5.55E-07	-3.49E-06
1900	11932	-2.61E-06	4.34E-07	-3.05E-06
2000	12560	-2.34E-06	3.45E-07	-2.68E-06



Title: GAP PREDICTION COMPARISSON FOR 9-BALL COMPLEMENT at 25g acceleration

Autor: PAPAKONSTANTINOUS ANTONIOS

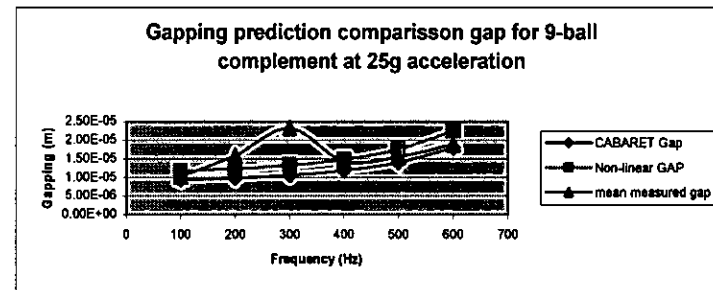
Date: 31-10-2003

Input data

Shaft assembly mass total (m_1)	1.9	kg
Outer housing assembly mass total (m_2)	0.783	kg
Input acceleration (α)	294.3	m/s^2
Input force (F)	789.6	N

frequency	angular velocity	CABARET Gap	Non-linear GAP	measured 1	measured 2	measured 3	mean measured gap
f (Hz)	ω (rad / s)	D (m)	D (m)	D (m)	D (m)	D (m)	D (m)
100	628	1.19E-05	1.22E-05	1.09E-05	8.84E-06	1.11E-05	1.03E-05
200	1256	1.24E-05	1.28E-05	1.45E-05	1.64E-05	1.68E-05	1.59E-05
300	1884	1.33E-05	1.38E-05	2.26E-05	2.36E-05	2.35E-05	2.32E-05
400	2512	1.49E-05	1.55E-05	1.42E-05	1.40E-05	1.52E-05	1.44E-05
500	3140	1.76E-05	1.84E-05	1.49E-05	1.62E-05	1.56E-05	1.56E-05
600	3768	2.25E-05	2.39E-05	1.82E-05	1.88E-05	1.97E-05	1.89E-05

frequency	CABARET Gap	Non-linear GAP	mean measured gap
100	9.49E-06	1.19E-05	1.03E-05
200	9.90E-06	1.24E-05	1.59E-05
300	1.06E-05	1.33E-05	2.32E-05
400	1.19E-05	1.49E-05	1.44E-05
500	1.41E-05	1.76E-05	1.56E-05
600	1.80E-05	2.25E-05	1.89E-05



Title: GAP PREDICTION FOR 9-BALL COMPLEMENT (using CABARET stiffness) at 30g acceleration

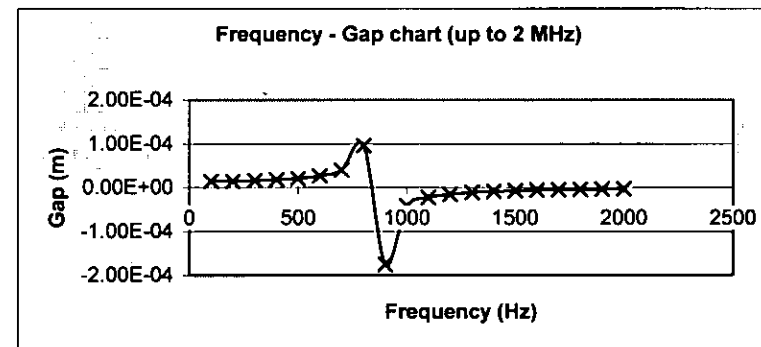
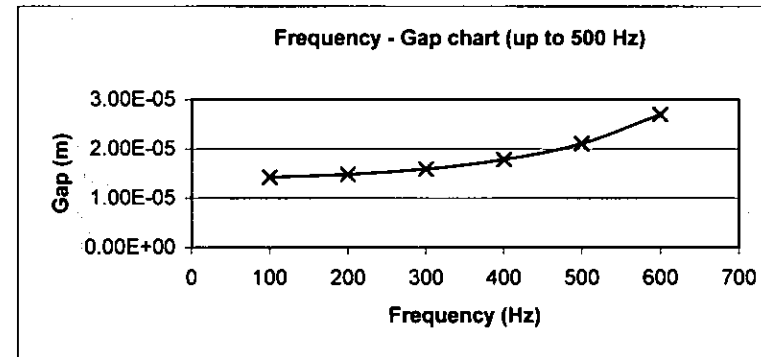
Autor: PAPAKONSTANTINOU ANTONIOS

Date: 31-10-2003

Input data

Shaft assembly mass total (m_1)	1.9	kg
Outer housing assembly mass total (m_2)	0.783	kg
Input acceleration (α)	294.3	m/s^2
Input force (F)	789.6	N
Stiffness (k)	16400000	N/m

frequency	angular velocity	amplitude	amplitude	Gap
f (Hz)	ω (rad / s)	A_1 (m)	A_2 (m)	D (m)
100	628	-7.42E-04	-7.56E-04	1.42E-05
200	1256	-1.82E-04	-1.97E-04	1.48E-05
300	1884	-7.83E-05	-9.42E-05	1.60E-05
400	2512	-4.14E-05	-5.93E-05	1.79E-05
500	3140	-2.37E-05	-4.48E-05	2.11E-05
600	3768	-1.28E-05	-3.99E-05	2.70E-05
700	4396	-3.40E-06	-4.39E-05	4.05E-05
800	5024	1.63E-05	-7.95E-05	9.58E-05
900	5652	-6.04E-05	1.15E-04	-1.75E-04
1000	6280	-1.98E-05	2.24E-05	-4.21E-05
1100	6908	-1.29E-05	1.01E-05	-2.29E-05
1200	7536	-9.64E-06	5.63E-06	-1.53E-05
1300	8164	-7.69E-06	3.52E-06	-1.12E-05
1400	8792	-6.35E-06	2.36E-06	-8.71E-06
1500	9420	-5.37E-06	1.66E-06	-7.02E-06
1600	10048	-4.61E-06	1.21E-06	-5.82E-06
1700	10676	-4.02E-06	9.05E-07	-4.92E-06
1800	11304	-3.54E-06	6.94E-07	-4.23E-06
1900	11932	-3.14E-06	5.42E-07	-3.68E-06
2000	12560	-2.81E-06	4.30E-07	-3.24E-06



Title: GAP PREDICTION FOR 9-BALL COMPLEMENT (using non-linear stiffness) at 30g acceleration

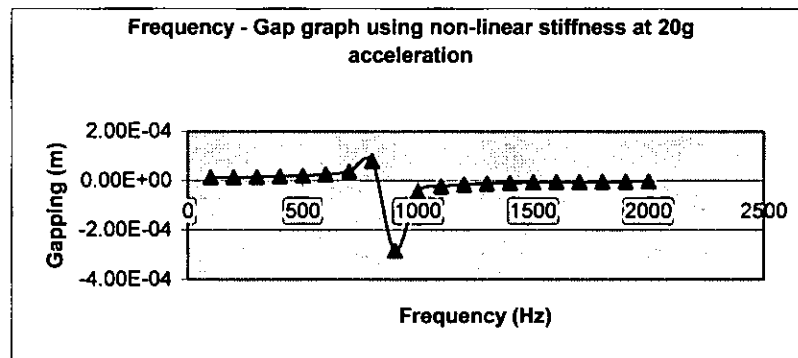
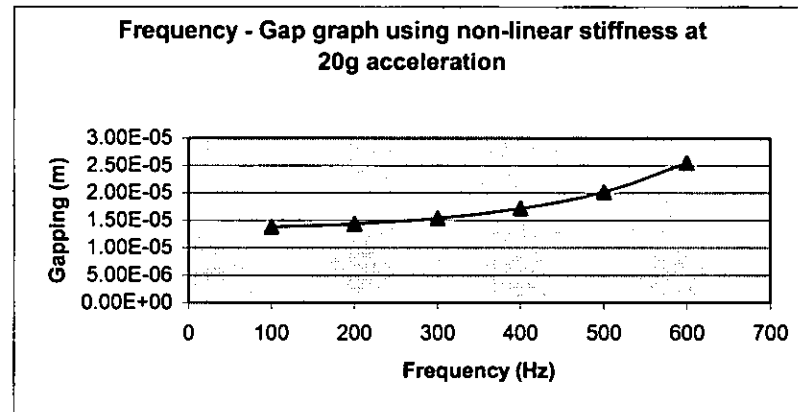
Autor: PAPAKONSTANTINOU ANTONIOS

Date: 31-10-2003

Input data

Shaft assembly mass total (m_1)	1.9	kg
Outer housing assembly mass total (m_2)	0.783	kg
Input acceleration (α)	294.3	m/s^2
Input force (F)	789.6	N
Stiffness (k)	16900000	N/m

frequency	angular velocity	amplitude	amplitude	Gap
f (Hz)	ω (rad / s)	A_1 (m)	A_2 (m)	D (m)
100	628	-7.42E-04	-7.56E-04	1.38E-05
200	1256	-1.82E-04	-1.97E-04	1.44E-05
300	1884	-7.84E-05	-9.38E-05	1.54E-05
400	2512	-4.16E-05	-5.88E-05	1.72E-05
500	3140	-2.40E-05	-4.41E-05	2.02E-05
600	3768	-1.33E-05	-3.88E-05	2.55E-05
700	4396	-4.36E-06	-4.16E-05	3.73E-05
800	5024	1.15E-05	-6.78E-05	7.93E-05
900	5652	-9.19E-05	1.91E-04	-2.83E-04
1000	6280	-2.10E-05	2.54E-05	-4.64E-05
1100	6908	-1.32E-05	1.09E-05	-2.41E-05
1200	7536	-9.79E-06	6.00E-06	-1.58E-05
1300	8164	-7.77E-06	3.72E-06	-1.15E-05
1400	8792	-6.40E-06	2.48E-06	-8.88E-06
1500	9420	-5.40E-06	1.74E-06	-7.13E-06
1600	10048	-4.64E-06	1.26E-06	-5.90E-06
1700	10676	-4.03E-06	9.43E-07	-4.98E-06
1800	11304	-3.55E-06	7.21E-07	-4.27E-06
1900	11932	-3.15E-06	5.63E-07	-3.71E-06
2000	12560	-2.82E-06	4.47E-07	-3.27E-06



Title: GAP PREDICTION COMPARISSON FOR 9-BALL COMPLEMENT at 30g acceleration

Autor: PAPAKONSTANTINOUS ANTONIOS

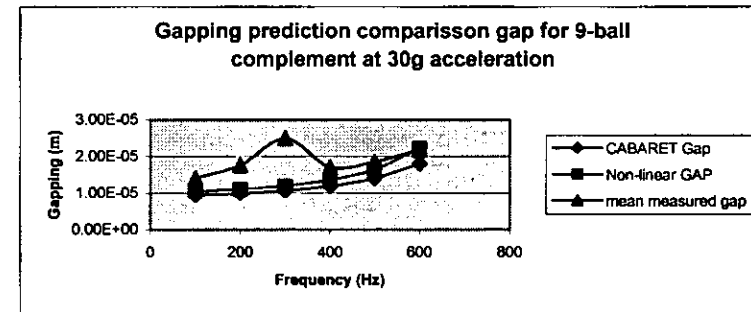
Date: 31-10-2003

Input data

Shaft assembly mass total (m_1)	1.9	kg
Outer housing assembly mass total (m_2)	0.783	kg
Input acceleration (α)	294.3	m/s^2
Input force (F)	789.6	N

frequency f (Hz)	angular velocity ω (rad / s)	CABARET Gap D (m)	Non-linear GAP D (m)	measured 1 D (m)	measured 2 D (m)	measured 3 D (m)	mean measured gap D (m)
100	628	1.42E-05	1.38E-05	1.16E-05	1.12E-05	1.96E-05	1.41E-05
200	1256	1.48E-05	1.44E-05	1.75E-05	1.77E-05	1.76E-05	1.76E-05
300	1884	1.60E-05	1.54E-05	2.13E-05	2.44E-05	2.91E-05	2.49E-05
400	2512	1.79E-05	1.72E-05	1.75E-05	1.69E-05	1.69E-05	1.71E-05
500	3140	2.11E-05	2.02E-05	1.83E-05	1.94E-05	1.81E-05	1.86E-05
600	3768	2.70E-05	2.55E-05	2.07E-05	2.35E-05	2.14E-05	2.19E-05

frequency	CABARET Gap	Non-linear GAP	mean measured gap
100	9.49E-06	1.05E-05	1.41E-05
200	9.90E-06	1.10E-05	1.76E-05
300	1.06E-05	1.20E-05	2.49E-05
400	1.19E-05	1.36E-05	1.71E-05
500	1.41E-05	1.65E-05	1.86E-05
600	1.80E-05	2.22E-05	2.19E-05



Title: GAP PREDICTION FOR 14-BALL COMPLEMENT (using CABARET stiffness) at 20g acceleration

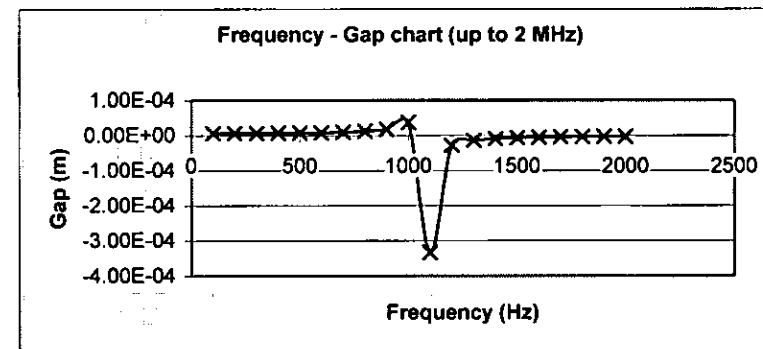
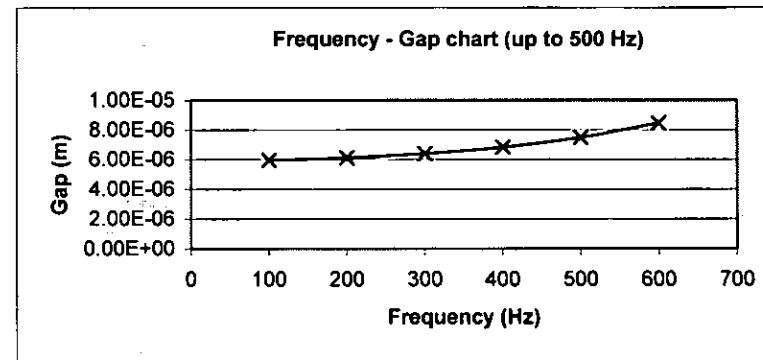
Autor: PAPAKONSTANTINOU ANTONIOS

Date: 31-10-2003

Input data

Shaft assembly mass total (m_1)	1.9	kg
Outer housing assembly mass total (m_2)	0.783	kg
Input acceleration (α)	196.2	m/s^2
Input force (F)	526.4	N
Stiffness (k)	26000000	N/m

frequency	angular velocity	amplitude	amplitude	Gap
f (Hz)	ω (rad / s)	A_1 (m)	A_2 (m)	D (m)
100	628	-4.96E-04	-5.02E-04	5.96E-06
200	1256	-1.23E-04	-1.29E-04	6.11E-06
300	1884	-5.34E-05	-5.98E-05	6.39E-06
400	2512	-2.91E-05	-3.59E-05	6.83E-06
500	3140	-1.77E-05	-2.52E-05	7.48E-06
600	3768	-1.13E-05	-1.98E-05	8.47E-06
700	4396	-7.22E-06	-1.73E-05	1.01E-05
800	5024	-4.04E-06	-1.68E-05	1.28E-05
900	5652	-7.32E-07	-1.93E-05	1.85E-05
1000	6280	5.88E-06	-3.13E-05	3.72E-05
1100	6908	-1.01E-04	2.32E-04	-3.34E-04
1200	7536	-1.16E-05	1.64E-05	-2.80E-05
1300	8164	-7.04E-06	6.98E-06	-1.40E-05
1400	8792	-5.20E-06	3.91E-06	-9.11E-06
1500	9420	-4.14E-06	2.48E-06	-6.62E-06
1600	10048	-3.44E-06	1.69E-06	-5.12E-06
1700	10676	-2.93E-06	1.20E-06	-4.13E-06
1800	11304	-2.54E-06	8.90E-07	-3.43E-06
1900	11932	-2.22E-06	6.77E-07	-2.90E-06
2000	12560	-1.97E-06	5.26E-07	-2.50E-06



Title: GAP PREDICTION FOR 14-BALL COMPLEMENT (using non-linear stiffness) at 20g acceleration

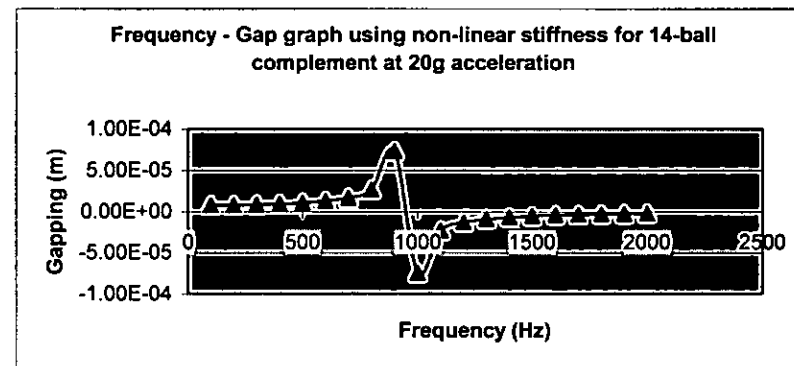
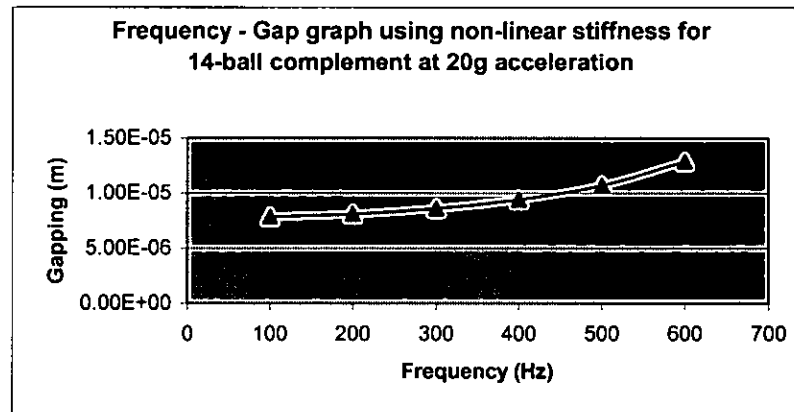
Autor: PAPAKONSTANTINOU ANTONIOS

Date: 31-10-2003

Input data

Shaft assembly mass total (m_1)	1.9	kg
Outer housing assembly mass total (m_2)	0.783	kg
Input acceleration (α)	196.2	m/s^2
Input force (F)	526.4	N
Stiffness (k)	19800000	N/m

frequency	angular velocity	amplitude	amplitude	Gap
f (Hz)	ω (rad / s)	A_1 (m)	A_2 (m)	D (m)
100	628	-4.95E-04	-5.03E-04	7.85E-06
200	1256	-1.22E-04	-1.30E-04	8.12E-06
300	1884	-5.28E-05	-6.14E-05	8.62E-06
400	2512	-2.83E-05	-3.78E-05	9.42E-06
500	3140	-1.68E-05	-2.75E-05	1.07E-05
600	3768	-1.01E-05	-2.29E-05	1.29E-05
700	4396	-5.22E-06	-2.21E-05	1.69E-05
800	5024	-4.91E-08	-2.65E-05	2.65E-05
900	5652	1.53E-05	-5.83E-05	7.36E-05
1000	6280	-2.67E-05	4.76E-05	-7.43E-05
1100	6908	-1.08E-05	1.22E-05	-2.31E-05
1200	7536	-7.29E-06	5.85E-06	-1.31E-05
1300	8164	-5.56E-06	3.40E-06	-8.95E-06
1400	8792	-4.48E-06	2.18E-06	-6.66E-06
1500	9420	-3.74E-06	1.49E-06	-5.22E-06
1600	10048	-3.18E-06	1.06E-06	-4.25E-06
1700	10676	-2.75E-06	7.85E-07	-3.54E-06
1800	11304	-2.41E-06	5.95E-07	-3.01E-06
1900	11932	-2.14E-06	4.61E-07	-2.60E-06
2000	12560	-1.91E-06	3.64E-07	-2.27E-06



Title: GAP PREDICTION COMPARISSON FOR 14-BALL COMPLEMENT at 20g acceleration

Autor: PAPAKONSTANTINOUS ANTONIOS

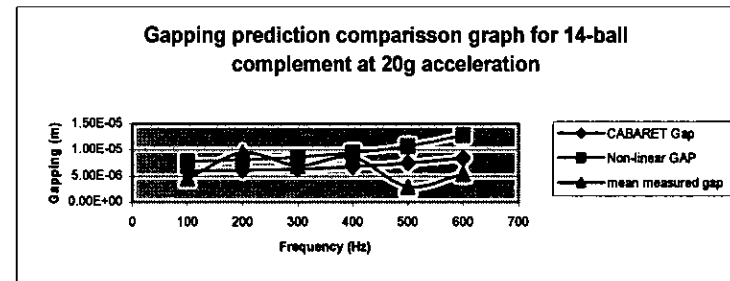
Date: 31-10-2003

Input data

Shaft assembly mass total (m_1)	1.9	kg
Outer housing assembly mass total (m_2)	0.783	kg
Input acceleration (a)	245.25	m/s^2
Input force (F)	658.0	N

frequency	angular velocity	CABARET Gap	Non-linear GAP	measured 1	measured 2	measured 3	mean measured gap
f (Hz)	ω (rad / s)	D (m)	D (m)	D (m)	D (m)	D (m)	D (m)
100	628	5.96E-06	7.85E-06	4.59E-06	5.01E-06	4.09E-06	4.56E-06
200	1256	6.11E-06	8.12E-06	6.41E-06	1.12E-05	1.07E-05	9.44E-06
300	1884	6.39E-06	8.62E-06	7.24E-06	6.84E-06	6.90E-06	6.99E-06
400	2512	6.83E-06	9.42E-06	1.04E-05	6.82E-06	8.69E-06	8.62E-06
500	3140	7.48E-06	1.07E-05	2.76E-05	2.79E-06	3.09E-06	2.94E-06
600		8.47E-06	1.29E-05	5.44E-06	5.48E-06	5.37E-06	5.43E-06

frequency	CABARET Gap	Non-linear GAP	mean measured gap
100	5.96E-06	7.85E-06	4.56E-06
200	6.11E-06	8.12E-06	9.44E-06
300	6.39E-06	8.62E-06	6.99E-06
400	6.83E-06	9.42E-06	8.62E-06
500	7.48E-06	1.07E-05	2.94E-06
600	8.47E-06	1.29E-05	5.43E-06



Title: GAP PREDICTION FOR 14-BALL COMPLEMENT (using CABARET stiffness) at 25g acceleration

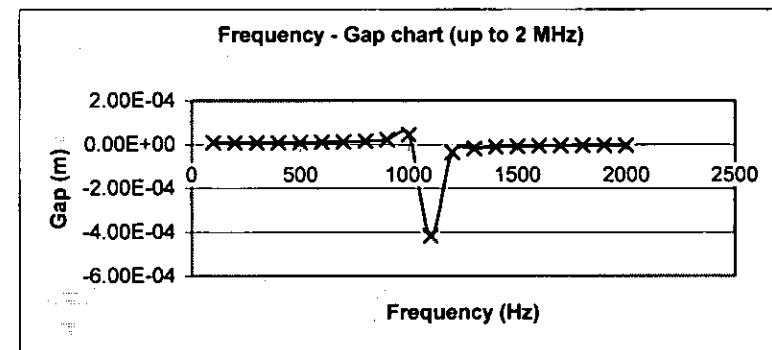
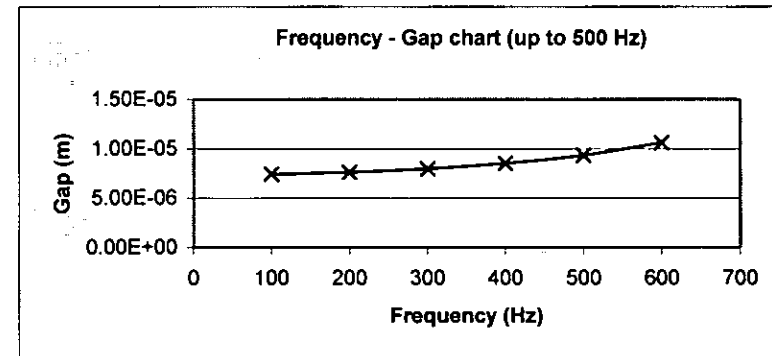
Autor: PAPAKONSTANTINOU ANTONIOS

Date: 31-10-2003

Input data

Shaft assembly mass total (m_1)	1.9	kg
Outer housing assembly mass total (m_2)	0.783	kg
Input acceleration (α)	245.25	m/s^2
Input force (F)	658.0	N
Stiffness (k)	26000000	N/m

frequency	angular velocity	amplitude	amplitude	Gap
f (Hz)	ω (rad / s)	A_1 (m)	A_2 (m)	D (m)
100	628	-6.20E-04	-6.27E-04	7.45E-06
200	1256	-1.53E-04	-1.61E-04	7.64E-06
300	1884	-6.68E-05	-7.48E-05	7.99E-06
400	2512	-3.64E-05	-4.49E-05	8.53E-06
500	3140	-2.21E-05	-3.15E-05	9.35E-06
600	3768	-1.42E-05	-2.48E-05	1.06E-05
700	4396	-9.02E-06	-2.16E-05	1.26E-05
800	5024	-5.05E-06	-2.10E-05	1.60E-05
900	5652	-9.14E-07	-2.41E-05	2.32E-05
1000	6280	7.35E-06	-3.91E-05	4.65E-05
1100	6908	-1.27E-04	2.90E-04	-4.17E-04
1200	7536	-1.45E-05	2.05E-05	-3.50E-05
1300	8164	-8.79E-06	8.73E-06	-1.75E-05
1400	8792	-6.50E-06	4.89E-06	-1.14E-05
1500	9420	-5.18E-06	3.10E-06	-8.28E-06
1600	10048	-4.30E-06	2.11E-06	-6.40E-06
1700	10676	-3.66E-06	1.50E-06	-5.16E-06
1800	11304	-3.17E-06	1.11E-06	-4.28E-06
1900	11932	-2.78E-06	8.46E-07	-3.63E-06
2000	12560	-2.47E-06	6.58E-07	-3.12E-06



Title: GAP PREDICTION FOR 9-BALL COMPLEMENT (using non-linear stiffness) at 25g acceleration

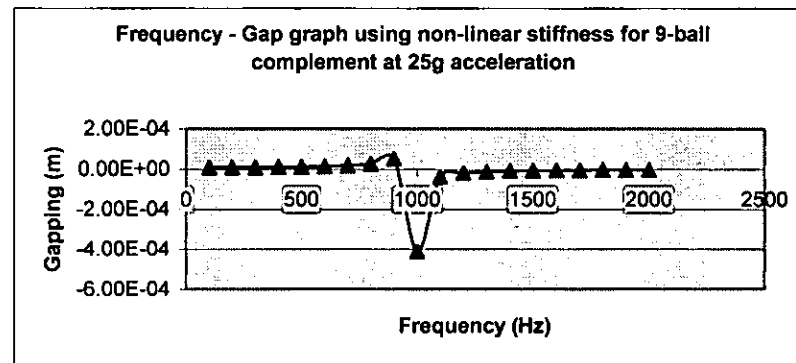
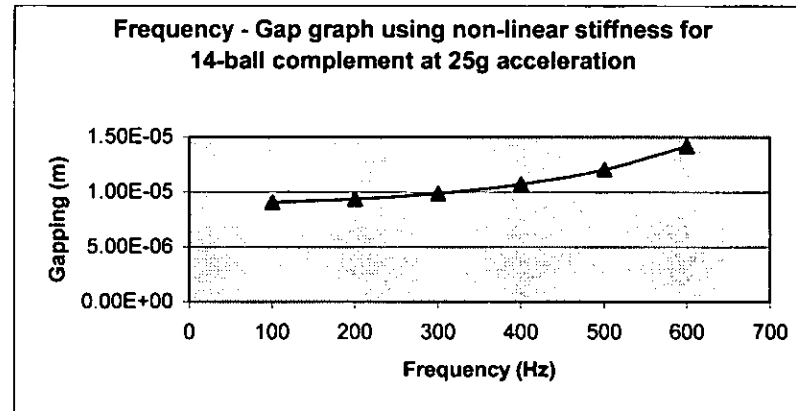
Autor: PAPAKONSTANTINOU ANTONIOS

Date: 31-10-2003

Input data

Shaft assembly mass total (m_1)	1.9	kg
Outer housing assembly mass total (m_2)	0.783	kg
Input acceleration (a)	245.25	m/s^2
Input force (F)	658.0	N
Stiffness (k)	21400000	N/m

frequency	angular velocity	amplitude	amplitude	Gap
f (Hz)	ω (rad / s)	A_1 (m)	A_2 (m)	D (m)
100	628	-6.19E-04	-6.28E-04	9.07E-06
200	1256	-1.53E-04	-1.62E-04	9.36E-06
300	1884	-6.62E-05	-7.61E-05	9.88E-06
400	2512	-3.57E-05	-4.65E-05	1.07E-05
500	3140	-2.14E-05	-3.34E-05	1.21E-05
600	3768	-1.31E-05	-2.73E-05	1.42E-05
700	4396	-7.45E-06	-2.54E-05	1.80E-05
800	5024	-2.15E-06	-2.81E-05	2.59E-05
900	5652	7.52E-06	-4.46E-05	5.21E-05
1000	6280	-1.26E-04	2.84E-04	-4.10E-04
1100	6908	-1.62E-05	2.17E-05	-3.79E-05
1200	7536	-9.87E-06	9.16E-06	-1.90E-05
1300	8164	-7.28E-06	5.06E-06	-1.23E-05
1400	8792	-5.78E-06	3.16E-06	-8.95E-06
1500	9420	-4.78E-06	2.13E-06	-6.91E-06
1600	10048	-4.05E-06	1.50E-06	-5.55E-06
1700	10676	-3.49E-06	1.10E-06	-4.59E-06
1800	11304	-3.05E-06	8.31E-07	-3.88E-06
1900	11932	-2.70E-06	6.41E-07	-3.34E-06
2000	12560	-2.40E-06	5.04E-07	-2.91E-06



Title: GAP PREDICTION COMPARISSON FOR 14-BALL COMPLEMENT at 25g acceleration

Autor: PAPAKONSTANTINOUS ANTONIOS

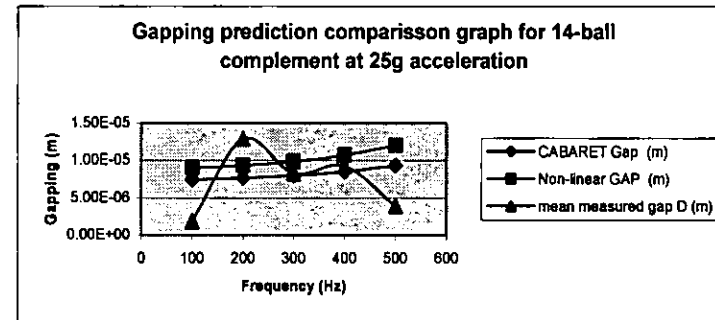
Date: 31-10-2003

Input data

Shaft assembly mass total (m_1)	1.9	kg
Outer housing assembly mass total (m_2)	0.783	kg
Input acceleration (α)	245.25	m/s^2
Input force (F)	658.0	N

frequency	angular velocity	CABARET Gap	Non-linear GAP	measured 1	measured 2	measured 3	mean measured gap
f (Hz)	ω (rad / s)	D (m)	D (m)	D (m)	D (m)	D (m)	D (m)
100	628	7.45E-06	9.07E-06	1.84E-06	1.11E-06	2.55E-06	1.83E-06
200	1256	7.64E-06	9.36E-06	1.30E-05	1.23E-05	1.33E-05	1.29E-05
300	1884	7.99E-06	9.88E-06	8.35E-06	8.59E-06	8.00E-06	8.31E-06
400	2512	8.53E-06	1.07E-05	9.87E-06	1.09E-05	6.94E-06	9.24E-06
500	3140	9.35E-06	1.21E-05	4.38E-06	3.16E-06	4.08E-06	3.87E-06
600				7.21E-06	7.23E-06	7.45E-06	7.30E-06

frequency	CABARET Gap	Non-linear GAP	mean measured gap
f (Hz)	(m)	(m)	D (m)
100	7.45E-06	9.07E-06	1.83E-06
200	7.64E-06	9.36E-06	1.29E-05
300	7.99E-06	9.88E-06	8.31E-06
400	8.53E-06	1.07E-05	9.24E-06
500	9.35E-06	1.21E-05	3.87E-06
			7.30E-06



Title: GAP PREDICTION FOR 14-BALL COMPLEMENT (using CABARET stiffness) at 30g acceleration

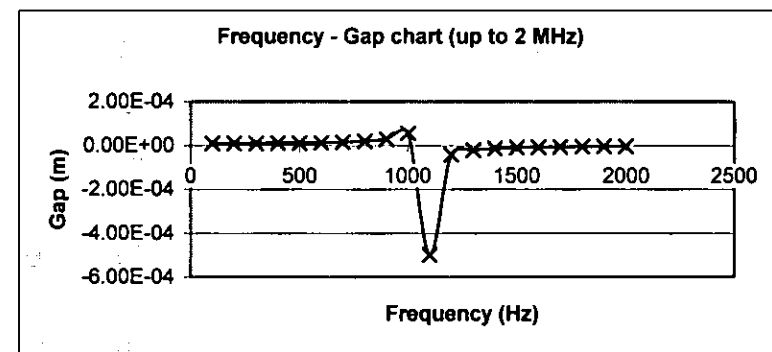
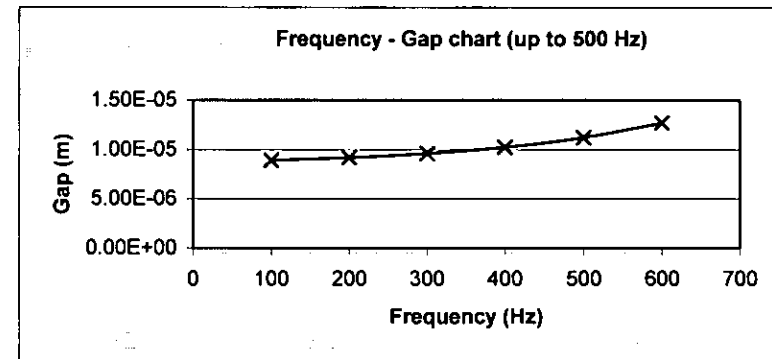
Author: PAPAKONSTANTINOU ANTONIOS

Date: 31-10-2003

Input data

Shaft assembly mass total (m_1)	1.9	kg
Outer housing assembly mass total (m_2)	0.783	kg
Input acceleration (α)	294.3	m/s^2
Input force (F)	789.6	N
Stiffness (k)	26000000	N/m

frequency	angular velocity	amplitude	amplitude	Gap
f (Hz)	ω (rad / s)	A_1 (m)	A_2 (m)	D (m)
100	628	-7.44E-04	-7.53E-04	8.94E-06
200	1256	-1.84E-04	-1.93E-04	9.17E-06
300	1884	-8.01E-05	-8.97E-05	9.59E-06
400	2512	-4.37E-05	-5.39E-05	1.02E-05
500	3140	-2.66E-05	-3.78E-05	1.12E-05
600	3768	-1.70E-05	-2.97E-05	1.27E-05
700	4396	-1.08E-05	-2.59E-05	1.51E-05
800	5024	-6.06E-06	-2.53E-05	1.92E-05
900	5652	-1.10E-06	-2.89E-05	2.78E-05
1000	6280	8.81E-06	-4.70E-05	5.58E-05
1100	6908	-1.52E-04	3.48E-04	-5.00E-04
1200	7536	-1.74E-05	2.45E-05	-4.20E-05
1300	8164	-1.06E-05	1.05E-05	-2.10E-05
1400	8792	-7.80E-06	5.87E-06	-1.37E-05
1500	9420	-6.21E-06	3.72E-06	-9.93E-06
1600	10048	-5.16E-06	2.53E-06	-7.69E-06
1700	10676	-4.39E-06	1.80E-06	-6.19E-06
1800	11304	-3.80E-06	1.34E-06	-5.14E-06
1900	11932	-3.34E-06	1.02E-06	-4.35E-06
2000	12560	-2.96E-06	7.89E-07	-3.75E-06



Title: GAP PREDICTION FOR 14-BALL COMPLEMENT (using non-linear stiffness) at 30g acceleration

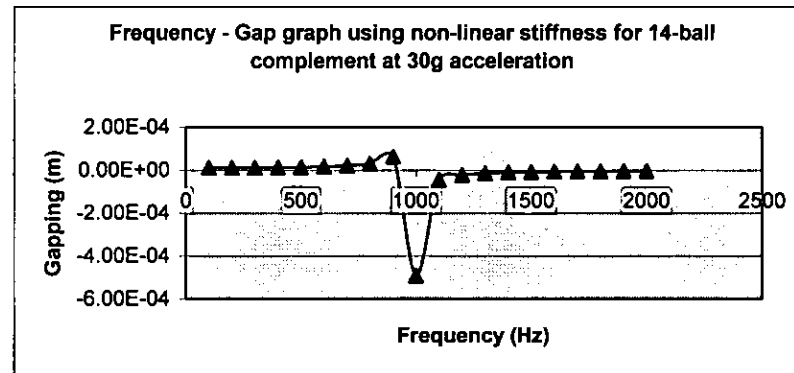
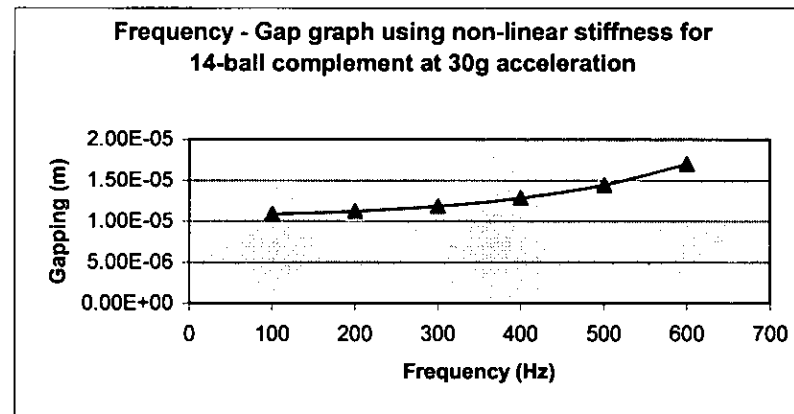
Autor: PAPAKONSTANTINOU ANTONIOS

Date: 31-10-2003

Input data

Shaft assembly mass total (m_1)	1.9	kg
Outer housing assembly mass total (m_2)	0.783	kg
Input acceleration (a)	294.3	m/s^2
Input force (F)	789.6	N
Stiffness (k)	21400000	N/m

frequency	angular velocity	amplitude	amplitude	Gap
f (Hz)	ω (rad / s)	A_1 (m)	A_2 (m)	D (m)
100	628	-7.43E-04	-7.54E-04	1.09E-05
200	1256	-1.83E-04	-1.95E-04	1.12E-05
300	1884	-7.95E-05	-9.13E-05	1.19E-05
400	2512	-4.29E-05	-5.58E-05	1.29E-05
500	3140	-2.56E-05	-4.01E-05	1.45E-05
600	3768	-1.58E-05	-3.28E-05	1.70E-05
700	4396	-8.93E-06	-3.05E-05	2.16E-05
800	5024	-2.58E-06	-3.37E-05	3.11E-05
900	5652	9.03E-06	-5.35E-05	6.25E-05
1000	6280	-1.51E-04	3.41E-04	-4.92E-04
1100	6908	-1.95E-05	2.61E-05	-4.55E-05
1200	7536	-1.18E-05	1.10E-05	-2.28E-05
1300	8164	-8.74E-06	6.07E-06	-1.48E-05
1400	8792	-6.94E-06	3.80E-06	-1.07E-05
1500	9420	-5.74E-06	2.55E-06	-8.29E-06
1600	10048	-4.86E-06	1.80E-06	-6.66E-06
1700	10676	-4.19E-06	1.32E-06	-5.51E-06
1800	11304	-3.66E-06	9.97E-07	-4.66E-06
1900	11932	-3.24E-06	7.69E-07	-4.00E-06
2000	12560	-2.88E-06	6.04E-07	-3.49E-06



Title: GAP PREDICTION COMPARISSON FOR 14-BALL COMPLEMENT at 30g acceleration

Autor: PAPAKONSTANTINOY ANTONIOS

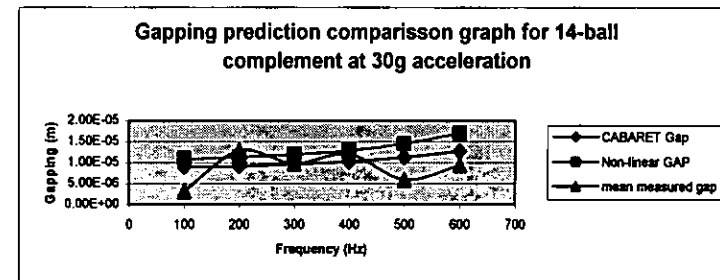
Date: 31-10-2003

Input data

Shaft assembly mass total (m_1)	1.9	kg
Outer housing assembly mass total (m_2)	0.783	kg
Input acceleration (α)	245.25	m/s^2
Input force (F)	658.0	N

frequency	angular velocity	CABARET Gap	Non-linear GAP	measured 1	measured 2	measured 3	mean measured gap
f (Hz)	ω (rad / s)	D (m)	D (m)	D (m)	D (m)	D (m)	D (m)
100	628	8.94E-06	1.09E-05	2.16E-06	3.48E-06	3.96E-06	3.20E-06
200	1256	9.17E-06	1.12E-05	1.37E-05	1.31E-05	1.16E-05	1.28E-05
300	1884	9.59E-06	1.19E-05	9.88E-06	9.59E-06	9.87E-06	9.78E-06
400	2512	1.02E-05	1.29E-05	1.47E-05	1.05E-05	1.08E-05	1.20E-05
500	3140	1.12E-05	1.45E-05	6.65E-06	5.48E-06	5.65E-06	5.93E-06
600		1.27E-05	1.70E-05	9.38E-06	9.23E-06	9.44E-06	9.35E-06

frequency	CABARET Gap	Non-linear GAP	mean measured gap
100	8.94E-06	1.09E-05	3.20E-06
200	9.17E-06	1.12E-05	1.28E-05
300	9.59E-06	1.19E-05	9.78E-06
400	1.02E-05	1.29E-05	1.20E-05
500	1.12E-05	1.45E-05	5.93E-06
600	1.27E-05	1.70E-05	9.35E-06



COLLISION ANALYSIS FOR 9-BALL COMPLEMENT

Input acce (g)	Applied Fc N	v_c m/s Veq	M/s^2 Aeq	N Fimp	GPA Stress
5	132	0.03	45	49	2.493
10	263	0.07	219	243	4.238
15	395	0.11	581	645	5.868
20	526	0.16	1178	1307	7.426
25	658	0.21	2050	2274	8.931
30	790	0.27	3234	3587	10.397
35	921	0.33	4764	5284	11.830
40	1053	0.39	6673	7402	13.237
45	1184	0.45	8992	9973	14.620
50	1316	0.51	11749	13032	15.984
55	1448	0.58	14974	16608	17.329
60	1579	0.65	18692	20733	18.659
65	1711	0.72	22932	25435	19.975
70	1842	0.79	27717	30743	21.278
75	1974	0.86	33074	36684	22.568
80	2106	0.93	39026	43286	23.848
85	2237	1.01	45596	50574	25.118
90	2369	1.09	52809	58574	26.378
95	2500	1.17	60686	67311	27.629
100	2632	1.25	69250	76810	28.872

